GELATION OF CELLULOSE NANOCRYSTALS

by

Lev Lewis

B.Sc., The University of New South Wales, 2012

A THESIS SUBMITTED IN PARTIAL FULFILLMENT OF

THE REQUIREMENTS FOR THE DEGREE OF

DOCTOR OF PHILOSOPHY

in

THE FACULTY OF GRADUATE AND POSTDOCTORAL STUDIES

(Chemistry)

THE UNIVERSITY OF BRITISH COLUMBIA

(Vancouver)

September 2019

The following individuals certify that they have read, and recommend to the Faculty of Graduate and Postdoctoral Studies for acceptance, the dissertation entitled:

GELATION OF CELLULOSE NANOCRYSTALS

submitted by Lev Lewis in partial fulfillment of the requirements for

the degree of Doctor of Philosophy

in Chemistry

Examining Committee:

Mark MacLachlan
Supervisor

Russ Algar
Supervisory Committee Member

Suzana Straus
University Examiner

Rizhi Wang
University Examiner

Additional Supervisory Committee Members:

Curtis Berlinguette
Supervisory Committee Member

Jason Hein
Supervisory Committee Member

Abstract

Colloidal gels of cellulose nanocrystals (CNCs) were prepared using three different strategies by manipulating their colloidal stability. In the first approach, colloidal gels were prepared by hydrothermally treating CNC suspensions. Desulfation of the CNCs at high temperature appears to be responsible for the gelation of the CNCs, giving highly porous networks.

In the second approach, a carbon dioxide-switchable (CO_2-switchable) hydrogel was prepared by adding imidazole to a suspension of CNCs. Sparging of CO_2 through the imidazole-containing CNC suspension led to gelation of the CNCs, which could be reversed by subsequent sparging with nitrogen gas (N_2) to form a low-viscosity CNC suspension. The gelation process and the properties of the hydrogels were investigated by rheology, zeta potential, pH, and conductivity measurements, and the gels were found to have tunable mechanical properties. This work describes a straightforward way to obtain switchable CNC hydrogels without the need to functionalize CNCs or add strong acids or bases. These CO_2-responsive CNC hydrogels have potential applications in stimuli-responsive adsorbents, filters, and flocculants.

Lastly, physical colloidal gels were prepared by freeze-thaw (FT) cycling of CNC suspensions. The aggregation of CNCs was driven by the physical confinement of CNCs between growing ice crystal domains. FT cycling was employed to form larger aggregates of CNCs without changing the surface chemistry or ionic strength of the suspensions. Gelation of CNC suspensions by FT cycling was demonstrated in water and other polar solvents. The mechanical and structural properties of the gels were investigated using rheometry, electron microscopy, X-ray diffraction and dynamic light scattering. It was found that the rheology could be tuned by varying the freezing time, the number of FT cycles, and concentration of CNCs in suspension.

Considering the wide natural abundance and biocompatibility of CNCs, these approaches to CNC-based hydrogels are attractive for producing materials that can be used in drug delivery, insulating materials, and as tissue scaffolds.

Lay Summary

Gels are soft materials that are mostly made up of water and can hold their shape. Dessert jelly is an example of a gel that contains a network of entangled strands, forming a self-supporting network. However, gels created using nanoscale particles that are 100,000 times smaller than the width of a human hair, are of interest as they have unique and interesting properties. These materials are called colloidal gels. Interestingly, colloidal gels can have self-healing properties and can be controllably switched between liquid and gel states. This thesis provides a foundation of strategies to gel nanoscale particles of cellulose, the major structural component of plants, and understand the properties of these gels. These insights may be extended to other particle systems for applications in environmental remediation, healthcare, and energy storage.

Preface

All the work presented in this thesis was carried out under the supervision of Prof. Mark MacLachlan. Dr. Wadood Hamad from FPInnovations, Vancouver, Canada collaborated on all the work presented here and kindly provided the cellulose nanocrystals used throughout this thesis. The rheological measurements were performed in collaboration with Prof. Savvas Hatzikiriakos. X-ray diffraction was performed by Anita Lam at the UBC Crystallography Facility. Scanning electron microscopy and transmission electron microscopy were performed at the UBC Bioimaging Facility with the assistance of Derrick Horne and Brad Ross. Elemental analysis was performed by Derek Smith at the UBC Mass Spectrometry Centre. X-ray photoelectron spectroscopy was performed by Dr. Ken Wong at the UBC Interfacial Analysis & Reactivity Lab.

The contents of **Chapter 2** have been published previously and I am the principal author.[a] The rheology measurements were performed by Dr. Maziar Derakhshandeh and me. I performed all other experiments and wrote the first draft of the manuscript. Reprinted with permission from footnote a. Copyright 2016 American Chemical Society.

The contents of **Chapter 3** have been published previously and I am co-first author.[b] This work was performed in collaboration with Anna-Lena Oechsle whom I mentored. I performed preliminary tests on a subset of amines and designed the experiments. Anna-Lena Oechsle

---

[a]**Lewis, L.**; Derakhshandeh, M.; Hatzikiriakos, S. G.; Hamad, W. Y.; MacLachlan, M. J. Hydrothermal Gelation of Aqueous Cellulose Nanocrystal Suspensions. *Biomacromolecules* **2016**, *17*, 2747–2754.

[b]Oechsle, A. L.*; **Lewis, L.***; Hamad, W. Y.; Hatzikiriakos, S. G.; MacLachlan, M. J. CO_2-Switchable Cellulose Nanocrystal Hydrogels. *Chem. Mater.* **2018**, *30*, 376–385. (*equal contribution)

screened additional amines and performed pH and conductivity measurements. All other characterization was done by Anna-Lena Oechsle and me. Anna-Lena Oechsle wrote the first draft and I edited the manuscript with Prof. Mark MacLachlan. Reprinted with permission from footnote b. Copyright 2018 American Chemical Society.

The contents of **Chapter 4** have been published previously and I am the principal author.[c] Andy Tran collected scanning electron micrographs. I performed all other experiments and wrote the first draft of the manuscript. Reprinted with permission from footnote c. Copyright 2019 American Chemical Society.

---

[c] **Lewis, L.**; Hatzikiriakos, S. G.; Hamad, W. Y.; MacLachlan, M. J. Freeze–Thaw Gelation of Cellulose Nanocrystals. *ACS Macro Lett.* **2019**, *8*, 486–491.

Table of Contents

List of Tables

List of Figures

List of Schemes

List of Symbols and Abbreviations

%	percentage
|G*|	complex modulus
°C	degrees Celsius
µm	micrometer (10^{-6} m)
µs	microsecond (10^{-6} s)
^{1}H	proton
1D	one-dimensional
2D	two-dimensional
3D	three-dimensional
Å	Angström (10^{-10} m)
a.u.	arbitrary units
BET	Brunauer-Emmett-Teller
BJH	Barrett-Joyner-Halenda
CCC	critical coagulation concentration
cm	centimeter (10^{-2} m)
cm^{-1}	wavenumber
CNC	cellulose nanocrystal
CNF	cellulose nanofibers
d	doublet (NMR)
DLVO	Derjaguin-Landau-Verwey-Overbeek

DMF dimethylformamide

DMSO dimethylsulfoxide

e.g. for example

EA elemental analysis

EtOH ethanol

eV electron volts

g grams

G′ storage modulus

G″ loss modulus

h hours

Hz hertz

i.e. note

J joule (kg m^2 s^{-2})

K kelvin

k Boltzmann's constant (1.38 x 10^{-23} m^2 kg s^{-2} K^{-1})

kg kilogram

kHz kilohertz (10^3 Hz)

kPa kilopascal (10^3 Pa)

L liter

LN2 liquid nitrogen

LVE linear viscoelastic region

M molarity (mol L^{-1})

m	meter
MFC	microfibrillated cellulose
MHz	megahertz (10^6 Hz)
min	minutes
mL	milliliter
mm	millimeter (10^{-3} m)
mmol	millimole
mol	mole
mV	millivolts (10^{-3} V)
nm	nanometer (10^{-9} m)
NMR	nuclear magnetic resonance
Pa	pascal
pH	power of hydrogen -log[H^+]
pK_{aH}	dissociation constant of conjugate acid
PXRD	powder X-ray diffraction
rad	radians
s	singlet (NMR)
s	second
S	siemens (kg^{-1} m^{-2} s^3 A^2)
SAOS	small amplitude oscillatory shear
SEM	scanning electron microscopy
T	temperature

TEM	transmission electron microscopy
TGA	thermal gravimetric analysis
UV	ultraviolet
V	volts
wt%	weight percentage
XPS	X-ray photoelectron spectroscopy
XRD	X-ray diffraction
~	approximately
γ	gamma
δ	NMR shift parts per million
ζ	zeta
η	viscosity
θ	theta
κ^{-1}	Debye length
λ	wavelength
μS	microsiemens

Acknowledgements

I had the pleasure of working with outstanding people during my time at the University of British Columbia, to whom I am indebted to for such unforgettable experiences.

First and foremost, I would like to thank my family for their continued love and support. Thank you for helping me grow into the person I am today, and Saba for sparking my curiosity and thirst for knowledge with a spectrophotometer and testing tablets. I am truly blessed.

I would like to thank my supervisor, Mark MacLachlan. I am extremely grateful for the freedom you have given me during my studies and for your support throughout my endeavors inside and outside the lab. I will always admire your passion and enthusiasm for chemistry and your ability to inspire others. Thank you to my supervisory committee Russ Algar, Curtis Berlinguette, and Jason Hein for all your comments and feedback.

I would also like to thank my collaborators. Wadood Hamad for your guidance and continued encouragement in the work I was doing. Savvas Hatzikiriakos, Maziar Derakhshandeh, and Tanja Tomkovic for all your help with rheology. Derrick Horne and Brad Ross for teaching me the art of electron microscopy and dealing with my all too frequent requests on how to improve my imaging. Anita Lam for your patience and enthusiasm whenever I had a new X-ray diffraction experiment to run. David Plackett and John Jackson for opening up your labs and giving your time to help with zeta potential measurements. Joseph Ho and Anna-Lena Oechsle for giving me the pleasure of being able to work with you.

Thank you to the entire MacLachlan and Wolf groups, past and present, for being my home away from home. The Roundbottoms for making those cold, dark, and wet nights something to look forward to. And to everyone I have met along the way, thank you. Words cannot begin to express my sincerest gratitude and appreciation. Thank you all.

Dedication

To my family.

הלב שלי מלא

Chapter 1: Introduction

The development of materials has pervaded society throughout history. Advancements in material chemistry innovation has evolved over the eras, from harnessing nature in the stone age for tools, to forging metals in the bronze age, through the industrial revolution of mass production, and towards the space age of putting man on the moon. These new technologies have solved challenges we have faced by being stronger, lighter, more durable, more flexible, and manufactured faster.

We can now build computers on a silicon wafer, harness the sun's power using solar cells, store energy in batteries between layers of carbon, grow cells in three dimensions in the lab, and fuel a car using hydrogen gas. We are able to push the boundaries of what is possible in materials science by understanding the fundamental principles governing how these systems behave. Continued efforts to broaden the utility and perception of materials science is needed to drive the next generation of progression in areas such as clean energy, tissue engineering, and electronics.

1.1 Gels

Gels are three-dimensional (3D) networks that are predominantly composed of solvent (>90 vol%). IUPAC defines a gel as a "non-fluid colloidal or polymer network that is expanded throughout its whole volume by a fluid" and has a finite, usually rather small, yield stress.[1] The yield stress of a material is the stress needed to plastically deform the material. Therefore, gels are highly solvated, self-supporting structures that typically do not flow under their own weight due to surface tension and intermolecular forces between the network. Nevertheless, there does not appear to be a consensus on the definition of a gel and it has varied over the decades.[2]

Gels are used in numerous applications including diapers, contact lenses, tissue scaffolds, adhesives, soft electronics, water purification, and drug delivery.[3–7] The physical, chemical, and biological properties of gels can be tuned to make them suitable for specific applications. For example, highly-stretchable conductive gels have been prepared that can form strong adhesions between various non-porous substrates that are typically difficult for gels to adhere to including glass, silicon, ceramics, gold, titanium, and aluminum, and have applications in biomedical adhesives, implantable electronics, and wound dressings.[8,9]

Figure 1.1 shows a subset of the gels that exist. Gels can be classified as either organogels or hydrogels, depending on whether the liquid phase is an organic solvent or water, respectively. Alternatively, the solvent can be removed by ambient drying to produce xerogels, or by freeze-drying or critical point drying from CO_2 to produce aerogels, which are low density, high surface area, porous networks that maintain the shape of the original gel.[10] Gels can also be distinguished between chemical gels and physical gels. Chemical gels are formed through covalent crosslinking of networked components. On the other hand, physical gels can form extended networks through non-covalent interactions, including hydrogen bonding, ionic interactions, and hydrophobic interactions.[7] The main structural classes of gels include polymeric, molecular, and colloidal, where the 3D structure-directing networking agent varies.

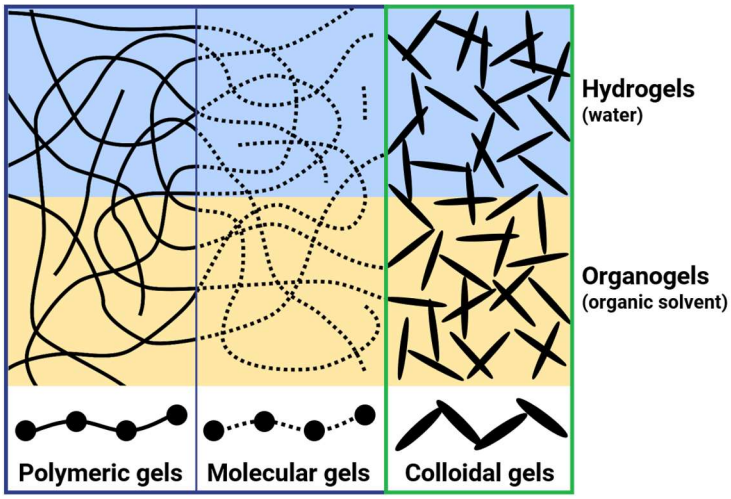

Figure 1.1. Three main structural classes of gels include polymeric, molecular, and colloidal systems. Depending on the solvent, gels can be classified as either hydrogels or organogels. Solid lines represent covalent attachment between monomers to form chains, while dotted lines represent non-covalent interactions between molecular building blocks. Crosslinks between chains, fibers, or particles, can be covalent or non-covalent.

Polymeric gels are examples of chemical gels, where the monomers are covalently bound to form elongated chains.[5] The polymeric chains can then entangle, or chemically crosslink, to create a 3D gel network. Examples include polyacrylamide, polydimethylsiloxane, and sodium polyacrylate and have uses in contact lenses, drug delivery, and diapers.[5–7]

Molecular gels, on the other hand, are examples of physical gels, where the monomers interact through non-covalent intermolecular forces to form fibers.[4,11] These fibers undergo similar physical entanglement to form an extended 3D gel network. Low-molecular-weight gelators are a class of molecular gels that can reversibly self-assemble into gels, for example by heating.[12] In contrast, permanently covalently crosslinked polymeric gels require irreversible bond-breaking to destroy the gel network.[11] Peptide amphiphiles such as,

naphthalene-protected diphenylalanine, can form robust hydrogelators and gelation can be triggered by pH, salt, solvent addition, or light.[4,13,14]

Colloidal gels are another example of physical gels. Colloidal gels consist of particles that are of the order of 1 to 1,000 nm in at least one dimension.[15] The particles form a 3D network that can form self-supporting hydrated structures.

Figure 1.2 gives examples of each type of gel and shows their microstructure by scanning electron microscopy (SEM). Each of these gels can self-support their own weight, either as a shape or when inverted, yet each relies on a different structure-directing component. These systems can be chemically designed with stimuli-responsive behavior such as the DNA-responsive shape-changing polyacrylamide hydrogels, **Figure 1.2A**,[16] or the azobenzene-containing light-responsive molecular gelator that switches between liquid and gelled states with UV irradiation, **Figure 1.2B**.[17] In addition, inorganic materials can form colloidal gels through the entanglement of high aspect ratio nanowires, **Figure 1.2C**.[18] Interestingly, the microstructure of each of these systems varies from largely amorphous networks in the polymeric gel (**Figure 1.2A**) to a flexible fibrillar network (**Figure 1.2B**), and rigid wire mesh networks (**Figure 1.2C**) depending on the structure-directing component. It is worth noting that care must be taken when comparing the microstructures of different gel systems as the drying process and imaging conditions can influence the final morphology observed.

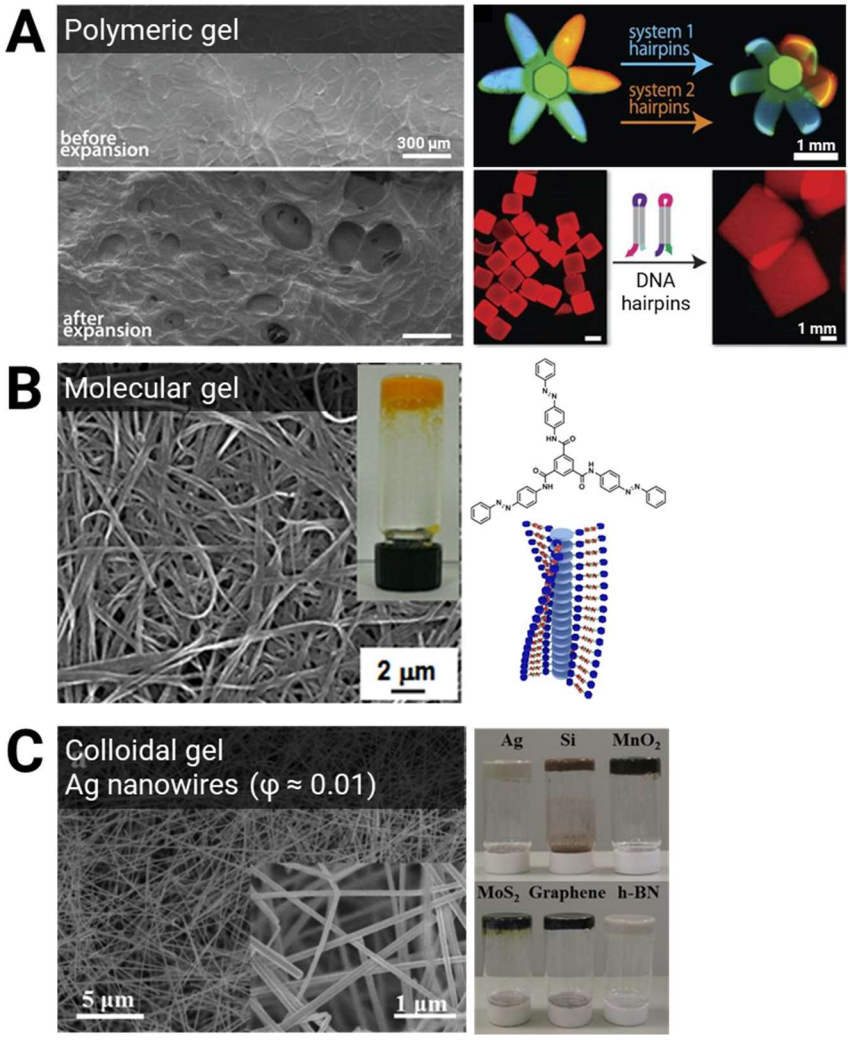

Figure 1.2. Examples of polymeric, molecular, and colloidal gels. (A) DNA-containing polyacrylamide polymeric hydrogel that shape-shift with the addition of DNA hairpins. SEM shows a relatively dense amorphous microstructure. The hydrogel can swell substantially in response to specific DNA hairpin sequences and can be patterned into various shapes and sizes.[16] From reference 16. Reprinted with permission from AAAS. (B) Light-responsive azobenzene-containing molecular gel, which self-assembles into stacked fibers. SEM shows a fibrillar meshed network and inset of inverted gel.[17] Reprinted with permission from reference 17. Copyright 2013 American Chemical Society. (C) Colloidal gel using silver nanowires at a volume fraction, φ, of ~0.01 v/v. SEM shows the high aspect ratio of the silver nanowires and the formation of an entangled meshed network. Colloidal gels were prepared with varying composition using 1D nanowires (Ag, Si, MnO_2) and 2D colloids (MoS_2, graphene, h-BN).[18] Reprinted from reference 18 licensed under CC BY-NC-ND 3.0.

The material properties of these gels can be designed for numerous applications by varying their composition and processing conditions. Hydrogels, in particular, are of interest for tissue engineering applications because their mechanical properties, for example their Young's modulus, can mimic those found in biological tissue including brain (0.1-1 kPa), muscle (8-17 kPa), and pre-mineralized bone (25-40 kPa).[7,19] Hydrogels are currently being explored as muscle-like materials that undergo stiffening when stretched, analogous to mechanical training of biological muscle to increase strength.[20,21]

1.1.1 Rheological Characterization of Gels

Generally, the gelling ability of a system can be evaluated by performing an inversion test.[2] During the inversion test, the sample is placed in a container and inverted. If the sample does not flow to the bottom of the container over a set time (e.g. 5 min), then the system is considered a gel. However, there are several limitations to this approach. For example, the size, shape, and composition of the container can influence the surface tension and adhesive properties of the sample to the container. In addition, the volume of the sample used, and the inversion time, are both factors that can influence the inversion test result. For example, smaller sample volumes, or samples being inverted for a shorter time, are more likely to pass the inversion test.

Therefore, rheology is used to help characterize gel formation, by quantitatively measuring the viscoelastic properties of a sample.[22] Viscoelasticity describes the combination of viscous and elastic properties of a material undergoing deformation. The viscosity of a material is its ability to resist flow, whereas the elasticity of a material is its ability to resist

deformation and return to its original shape when the stress is removed. Rheology can be used to measure the viscoelastic properties of a sample under oscillatory or continuous shear.[23] The loss modulus, G″, is related to the viscous component of a sample while the storage modulus, G′, is related to the elastic component. The complex modulus, G*, is related to the stiffness of the material and can be calculated from the loss and storage moduli using **Equation 1.1**.

$$|\boldsymbol{G}^*| = \sqrt{(\boldsymbol{G}')^2 + (\boldsymbol{G}'')^2} \quad \textbf{(1.1)}$$

A system is said to be gel-like when the storage modulus, G′, is greater than the loss modulus, G″, during oscillatory shear measurements. G′ is a measure of the elastic response of a material, while G″ is a measure of its viscous response, so a gel exhibits greater elastic-like behavior than viscous-like behavior. Ultimately, the inversion test should not be used as the only metric to evaluate the gelling ability of various systems.

1.1.2 Colloidal Gels

Colloids are systems that consist of a dispersed phase suspended in a continuous phase, which do not settle, aggregate, sediment, or precipitate over reasonable time scales (i.e. weeks or months).[15,24–26] There are several examples of colloids in natural and man-made systems including milk, blood, soil, ink, and paint.[27] Colloids can form gels when the dispersed phase is a solid and the continuous phase is a liquid. For example, the dispersed phase in dessert jelly contains solid gelatin proteins while the continuous phase is water, along with some sugar and artificial coloring and flavoring. Physical gels of colloidal systems are dynamic in nature,

allowing them to assemble and disassemble due to non-covalent interactions between individual dispersed particles to form extended 3D networks.[28]

One of the earliest reports of a colloidal gel was that of vanadium pentoxide in 1885,[29] and since then others have been prepared.[30] The mechanism of network formation can vary for colloidal systems between entanglement, for long nanowires,[18] to a percolation of rigid sheet-like particles depending on the nature of the colloid.[31] Alternatively, colloids can form gels by the glassy arrest of particles in the system, where each particle is caged by its neighbours.[32,33] Despite significant progress, the kinetics of colloidal gelation are still not well understood.[34]

Colloidal gels have been made using a variety of materials including metal and metal oxide nanowires,[18] graphene oxide,[31] carbon nanotubes,[35] clays,[36–38] and cellulose nanocrystals.[39] Understanding these particulate systems is important and parallels many systems we currently study including silica and alumina column chromatography, cosmetics, water treatment, river sedimentation, catalytic coatings, and biological separations.[25,26,40] However, the gelation of colloidal systems is not well understood, yet it is of interest to prepare soft materials with varying material properties.[41] By furthering our understanding of colloidal systems we can broaden the scope and applicability of these materials to improve their form, function, efficiency, and utility.

1.2 Cellulose Nanocrystals

Cellulose is the most abundant biopolymer on earth. Plant biomass is predominantly made of cellulose (35-50% by weight) and contains hemicellulose (20-35% by weight) and lignin (10-25% by weight) but can also be found in some bacteria, fungi, and tunicates.[42] The microstructure of wood consists of the plant cell wall, which is composed of macrofibrils and microfibrils, **Figure 1.3**. These fibrils are held together by other components including hemicellulose and lignin, and contain regions of amorphous and crystalline cellulose, which form a cellulose I crystal structure through hydrogen bonding.[43]

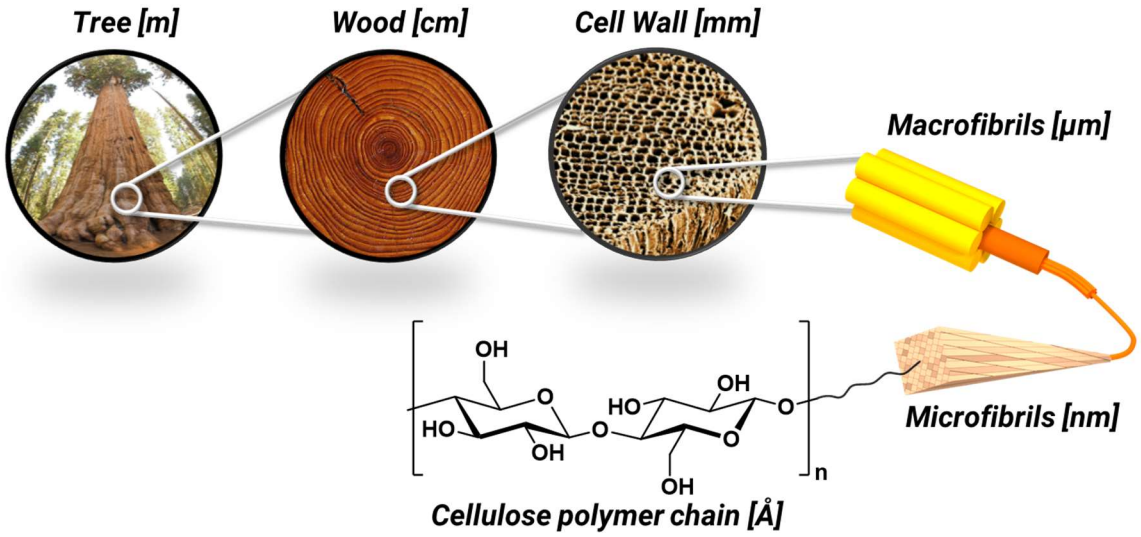

Figure 1.3. Microstructure of wood showing the structural components and their relative length scales. (Tree: "German Sherman Tree" by Jim Bahn (https://commons.wikimedia.org/wiki/File:General_Sherman_tree_looking_up.jpg) is licensed under CC BY 2.0. Wood: "Rings of Fire" by Seth Anderson (https://www.flickr.com/photos/swanksalot/4803155) is licensed under CC BY-NC-SA 2.0. Cell Wall: "Hard Soft Wood" by Mckdandy (https://commons.wikimedia.org/wiki/File:Hard_Soft_Wood.jpg) is licensed under CC BY-SA 3.0.)

Natural Resources Canada has stated that no nation derives more net benefit from trade in forest products than Canada.[44] This has spurred several government initiatives to develop high value materials using nanocelluloses derived from forest products.[45] Nanocelluloses include cellulose nanocrystals (CNCs), cellulose nanofibrils (CNFs), and microfibrillated cellulose (MFC).[46–49] CNCs are crystalline rod-like nanoparticles typically prepared through a chemical treatment, whereas CNFs and MFCs are long flexible fibers with lower crystallinity, typically prepared by mechanical treatment. Cellulose nanocrystals are transformative pulp-based products due to their high crystallinity and mechanical strength.

1.2.1 Preparation of Cellulose Nanocrystals

Cellulose nanocrystals (CNCs) can be prepared by treating wood pulp with concentrated sulfuric acid, **Figure 1.4**. The sulfuric acid treatment selectively hydrolyzes the amorphous cellulose, leaving behind crystalline rod-shaped particles with dimensions of 100-300 nm by 5-20 nm, depending on the source of the pulp and the processing conditions.[43] Importantly, the sulfuric acid hydrolysis introduces negatively charged sulfate half-ester groups onto the surface of CNCs. These negatively charged groups electrostatically stabilize CNCs in water to make a colloidally stable system. Other acids, including hydrochloric, hydrobromic, and phosphoric acids, can be used to prepare CNCs. However, sulfuric acid hydrolysis tends to produce CNCs with superior colloidal stability.[43,50] Depending on the sulfate group counterion, proton or sodium ion, CNCs can be abbreviated as CNC-H^+ or CNC-Na^+, respectively. The colloidal stabilities of CNC-H^+ and CNC-Na^+ suspensions are similar. However, CNC-H^+ suspensions tend to be more acidic (pH ~2), compared to CNC-Na^+ (pH

~7). The surface chemistry of CNCs can also be modified through other synthetic strategies to control their interactions and colloidal stability.[51,52]

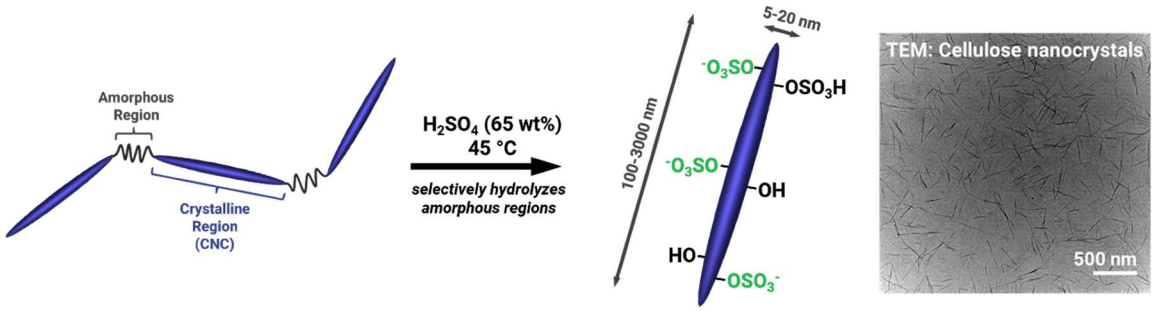

Figure 1.4. Schematic showing the preparation of CNCs by sulfuric acid hydrolysis selectively hydrolyzes the amorphous regions in the cellulosic source producing crystalline rod-like particles with negatively charged sulfate half-ester groups on their surface. A representative transmission electron microscopy (TEM) image of CNCs shows their rod-like shape and varied size distribution.

CNCs are an emerging material whose use in technology offers economic and environmental benefits, and utilizes Canada's abundant forest resource. CNCs are attractive due to their biocompatibility, biodegradability, high strength, low density, renewability, and liquid crystalline properties.[53] CNCs are currently being explored as additives and fillers in polymer melts, cements, and cosmetics.[54,55] Research into the fundamental properties of CNCs and their applications is ongoing.[56]

1.2.2 Colloidal Stability of Cellulose Nanocrystals

CNCs dispersed in water are an example of a colloidal system. The surface chemistry of CNCs plays an important role in keeping CNCs dispersed without precipitating or aggregating. CNCs have an overall negative charge due to the presence of negatively charged sulfate half-ester groups on their surface. These negatively charged sulfate groups electrostatically stabilize CNCs in suspension and have been shown to be dispersible in various solvents including water, dimethylsulfoxide, and dimethylformamide.[53]

There are several underlying principles that are critical to evaluating the colloidal stability of CNCs that will be discussed, including surface charge, ionic strength, and kinetic stabilization. A conceptual understanding of the interfacial interactions at the surface of CNCs is important in developing strategies to controllably manipulate colloids in dispersion.

The electric potential from the surface of a dispersed charged particle changes as a function of distance and is known as the electric double layer, **Figure 1.5**. Typically, a negatively charged particle will have a layer of tightly bound counter ions on the surface, known as the Stern layer. Further from the surface are loosely bound ions that associate with the particle as it diffuses through the solvent. This boundary of loosely bound ions is known as the slipping plane. The slipping plane is the surface at which the zeta potential, **ζ**, is measured for charged particles. Although the electrostatic effects of the charged particle extend to infinity, ions beyond the slipping plane do not strongly associate with the particle and move through the solvent independently. Experimentally, these layers of associated ions extend only a few nanometers from the particle's surface and form the electric double layer. The potential landscape of this electric double layer depends on a number of factors including pH, ionic strength, concentration, and temperature.[27]

Figure 1.5 shows a schematic representation of the electrostatic potential as a function of distance, and the association of ions to the surface of a negatively charged particle into various layers. The electric potential decays exponentially from the surface of the particle as ions in solution shield the surface potential of the charged particle. The electrostatic potential decays more rapidly when the ionic strength is increased (i.e. increased concentration of ions in solution), for example, by the addition of sodium chloride.

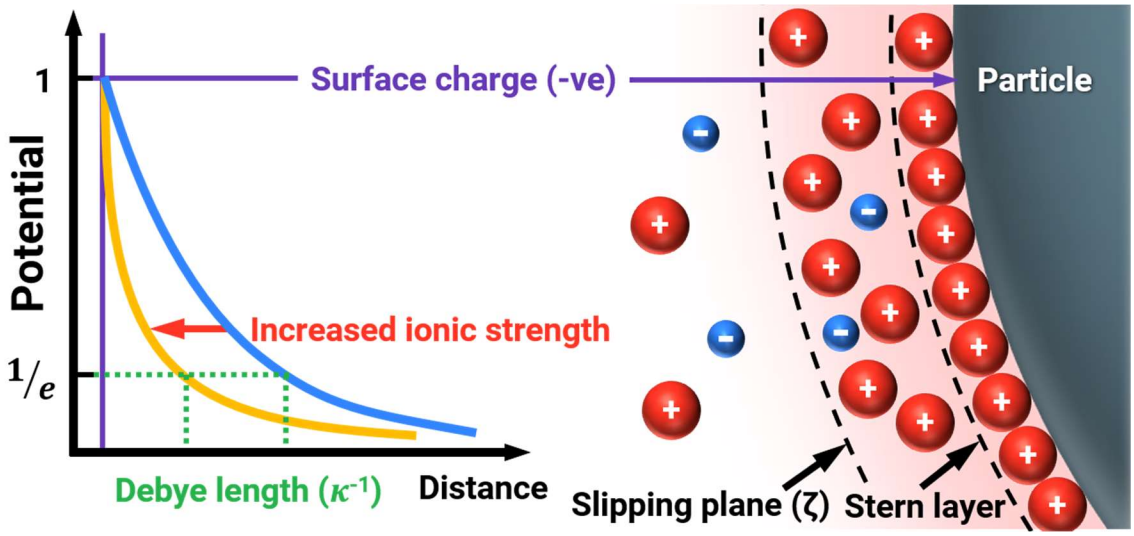

Figure 1.5. Schematic representation of the electric double layer that forms on a charged surface showing the change in surface potential as a function of distance, and the association of ions on their surface. Adapted from reference.[27]

The zeta potential, **ζ**, is a measure of electric potential of a charged particle dispersed in a medium and is a key indicator for the overall stability of a colloidal system. Typically, particles with zeta potential values greater than 20 mV in magnitude are considered stable dispersions.[57] CNCs tend to have zeta potentials ranging from −20 mV to −50 mV depending on their source and preparation conditions.[43] This makes CNCs prepared with sulfuric acid

strongly charged and stable, since the pK_a of the sulfate group is ~2 and are therefore ionized in water over a wide range of pH values.[50] However, CNCs prepared with hydrochloric acid are weakly charged and show limited dispersibility due to the difficulty of hydroxyl groups to ionize at lower pH, generally making them colloidally unstable in water.

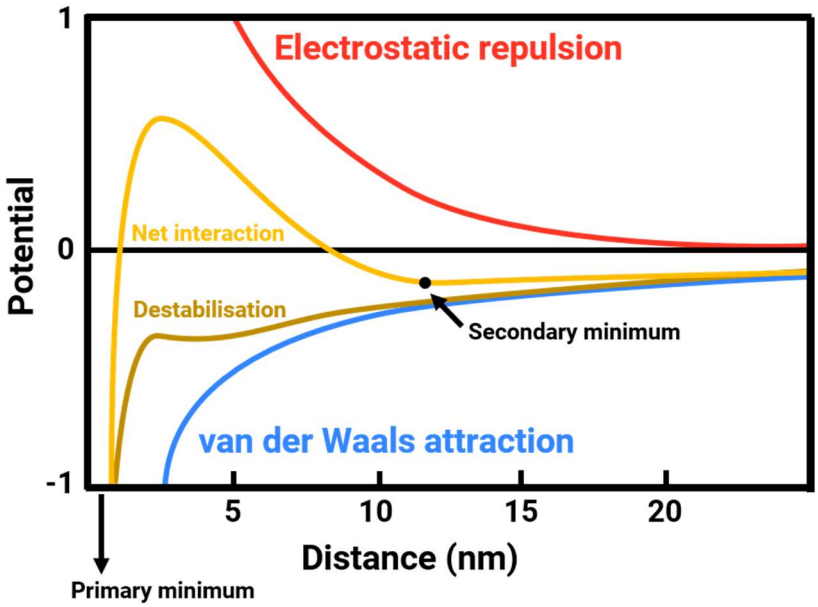

Figure 1.6. Schematic representation of the forces exerted on a charge particle. The net interaction can be used to describe their colloidal stability. Destabilization by increasing ionic strength or decreasing surface charge can lower the energetic barrier to aggregation and drive particles to their thermodynamic minimum. Adapted from references.[27,58]

The stability of charged particles in a colloidal system depends on the net interaction of attractive van der Waals forces and repulsive electrostatic forces, and forms the basis of DLVO theory, named after Derjaguin and Landau,[59] and Verwey and Overbeek.[60,61]

Thermodynamically, particles want to aggregate due to van der Waals attraction, however colloids are kinetically trapped systems due to their strong electrostatic repulsion, **Figure 1.6**. In the absence of surface charge, where there is zero electrostatic repulsion between particles, the net interaction approaches that of pure van der Waals forces and the two particles will strongly attract each other over all distances. For highly charged particles in a low ionic strength system, the energetic barrier is large and the particles are kinetically trapped at a distance of approximately 1-5 nm.[58] In this case, although thermodynamically the particles want to aggregate, the energetic barrier may be too large to overcome under ambient conditions. Therefore, the particles will remain at a distance defined by the secondary minimum and are considered kinetically stable systems.

The energetic barrier decreases as the surface charge decreases or as the ionic strength increases. Once the barrier is sufficiently small, the particles begin to aggregate, and the colloid is destabilized. Therefore, these systems are highly dynamic and can be manipulated in various ways to change their net interaction potentials.

The Schulze-Hardy rule empirically describes the strong valency dependency of ions on the aggregation of hydrophobic colloidal particles.[62] Multivalent ions are said to destabilize colloids much more strongly than monovalent ions. DLVO theory was able to predict the critical coagulation concentration, CCC, that would destabilize a colloidal system, and found it to be inversely proportional to the sixth power of the ion valency, z (**Equation 1.2**).

$$CCC \propto \frac{1}{z^6} \qquad \textbf{(1.2)}$$

However, the assumptions made in the Schulze-Hardy rule are not representative of most systems and their effects are still being explored.[63] More generally, the ionic strength and the surface charge can be used as a measure of the colloidal stability. The ionic strength, *I*, is defined in **Equation 1.3** and depends on the concentration, *c*, of ions with valence *z*.

$$I = \frac{1}{2}\sum_{i=1}^{n} c_i z_i^2 \qquad \textbf{(1.3)}$$

The ionic strength gives an indication of the amount of salt in the system and the degree of charge shielding of the colloidal particles. The Debye length, κ^{-1}, is inversely proportional to the ionic strength and is defined by **Equation 1.4**, where *I* is the ionic strength, ε_r is the dielectric constant, ε_0 is the permittivity of free space, k_B is the Boltzmann constant, *T* is temperature, N_A is the Avogadro number, and *e* is the elementary charge.[24]

$$\kappa^{-1} = \sqrt{\frac{\varepsilon_r \varepsilon_0 k_B T}{2 \times 10^3 N_A e^2 I}} \qquad \textbf{(1.4)}$$

The Debye length, κ^{-1}, can also be represented as the distance from a charged surface at which the particle's surface potential drops by a factor of e^{-1} (Euler's number), depending on the nature of the electrolyte. The Debye length is dependent only on the ionic strength and is roughly 10 nm for systems containing 1 mM of NaCl and does not depend on the overall charge of the particle.[58] This distance can be used as a measure of how close two charged particles can approach each other at a particular electrostatic potential.

Ultimately, the colloidal stability can be disrupted by changing either the surface charge or the ionic strength, and drive the aggregation of a colloid to its thermodynamic minimum. CNCs are stabilized in water by a high negative surface charge and low ionic strength system. Decreasing the overall surface charge, by surface treatment with surfactants or functionalization, can destabilize CNCs.[51] Alternatively, increasing the ionic strength with the addition of salt can also destabilized CNCs by charge shielding the negative surface charge and may lead to gelation.

It is important to first understand the electrostatic potential landscape of the charged surface of CNCs, before we can manipulate these systems to modify their stability and control their interactions.

1.2.3 Cellulose Nanocrystal Gels

Gels using CNCs have been prepared and are promising in various applications including coatings, substrates for catalysis, filtration, and 3D cell cultures.[64,65] The two main types of CNC gels are those composed of CNCs only, and those that contain CNCs along with another structural components including synthetic or natural polymers such as agarose,[66] gelatin,[67] alginate,[68] polyvinyl alcohol,[69] and polyacrylamide.[70] CNC-containing gels can be combined with other polymers through a variety of processing methods to improve their swelling behavior and produce hydrogels that are more mechanically robust and stimuli-responsive. However, these CNC-containing systems tend to rely on entanglement as the gelation mechanism, where the polymers bend, wrap around, or are chemically crosslinked with CNCs, forming an extended mesh network.

Alternatively, CNCs can be used as the only structural component in the gel. CNCs are rigid rod-like particles that are not susceptible to bending or entanglement, but are still able to form self-supporting percolated networks due to non-covalent interactions, including hydrophobic/hydrophilic interactions and hydrogen bonding interactions, between individual particles to form stabilized extended clusters. Percolating networks consist of a continuous connected path of touching particles from one side of the system to the other. The concentration and aspect ratio of the colloid are key features that can be used to evaluate their ability to form percolated networks.[71,72] **Figure 1.7** shows the approximate particle density of 4 wt% dispersions of CNCs and their potential to form percolated networks. The traditional representation of CNC suspensions, **Figure 1.7A**, does not provide a representative model of the number of interactions that exist in CNC suspensions. We estimated the particle density based on the weight concentration, particle size, and the density of cellulose in a typical 4 wt% suspension, **Figure 1.7B**, to be ~5000 particles per cubic micron. We assumed the cellulose particles have a density of 1.6 g cm^{-3} and are monodisperse rectangular prisms with dimensions of 200 nm by 5 nm by 5 nm.[73] Nanoparticle tracking analysis was used to quantify the number concentration of CNCs in suspension to be ~1500 particles per cubic micron, **Figure 1.7C**. Nanoparticle tracking analysis is a technique that relies on laser scattering from a particle (or aggregate of particles) to track their diffusion and determine their size. As a result of possible particle aggregation and clustering, the calculated number concentration is likely lower than reality.[74] The dense nature of CNCs in these colloidal systems provides the foundation for the formation mechanism of CNC-only gels. A large interaction number is favorable for the formation of self-supporting 3D networks. At lower concentrations, the interparticle distance

between CNCs may be too large to effectively produce extended networks. Therefore, it is important to consider the concentration and particle density when preparing colloidal gels.

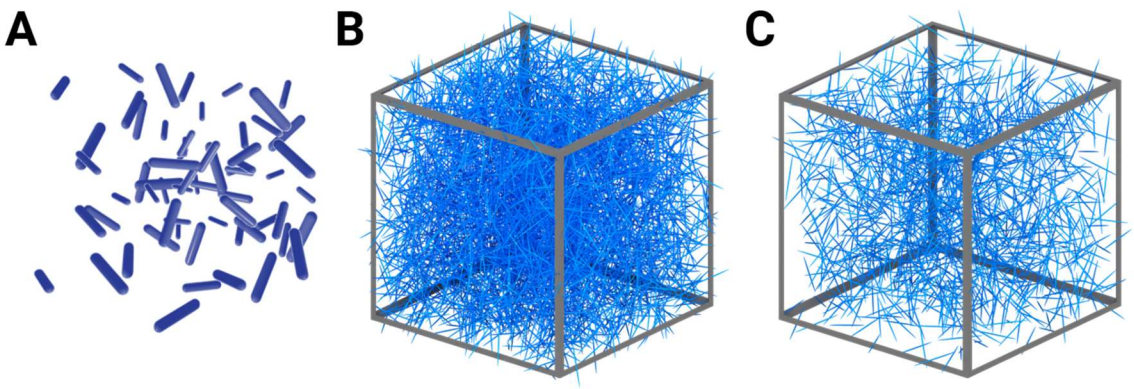

Figure 1.7. Representations of the particle density of CNCs in suspension. (A) Schematic representation of CNCs in suspension.[75] Reprinted with permission from reference 73. Copyright 2013 American Chemical Society (B) Calculation of particle density based on the size (200 nm x 5 nm x 5 nm rectangular prisms), the concentration (4 wt%), and the density (1.6 g cm^{-3}) of CNC suspensions, resulting in ~5000 particles in 1 μm^3 rendered to scale. (C) Particle density based on nanoparticle tracking analysis (**Figure A.1.1**) of 4 wt% CNC suspensions resulting in ~1500 particles in 1 μm^3 rendered to scale.

CNC-only gels can be prepared in a number of ways including increasing the concentration of CNCs,[76] sonication,[77] increasing the salt concentration,[78,79] and chemically crosslinking CNCs.[80] It has been shown that simply increasing the concentration of dispersed CNCs or sonicating can result in gel formation.[76,77] In these cases, it is still not clear what the mechanism of gelation is, for example through glassy arrest due to caging of particles around each other, or aggregation due to a destabilization of the electric double layer at higher particle concentrations, or the hydrophobic/hydrophilic interaction of CNC crystallite faces, or simply physical proximity of particles to allow attractive forces, such as hydrogen bonding, to

dominate. The addition of monovalent and multivalent salts is known to destabilize colloidal systems and can be used to gel CNC suspensions.[78,79] Gelation has also be achieved by chemically crosslinking CNCs covalently, which are orthogonally functionalized with terminal aldehyde and hydrazide moieties, through hydrazone linkages to form extended networks.[80] Each of these strategies exploit the colloid stability and percolating ability of CNCs to form extended 3D networks. Ultimately, however, the differences in network formation between entanglement and rigid percolation, and physical versus covalent crosslinking, are not well understood for colloidal systems. Exploring the gelation of these systems may shed light on the mechanism of formation and how these strategies can be translated to other colloids.

1.3 Goals and Scope

Colloidal gels are systems that are not well understood in terms of their mechanism of formation and control over their gelation. Control over their stability is of interest to access new material properties. The focus of this thesis is to explore various ways in which we can manipulate the colloidal properties of CNCs without chemically functionalizing their surface to produce colloidal gels.

In **Chapter 2**, a decrease in surface charge causes the gelation of heat treated CNCs.[81] Sulfate groups on the surface of CNCs are susceptible to rapid hydrolysis at elevated temperatures. The hydrolysis of these sulfate groups decreases the overall charge of CNCs and the decrease in electrostatic repulsion causes CNCs to aggregate and form a gel. Changes in the CNC counterion, concentration, and treatment temperature are explored, and the resultant structural and morphological properties of the gels are characterized.

In **Chapter 3**, an oscillation in ionic strength is used to cycle between liquid and gel states of cellulose nanocrystals.[82] Amine-containing additives in the suspension can react with CO_2 and N_2 to form the protonated and neutral species of the amine, respectively. The switch between charged and neutral forms causes a drastic change in ionic strength that causes CNCs to destabilize and form a gel. The reversible nature of the protonation event can be used to cycle the material properties of the system between a gel and a liquid upon bubbling with CO_2 and N_2, respectively.

In **Chapter 4**, the aggregation of physically confined cellulose nanocrystals between growing ice crystals is shown to cause gelation.[83] Thermodynamically, CNCs want to aggregate but are kinetically trapped systems due to electrostatic repulsion. Freezing suspensions of CNCs forces the particles into close proximity such that van der Waals forces

dominate, and the particles do not fully redisperse upon thawing. Cycling this freeze-thaw process causes the buildup of aggregated clusters in the system which can then form self-supporting networks.

Each of these chapters explores an individual mechanism in which colloid systems can be destabilized to produce colloidal gels from CNCs. Although cellulose nanocrystals were used throughout this work, having a deeper understanding into why these colloidal gels form can hopefully be extended to other colloidal systems with varying composition, size, shape, and surface chemistry, to access different colloidal soft material gels.

Chapter 2: Hydrothermal Gelation of Cellulose Nanocrystals

2.1 Introduction

Hydrogels are three-dimensional (3D) hydrophilic networks that can undergo large dimensional changes when hydrated and can reach over 90% water in composition.[6,7] They are used for baby diapers, contact lenses, tissue scaffolds, drug delivery, and many other applications. Hydrogels based on cellulose and cellulose nanofibers are known,[77,84,85] and they are attractive as substrates for thermal insulators,[86] oil absorbents,[87–89] and 3D tissue engineering scaffolds[90] due to their biocompatibility, mechanical properties, and wide natural abundance.

Cellulose nanocrystals (CNCs) can be obtained by treating wood pulp with sulfuric acid.[91–93] The CNCs obtained are typically ~5–20 nm × 100–500 nm in dimension, depending on the source of the pulp.[50,73,94] Sulfate ester groups on the crystals give CNCs a negative surface charge and render them dispersible in water. CNCs are being explored as additives to polymers and other materials, because of their self-assembly, high crystallinity, high aspect ratios, rheological properties, and mechanical properties.[69,95–97] The unique liquid crystalline properties of CNCs are also being investigated for their photonic properties in iridescent films and as templates for other materials.[98–103] Kelly et al. constructed photonic stimuli-responsive composite hydrogels from CNCs and various polymers, including polyacrylamide.[70]

Constructing hydrogels from CNCs is a desirable goal since these materials are a renewable resource. In fact, there has been much recent progress in the development of hydrogels from CNCs.[104–108] Yang et al. used surface-modified cellulose nanocrystals as a reinforcing agent to prepare injectable carboxymethylcellulose/dextran composite

hydrogels.[109] The improved mechanical properties and minimal toxicity of this system support its use in tissue engineering applications.[110,111]

Importantly, the stability of CNCs in suspension is strongly dependent on the surface charge of the individual crystals and the ionic strength of the solution.[79,112,113] Electrostatic repulsion between negatively charged crystals stabilizes CNCs in suspension. The preparation of CNC gels can thus be achieved by exploiting these two conditions: (a) an increase in ionic strength or (b) a decrease in the surface charge of the individual CNCs; both result in a decreased colloidal stability and may lead to gelation.

Gelation of CNC suspensions have been realized in a variety of ways. Simply increasing the concentration of CNCs in suspension is known to lead to gelation due to a decrease in the electrostatic double layer distance between CNCs.[39,76,113] Moreover, sonication of CNC suspensions can result in gelation.[77] Chau et al. showed that hydrogels with viscoelastic properties can be obtained by combining CNCs with alkali metal salts.[112]

Alternatively, surface functionalization of CNCs can also lead to hydrogel formation. For example, hydrazone crosslinking has been shown to occur between hydrazide and aldehyde-functionalized CNCs to form self-supporting hydrogels.[80] The coassembly of these hydrazone-crosslinked CNC hydrogels with polypyrrole nanofibers, polypyrrole-coated carbon nanotubes, or MnO_2, give composite materials that are good supercapacitor electrode materials owing to their high porosity and mechanical properties.[114] Other examples of hydrogels constructed from CNCs are also known.[79,97,115]

Hydrogels can be dried to afford lightweight aerogels that can be used as substrates for various applications. For example, Wicklein et al. showed that freeze-cast aerogel composites of cellulose nanofibers, graphene oxide, and sepiolite nanorods exhibit lower thermal

conductivities and better fire-retardant properties than traditional insulating materials, including expanded polystyrene and polyurethane foams.[116] Moreover, Smith et al. used atomic layer deposition to coat CNC aerogels with Al_2O_3 to improve their oxidation resistance, potentially allowing them to be added as reinforcing fillers in polymers with high-temperature (~175 °C) processing conditions.[117]

Here we report the facile and controlled preparation of hydrogels by the hydrothermal treatment of suspensions of CNCs. At elevated temperature, the CNCs undergo desulfation that reduces the surface charge of the crystals and induces gelation. The structural properties of the hydrogels obtained have been investigated by electron microscopy, X-ray diffraction, nitrogen adsorption, and rheology. This new, straightforward aqueous method to form CNC hydrogels does not require the addition of polymers, metal salts, reagents, or other solvents in order to control the degree of sulfation.

2.2 Experimental

2.2.1 Materials and Instrumentation

All compounds were used as received without any further purification. Aqueous suspensions of cellulose nanocrystals (CNCs) were provided by CelluForce Inc. in acidic form (CNC-H^+, 4 wt%, pH 2.3) or neutral form (CNC-Na^+, 4 wt%, pH 6.9).[98] In brief, ultrapure aqueous CNC suspensions were prepared by dispersing spray-dried CNCs (CelluForce Inc.) in deionized water, at a concentration of 2 wt%, by stirring overnight using a mechanical stirrer. The dispersed CNC suspension was then sonicated at 70% power for 30 min (in batches of 3 L) using an ultrasonicator Vibra-Cell VC 750 (Sonics & Materials Inc.). The average energy input was ~9000 J g^{-1} of CNCs. The suspension was then filtered, first using grade 4 Whatman filter paper, followed by grade 42 Whatman filter paper. The filtered CNC suspension was dialyzed against deionized water overnight. The dialyzed suspension was concentrated to the desired concentration using a rotary evaporator then stored in the fridge at 4 °C until further use. The final pH and conductivity of the ultrapure CNC aqueous suspension was adjusted to acidic form (CNC-H^+, pH 2.3) using an ion-exchange resin (Dowex Marathon C hydrogen form, 23–27 mesh particle size, Sigma-Aldrich), or neutral form (CNC-Na^+, pH 6.9) by neutralizing with NaOH, followed by filtration. The typical dimensions of CNC spindles were determined by transmission electron microscopy size distribution analysis to be 191 ± 80 nm by 13 ± 3 nm (**Figure A.2.3**) and have an electrophoretic surface charge of −4.44 C m^{-2}.

Teflon-lined stainless steel autoclaves (23 mL, Parr Instrument Company, Illinois, U.S.A.) were used during hydrothermal treatment of aqueous CNC suspensions. Scanning electron microscopy (SEM) was performed at the UBC Bioimaging Facility on a Hitachi S4700 electron microscope with samples sputter-coated with platinum/palladium alloy. Hydrogels

were solvent exchanged with ethanol prior to critical point drying using supercritical CO_2 with an autosamdri-815 critical point dryer (Tousimis Research Corporation, Rockville, Maryland, U.S.A.). Nitrogen sorption isotherms were acquired at 77 K using a Micromeritics ASAP 2020 analyzer. Pore-size distributions and specific surface areas were calculated from the adsorption branches using the Barrett–Joyner–Halenda (BJH) and Brunauer–Emmett–Teller (BET) methods, respectively. Thermogravimetric analysis was performed with a Pyris 6 thermogravimetric analyzer (PerkinElmer) under nitrogen gas with a heating rate of 5 °C min^{-1}. Powder X-ray diffraction patterns were recorded on a Bruker D8 Advance diffractometer equipped with a Cu Kα sealed tube X-ray source and a NaI scintillation detector. Elemental analysis (EA) was performed at the UBC Mass Spectrometry and Microanalytical Laboratory on a Fisons Instruments Elemental Analyzer EA 1108 using flash combustion. Samples were freeze-dried and rinsed with double-distilled H_2O to remove any unbound sulfate ions by vacuum filtration and freeze-dried again prior to elemental analysis. X-ray photoelectron spectroscopy (XPS) was performed on a Leybold Max200 spectrometer using an aluminum X-ray source operating at a base pressure of 1×10^{-9} Torr. Initial survey scans were acquired with a pass energy of 192 eV, while higher resolution scans were acquired with a pass energy of 48 eV. XPS spectra were deconvoluted using XPSPEAK by curve fitting with a mixed Gaussian–Lorentzian function after a Shirley type background subtraction. Samples were freeze-dried and rinsed with double-distilled H_2O to remove any unbound sulfate ions by vacuum filtration and freeze-dried again prior to XPS analysis.

2.2.2 Preparation of CNC Hydrogels

An aqueous suspension of CNC-H^+ (10 mL, 4 wt%) was added to a Teflon-lined stainless steel autoclave. The autoclave was sealed and heated to the desired temperature, between 60 and 120 °C over 20 min, and held at the desired temperature for 20 h. After cooling the autoclave to room temperature, the CNC hydrogel was collected and stored at room temperature in sealed glass vials until further characterization was performed. Samples are named CNC-TEMP, where TEMP denotes the treatment temperature (e.g., CNC-80, CNC-120) or CNC-NT for no treatment. The conditions are explicitly described when conditions including concentration (1, 2, or 4 wt%), treatment time, and CNC suspension pH (CNC-H^+ pH 2.3 or CNC-Na^+ pH 6.9) were varied.

2.2.3 Rheology

Rheological properties were characterized by a stress-controlled rotational rheometer (Anton Paar MCR501) in strain-controlled or oscillatory mode using a parallel plate (diameter 50 mm) or a cone–plate geometry (diameter 25 mm, angle 4°). All measurements were conducted at 25 °C. A thin film of mineral oil was applied to the sample periphery to suppress water evaporation during the experiments.

Frequency sweep experiments were performed from 0.01 to 100 Hz within the linear viscoelastic region (5% strain amplitude) in order to determine the viscoelastic moduli of the samples, namely the storage modulus G′ and the loss modulus G″. Continuous shear ramps were performed using shear rates ranging from 0.01 to 100 s^{-1} and a gap of 0.5 mm in order to determine the viscosity material function of the samples. A gap size of 0.5 mm was chosen since the upper limit of the shear rate examined in this study is large (100 s^{-1}), which can

induce edge failure if a larger gap size is used.[118] The rheological properties such as storage and loss modulus were compared with those obtained using a cone and plate geometry in order to check for data consistency. The obtained results from both geometries were similar within experimental error (data not shown).

Thixotropic experiments were performed in three intervals/steps using a cone–plate geometry (diameter 25 mm, angle 4°). The sample was initially subjected to small amplitude oscillatory shear (SAOS) at a certain frequency (10 Hz) for 5 min within the linear viscoelastic region (LVE), followed by a large shear rate (200 s^{-1}) for 5 min to break down the structure of the gel, and finally, the material recovery was monitored over time under SAOS using the same frequency used in the first interval.[119] Interval (1) was performed at 10 Hz oscillatory frequency and 5% strain (within LVE) for ∼5 min to reach steady state.

2.3 Results and Discussion

2.3.1 Synthesis of CNC Hydrogels

While conducting preliminary experiments to carbonize CNCs under hydrothermal conditions, we heated aqueous CNC suspensions in sealed Teflon-lined stainless-steel autoclaves. Hydrothermal treatments have been used to prepare carbonaceous and other functional materials, by heating water to mild temperatures (<200 °C) in a sealed, self-pressurizing environment.[120,121] Unexpectedly, this hydrothermal treatment resulted in gelation of the CNC suspension at temperatures above 80 °C. We attribute the gelation to the desulfation of CNCs, which destabilizes CNCs in suspension, forming a gel (**Figure 2.1**). Autocatalyzed desulfation has already been shown to occur spontaneously at ambient conditions and is accelerated at elevated temperatures ranging between 70 and 100 °C in sealed glass vials.[122] However, the structural or rheological properties of these desulfated suspensions have not yet been studied.

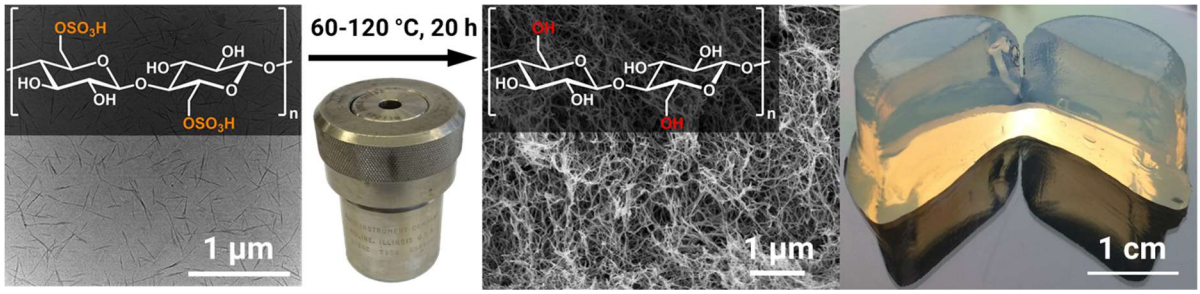

Figure 2.1. Overall synthetic route to CNC hydrogels. CNC suspensions treated hydrothermally undergo desulfation, destabilizing them in suspension, causing gelation. Optical photograph (far right) of 2 wt% CNC-H^+ suspension treated at 120 °C for 20 h.

To the best of our knowledge, CNC hydrogels with tunable mechanical properties have not been demonstrated without the addition of added polymer, solvent, salt, or chemical functionalization. Here we show that hydrothermal desulfation of CNC suspensions can produce hydrogels with tunable mechanical properties by varying conditions including treatment temperature, time, pH, and concentration. We also discuss the changes in CNC composition and structure following hydrothermal treatment.

Figure 2.2 shows hydrogels obtained from CNCs treated at various temperatures, concentrations, and time. We focused on further characterizing hydrogels prepared using CNC-H^+ suspensions (pH 2.3) at a concentration of 4 wt% and heated for 20 h at various temperatures. These conditions produced gels with a broad range of mechanical properties, as seen in **Figure 2.2A**. Thermal treatments performed at elevated temperatures above 120 °C (150, 180, and 210 °C) for 20 h caused discoloration, attributed to hydrothermal carbonization.[121] Therefore, subsequent thermal treatments were kept at, or below, 120 °C.

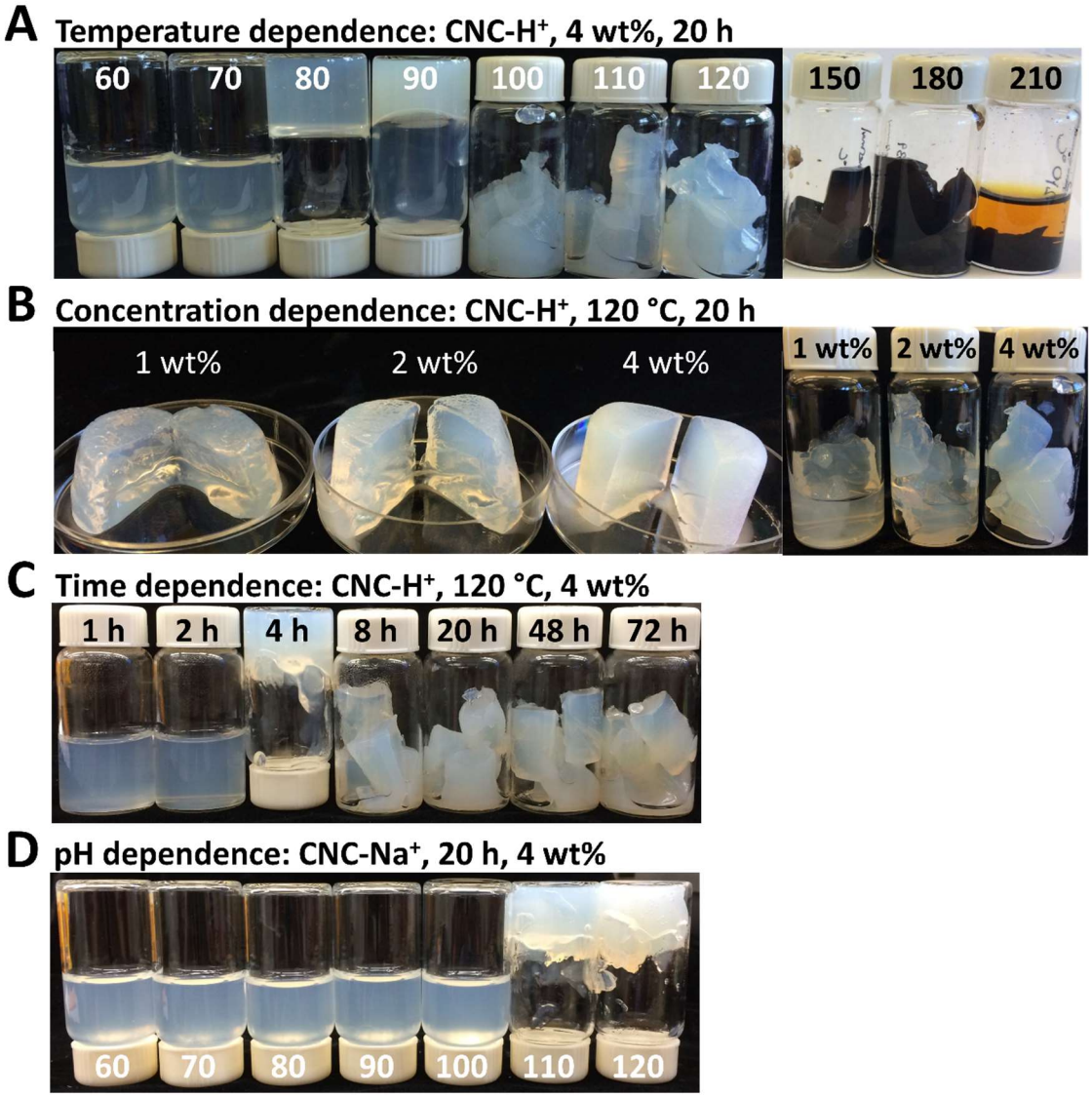

Figure 2.2. Photographs of hydrothermally treated CNC suspensions. (A) Temperature dependence: Hydrogels of 4 wt% CNC-H^+ suspension (pH 2.3) treated at the indicated temperatures (°C) for 20 h. (B) Concentration dependence: Hydrogels of CNC-H^+ suspensions treated at 120 °C for 20 h at the indicated concentrations. (C) Time dependence: Hydrogels of 4 wt% CNC-H^+ suspensions treated at 120 °C for the indicated times. (D) pH dependence: Hydrogels of 4 wt% CNC-Na^+ suspensions (pH 6.9) treated at the indicated temperatures for 20 h, showing the effect of pH on gelation; a higher temperature is required for gelation of CNC suspensions at higher pH.

Figure 2.2B shows CNC-H^+ suspensions treated at varying concentrations (1, 2, and 4 wt%) at 120 °C for 20 h. Gel integrity decreased with decreasing concentration. A significant amount of water was expelled from the hydrogel when the concentration of the treated CNC-H^+ suspension was 1 wt%. CNCs act as the structural framework within the hydrogel network. Thus, at lower concentrations there are fewer CNCs supporting the gel structure, causing the hydrogel to collapse slightly and expel water.

Moreover, the treatment time was varied (1, 2, 4, 8, 20, 48, and 72 h) for 4 wt% CNC-H^+ suspensions treated at 120 °C and was shown to influence gel integrity, as seen in **Figure 2.2C**. Excessive treatment time (72 h) caused slight discoloration due to partial hydrothermal carbonization of CNCs.

Figure 2.2D shows hydrogels using CNC-Na^+ suspensions (pH 6.9) at a concentration of 4 wt% and heated for 20 h at various temperatures. The pH of the initial suspension influences the critical temperature for gelation. A comparison of **Figure 2.2A and D** shows that acidic CNC-H^+ suspensions (pH 2.3) begin to gel at ∼80 °C following 20 h of treatment, whereas neutral CNC-Na^+ suspensions (pH 6.9) require higher treatment temperatures, ∼110 °C, before gelation is observed.

2.3.2 Desulfation of Aqueous CNC Suspensions by Hydrothermal Treatment

Elemental analysis (EA) and X-ray photoelectron spectroscopy (XPS) both support the desulfation of CNC due to hydrothermal treatment. The degree of sulfation decreases significantly with increased treatment temperature. **Table 2.1** shows the relative decrease in sulfur content after hydrothermal treatment between CNC-H^+ suspensions treated at 120 °C (CNC-120) and nontreated (CNC-NT). Although the amount of sulfur in CNC-120 was below

the detection limit for elemental analysis, the sulfur content decreases significantly as treatment temperature increases.

Table 2.1. Elemental analysis (EA) of 4 wt% CNC-H^+ suspensions treated at various temperatures for 20 h, showing the weight percentage of sulfur, carbon, and hydrogen in each sample

	CNC-NT	CNC-60	CNC-80	CNC-100	CNC-120
wt% sulfur	0.61	<0.4[a]	<0.4[a]	<0.4[a]	<0.1[b]
wt% carbon	41.06	41.73	42.44	41.48	41.61
wt% hydrogen	6.31	6.30	6.52	6.48	6.05

[a]Below the quantification limit.
[b]Below the detection limit.

Figure 2.3 shows the sulfur content (atomic %) determined from XPS, confirming a decrease in the amount of sulfur between CNC-NT and CNC-120, further validating the desulfation of the CNC surface at elevated temperature via hydrothermal treatment. Therefore, the degree of sulfation can be tuned by varying the treatment temperature. This hydrothermal method is advantageous over traditional methods, which require extensive reaction and purification steps and the addition of reagents with limited control over extent of desulfation.[96,123,124]

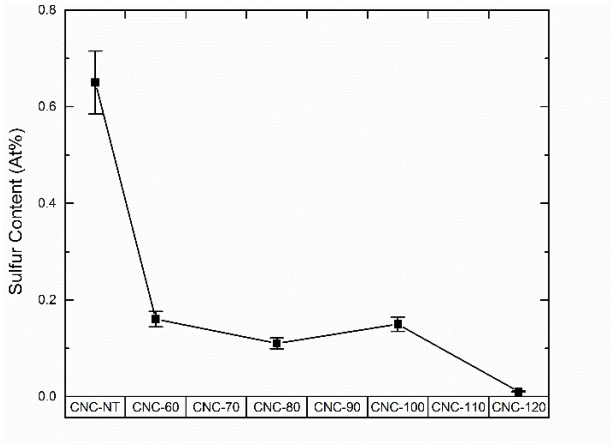

Figure 2.3. Atomic percent of sulfur in each sample as determined by X-ray photoelectron spectroscopy. The samples were prepared by heating 4 wt% CNC-H^+ suspensions at various temperatures for 20 h.

The thermal stability of CNC samples treated at various temperatures was measured by thermogravimetric analysis (TGA). The thermal stability of CNCs is known to increase with decreasing degree of sulfation,[125] and therefore, the higher the thermal stability, the greater the extent of desulfation. The temperature at which the TGA curve intersects at 80 wt% remaining was determined for each sample, and is represented as T80% (**Figure A.2.1 and Figure A.2.2**). However, there is no clear trend of degradation temperature between samples, suggesting that the thermal stability is not only dependent on the degree of sulfation but also other factors such as surface area, crystallinity, and drying conditions.

2.3.3 Characterization of CNC Hydrogel Structure

CNC hydrogels were dried by critical point drying with supercritical CO_2, following solvent exchange with ethanol, to afford highly porous aerogels. Scanning electron microscopy (SEM) of CNC aerogels treated at various temperatures shows a highly porous interconnected cellulosic network, as seen in **Figure 2.4**.

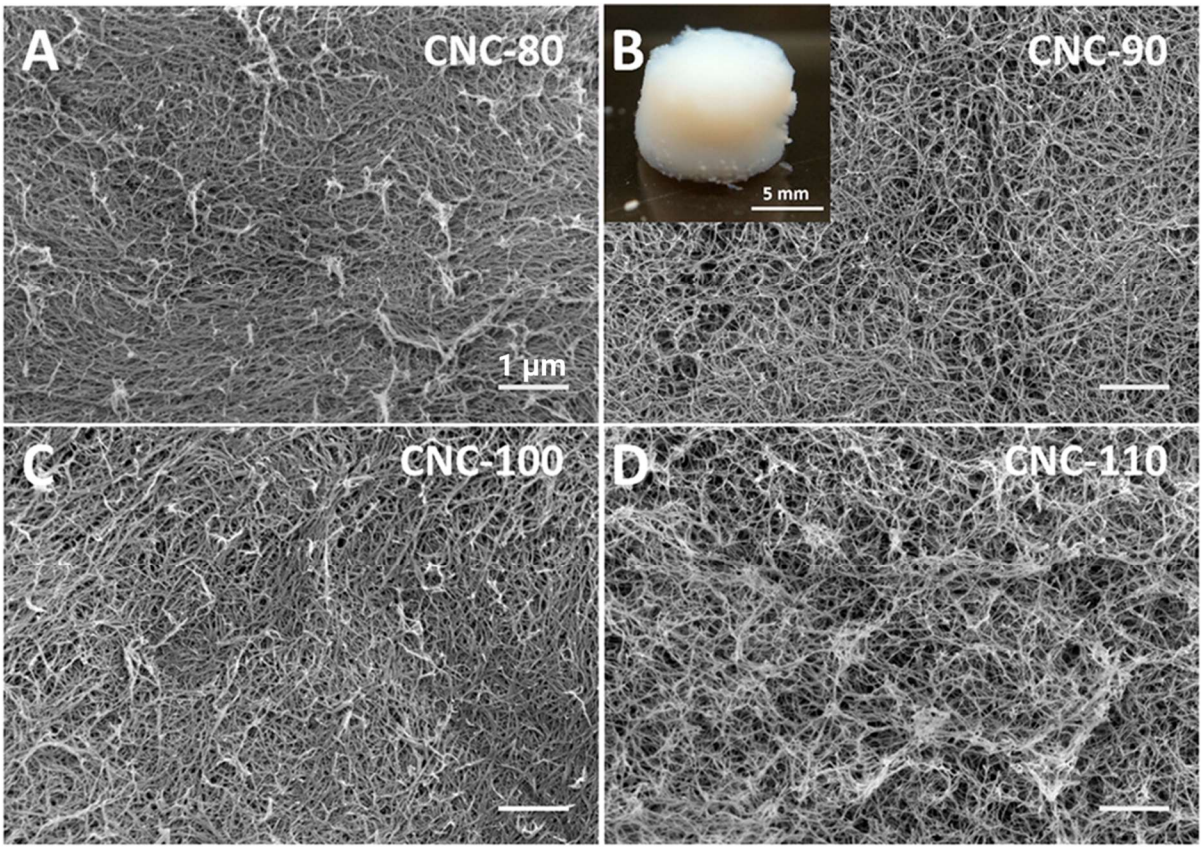

Figure 2.4. Scanning electron microscopy (SEM) micrographs of 4 wt% CNC-H^+ suspensions treated at different temperatures for 20 h, (A) 80, (B) 90, (C) 100, and (D) 110 °C, followed by critical point drying with supercritical CO_2. Scale bar represents 1 µm. The inset of (B) shows a photograph of a typical CNC aerogel (CNC-90).

CNC suspensions with varying concentrations of 1, 2, and 4 wt% were treated at 120 °C for 20 h to yield aerogels with densities of 0.026, 0.036, and 0.068 g cm^{-3}, and BET specific surface areas of 354, 272, and 158 m^2 g^{-1}, respectively (**Figure 2.5**). These experiments clearly show that we can tune the density and surface area of the final aerogel by varying the initial concentration of CNC suspension.

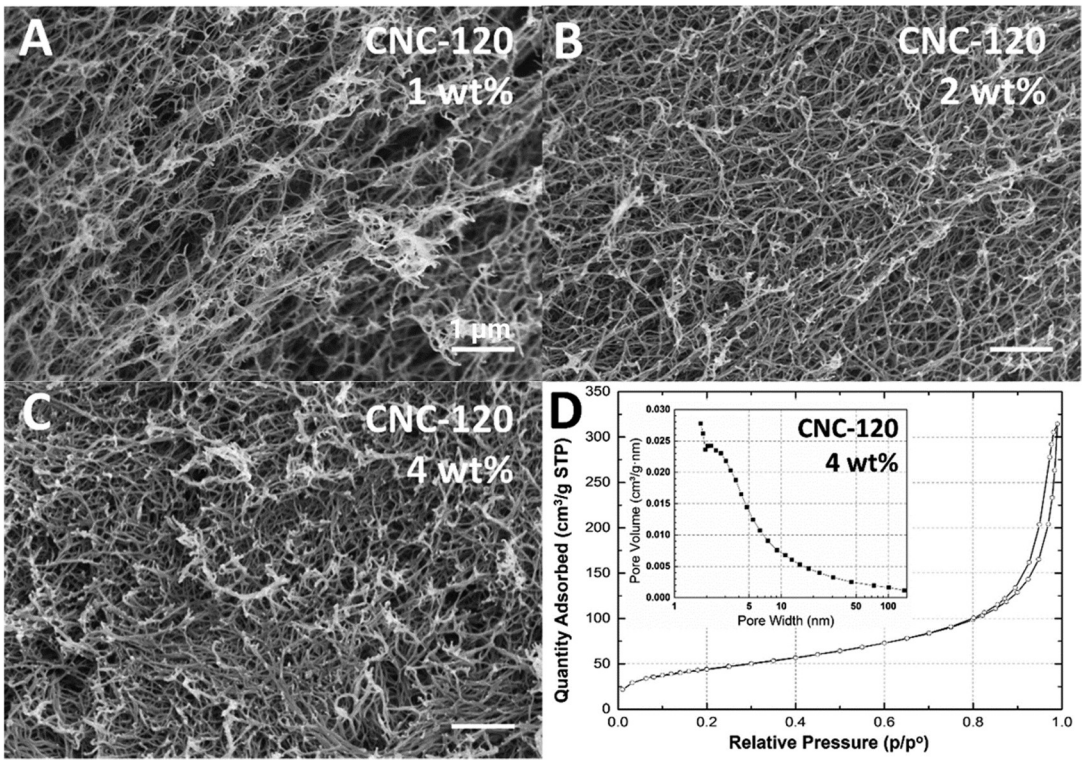

Figure 2.5. SEM micrographs of CNC-H^+ suspensions treated at 120 °C for 20 h with varying concentrations of (A) 1, (B) 2, and (C) 4 wt%, followed by critical point drying with supercritical CO_2. Scale bar represents 1 μm. (D) Typical nitrogen sorption isotherm and inset of BJH pore size distribution of CNC aerogel (4 wt% CNC-120).

Powder X-ray diffraction (PXRD, **Figure 2.6**) confirmed that the CNCs remain crystalline within the hydrogels. There appears to be minimal structural change even in the nanocrystals processed at 120 °C, as the peaks at 15°, 16°, 22°, and 34° 2θ are indicative of the characteristic crystalline planes of cellulose Iα (1−10), (110), (200), and (004), respectively.[126] The characteristic CNC PXRD pattern supports the notion that it is primarily the CNC surface charge that results in hydrogel formation, rather than the formation of an amorphous cellulose network. Thus, the hydrothermal treatment can controllably and selectively catalyze the hydrolysis of negatively charged sulfate half-esters on the surface of the nanocrystals without causing significant degradation of the CNCs themselves.

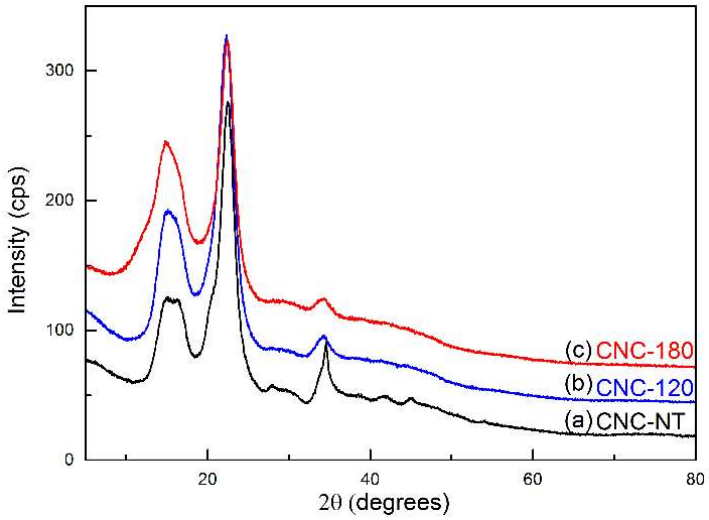

Figure 2.6. Powder X-ray diffraction patterns of CNCs for (a) untreated CNCs (CNC-NT), (b) CNC suspension treated at 120 °C for 20 h (CNC-120), and (c) CNC suspension treated at 180 °C for 20 h (CNC-180).

2.3.4 Rheological Properties of CNC Hydrogels

The rheological properties of CNC hydrogels were investigated using a stress-controlled rotational rheometer equipped with a parallel plate or a cone-and-plate geometry. Dynamic frequency sweeps and continuous shear ramps were performed in order to examine the rheological properties of CNC hydrogels treated at various temperatures. **Figure 2.7** depicts the viscoelastic moduli of CNC hydrogels prepared from 4 wt% suspensions ($CNC{-}H^{+}$) treated at various temperatures from 60 to 90 °C. **Figure 2.7** shows that CNC hydrogels treated at temperatures greater than 80 °C exhibit gel-like characteristics, since the storage modulus (G′) is greater than the loss modulus (G″) and both of these properties (G′ and G″) are independent of frequency. However, only CNC-80 and CNC-90 exhibited G′ > G″ over the entire frequency range tested, suggesting that these hydrogels form robust three-dimensional networks. The transition from liquid-like to gel-like behavior seems to occur at a

temperature between 70 and 80 °C for 4 wt% suspensions, which is in agreement with inversion test results in **Figure 2.2A**.

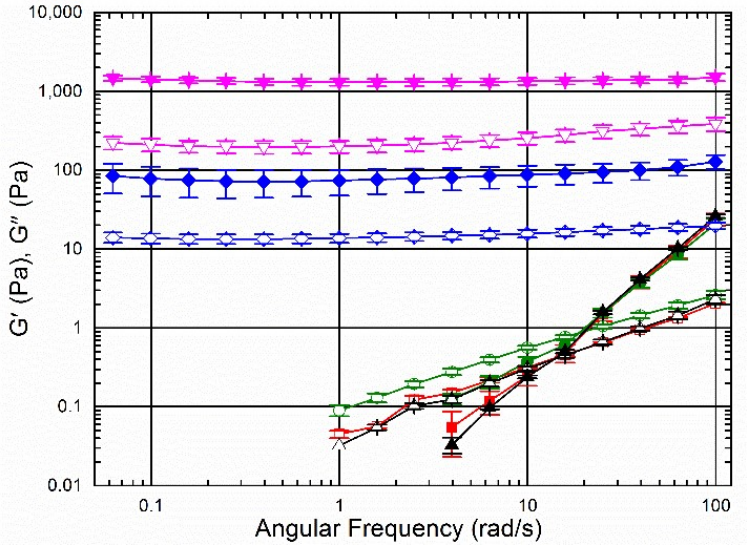

Figure 2.7. Frequency sweep of 4 wt% CNC-H^+ suspensions treated at various temperatures for 20 h. CNC-NT (black ▲), CNC-60 (red ■), CNC-70 (green ●), CNC-80 (blue ◆), and CNC-90 (magenta ▼). Storage modulus (G′, closed symbol) and loss modulus (G″, open symbol) as a function of angular frequency measured at a strain of 5%. Error bars correspond to average standard deviation, $n = 5$.

Figure 2.8 shows the viscosity of 4 wt% CNC-H^+ suspensions treated at various temperatures as a function of shear rate. As the shear rate increases, the viscosity decreases for all samples, demonstrating that these hydrogels are shear thinning. Thus, they can be delivered through syringe injection, making them applicable for biological applications including localized drug delivery, 3D printing, and tissue engineering. The viscosity can be tuned by varying the treatment temperature resulting in materials with a range of viscosities. Control over the final viscoelastic properties of these materials provides flexibility to leverage specific material characteristics for particular material requirements.

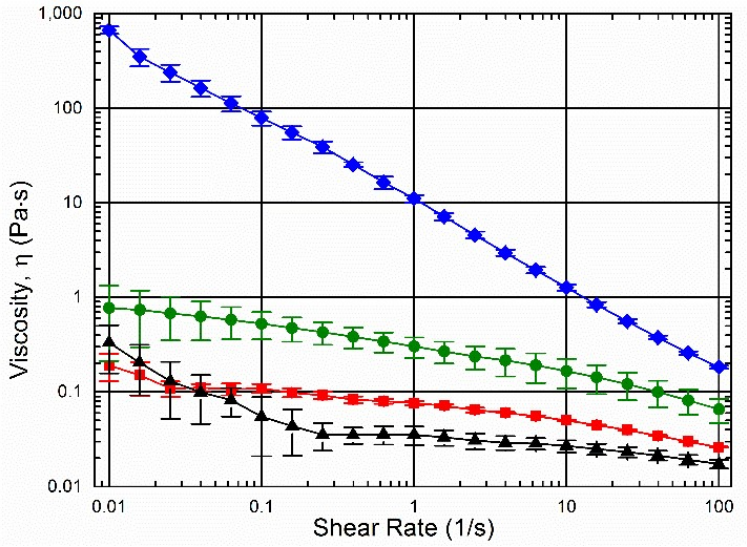

Figure 2.8. Continuous shear ramp of CNC hydrogels using rotational rheology. The viscosity as a function of shear rate is plotted for CNC hydrogels treated at various temperatures. CNC-NT (black ▲), CNC-60 (red ■), CNC-70 (green ●), and CNC-80 (blue ◆). Error bars correspond to average standard deviation, $n = 5$.

Figure 2.9 shows the thixotropic recovery of CNC hydrogels after continuously shearing the sample for 5 min (break in horizontal axis from 5 to 10 min in the graphs of **Figure 2.9**). The recovery of the storage modulus (G′) and loss modulus (G″) was monitored after cessation of destructive shear (breakdown of structure) until a plateau was reached. Each hydrogel sample readily recovers its viscoelastic properties as both G′ and G″ gradually increase over time. The gelation time, t_G, is described as the time at which G′ begins to exceed G″ and occurs <5 s after cessation of destructive shear for all samples. Since the gelation time is short, the contribution of motor inertia to the gelation time may not be neglected. **Figure 2.9A and B** show no thixotropic behavior, as these fluids are simply viscoelastic ones (below gelation as shown in **Figure 2.7**). However, **Figure 2.9C and D** show a gradual plateau recovery of the G′ and G″ over the course of several minutes which implies strong thixotropic

behavior and recovery. The recovery time decreases as the treatment temperature increases from 80 to 90 °C (**Figure 2.9C and D**), suggesting a stronger network formation and faster recovery due to a greater degree of desulfation and fewer repulsive interactions. In some instances, the hydrogels recover to a greater or lower stiffness than observed initially, suggesting that the hydrogels undergo restructuring during continuous shear and can recover to form a more or less robust gel after structural breakdown caused by shear (**Figure 2.9C**).

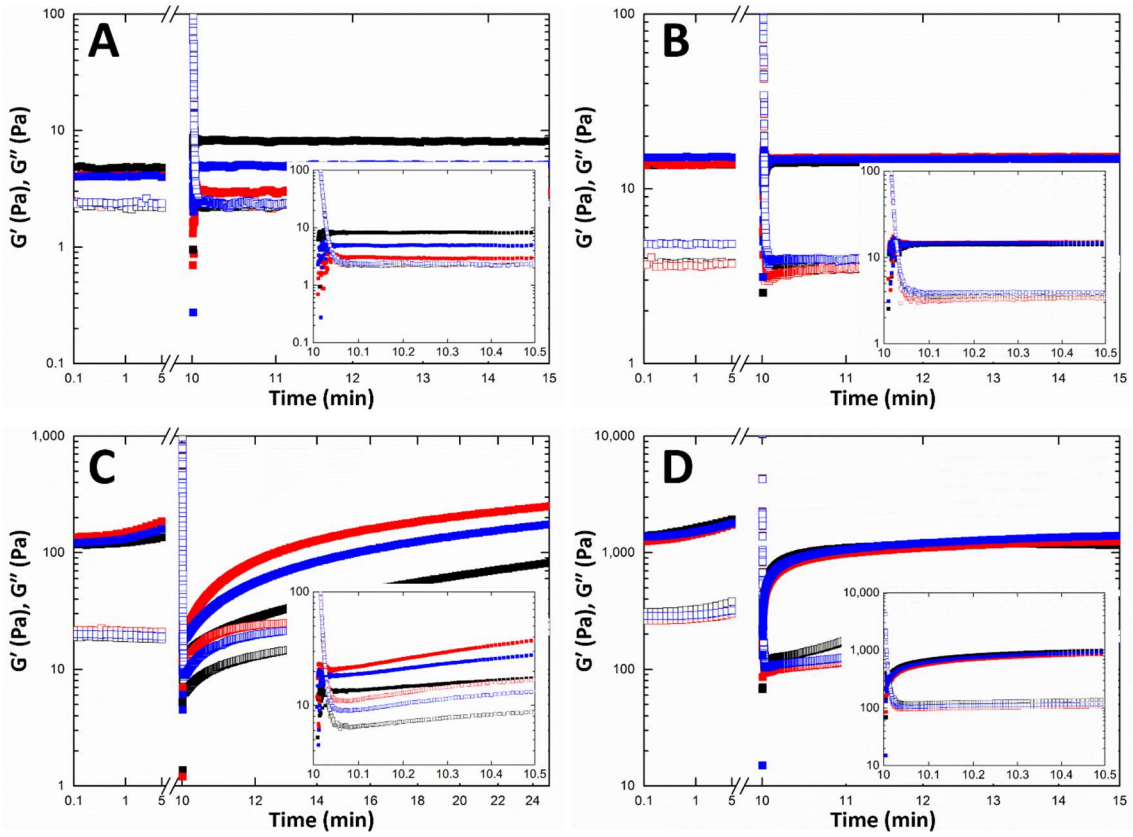

Figure 2.9. Thixotropic investigation of CNC samples treated at different temperatures. (A) CNC-60, (B) CNC-70, (C) CNC-80, and (D) CNC-90 hydrogel recovery over time after continuous shear that causes a breakdown of the structure of the hydrogel network. The storage modulus (G′, closed symbol) and loss modulus (G″, open symbol) gradually increase demonstrating thixotropic recovery of these hydrogel networks. The various colors show repeats of the same test.

2.4 Conclusions

We have shown that CNC hydrogels can be prepared through a straightforward hydrothermal treatment of aqueous suspensions of CNCs at elevated temperatures. Desulfation of the CNC surface occurs during hydrothermal treatment, resulting in a destabilization of CNCs in suspension. The loss of negatively charged sulfate groups from the surface disrupts the electrostatic repulsion between CNCs, causing gelation. Using this approach, we can prepare CNC hydrogels with a range of mechanical properties, including hydrogels that exhibit thixotropic recovery and shear thinning characteristics. CNC hydrogels prepared in this manner could be leveraged for biological applications, since no added salts or other solvents are required, they are syringe injectable, and they are able to recover their mechanical properties. We can dry these hydrogels to produce highly porous, low density, self-supporting aerogel networks as a support for different applications.

Chapter 3: CO_2-Switchable Cellulose Nanocrystal Hydrogels

3.1 Introduction

Hydrogels are three-dimensional hydrophilic networks that swell when hydrated and can hold up to 40 times more water compared to their dry weight.[5–7] The physical, chemical, and biological properties of hydrogels can be tuned to make them suitable for a wide variety of biomedical applications, including tissue scaffolds, drug-delivery vehicles, and contact lenses.[6,81,127,128] Hydrogels that can change their dimensions and properties in response to stimuli are attractive as carriers for controlled drug release, scaffolds for tissue engineering, and actuators.[129–132] Recently, Kim et al. created a hydrogel actuator with a layered structure consisting of cofacially oriented electrolyte nanosheets [unilamellar titanate-(IV)] embedded in an electrostatically anisotropic hydrogel matrix [poly-(*N*-isopropylacrylamide)] that can undergo thermoresponsive deformation enabled by a permittivity switch.[133,134] Other hydrogels that can respond to temperature,[135–137] pH,[138–140] light,[141–143] ionic strength,[144–146] concentration of specific biomolecules,[147–149] electric fields,[150,151] and magnetic fields[152,153] have also been explored.[129]

Cellulose is the most abundant natural and renewable organic biopolymer produced on earth, present in plants, tunicates, algae, fungi, and bacteria.[154–156] Cellulose nanocrystals (CNCs) can be obtained by the acid hydrolysis of cellulose fibers with concentrated sulfuric acid, yielding highly crystalline (54–88%) rod-like nanoparticles with widths of 5–70 nm, and lengths of 100–500 nm depending on the cellulose source.[50,64,73,94,157] In recent years, there has been enormous interest in using CNCs in a wide range of applications owing to its renewability, biocompatibility, and its physicochemical properties such as low density, high specific surface area, liquid crystallinity, and high mechanical strength.[48,50,93,95,98,158–161]

Hydrogels incorporating CNCs have a number of advantageous properties including biocompatibility, renewability, and high mechanical strength that make them suitable for a range of promising applications including coatings, wound dressings, tissue engineering scaffolds, and drug delivery systems.[64] There are many ways in which these hydrogels have been constructed. For example, Ureña-Benavides et al. made CNC-only hydrogels by increasing the concentration of aqueous dispersions of sulfonated CNCs.[39] Gonzales et al. prepared physically entrapped nanocomposite hydrogels using poly-(vinyl alcohol) and CNCs for wound dressing applications.[162] Also, Yang et al. reported tough, stretchable, and isotropic nanocomposite hydrogels, where CNCs are encapsulated by flexible polymer chains of poly-(*N*,*N*-dimethylacrylamide), examples of chemically entrapped CNC hydrogels.[163] Other examples of hydrogels incorporating CNCs have been reported.[70,164–166]

Sulfate half-ester groups are functionalized onto the surface of CNCs during sulfuric acid catalyzed hydrolysis of cellulose pulp. These sulfate groups give CNCs an overall negative charge and render them dispersible in water, because of electrostatic repulsion.[167,168] Destabilizing CNCs, either through a decrease in surface charge or an increase in ionic strength, can cause attractive interactions (e.g. van der Waals forces and hydrogen bonding) to dominate, resulting in hydrogel formation.[112,113] We have shown previously, in **Chapter 2**, that decreasing the surface charge by hydrothermal desulfation decreases the electrostatic repulsion and results in gelation.[81] Shafiei-Sabet et al. and Chau et al. showed that increasing the ionic strength of a CNC suspension by addition of salt decreases the Debye length, causing aggregation of the CNCs and hydrogel formation.[79,112] Furthermore, even a simple increase in the CNC concentration or sonication of the suspensions might result in gelation.[76,77,79,113]

Previous studies on CNC hydrogels have explored the reversibility of the gelation process; for example, Kan et al. reported poly-(4-vinylpyridine)-grafted CNCs that show pH-responsive flocculation and sedimentation.[169] Also, Way et al. showed that functionalization of CNCs with carboxylic acid or amine yields pH-responsive CNC suspensions.[170] However, the repeated switching using acids and bases results in the accumulation of salt over several cycles, which leads to an increase of the ionic strength and influences the dispersibility of CNCs in suspension, and further purification is necessary to remove the accumulated salt.[171,172]

Carbon dioxide (CO_2) is a naturally abundant, biocompatible, and inexpensive gas that can react with amines to form ammonium bicarbonate salts. Removal of CO_2 can be achieved by simply heating, sonicating, or sparging the solution with an inert gas such as N_2 or Ar.[172] Mercer et al. reported that the ionic strength of an aqueous amine-containing solution can significantly increase with the addition of CO_2 because of the formation of carbonic acid, which protonates the amine and leads to charged hydrogen carbonate and ammonium salts. Heating or sparging the solution with N_2 or air reverses the reaction, removing CO_2 and decreasing the ionic strength.[173] CO_2-switchable amine-containing ABA triblock copolymer hydrogels have been investigated by Han et al.[174] Robert et al. demonstrated the use of nitrogen-containing polymers as CO_2-switchable water treatment additives that were able to settle out fine particulates such as kaolinites and montmorillonite clays.[175] Furthermore, Wang et al. demonstrated the CO_2-responsive gelation of CNC suspensions by functionalizing CNCs with terminal imidazole groups.[171] However, these approaches typically require chemical functionalization to achieve CO_2-responsive gelation.

Su et al. demonstrated the reversible aggregation and dispersion of dodecane/water emulsions and polystyrene latexes using a “switchable water” system, with the simple addition

of *N*,*N*-dimethylethanolamine, that undergoes a CO_2-triggered change in ionic strength.[176] However, the system was not designed to gel.

In this chapter, we report the CO_2-switchable gelation of CNC suspensions containing imidazole without the need for any covalent functionalization. The gelation process can be reversed by the removal of CO_2 by sparging the gel with N_2. The CO_2-triggered gelation is attributed to an increase in ionic strength due to the protonation of imidazole and the formation of bicarbonate in solution. This significant increase in ionic strength results in the destabilization of CNCs in suspension, forming a gel. Rheology, zeta potential, pH, and conductivity measurements were used to investigate the gelation process and the properties of the stimuli-responsive hydrogels.

3.2 Experimental

3.2.1 Materials

All compounds were used as received without any further purification. Imidazole was obtained from Acros. The ultrapure aqueous suspension of cellulose nanocrystals (CNCs) was provided by FPInnovations in acidic form (CNC-H^+, 4 wt%, pH 2.3) and was prepared by a previously reported method.[177] In brief, spray-dried CNCs were mechanically stirred overnight in deionized water at a concentration of 2 wt%. An ultrasonicator Vibra-Cell VC 750 (Sonics & Materials Inc.) instrument was used to sonicate the CNC suspension in 3 L batches for 30 min at 70% power, which corresponds to an average energy input of ~9000 J g^{-1} of CNC. The suspension was then filtered through grade 4 Whatman filter paper, followed by grade 42 Whatman filter paper, and then dialyzed overnight against deionized water. The desired concentration was adjusted using a rotary evaporator, and an ion-exchange resin (Dowex Marathon C hydrogel form, 23–27 mesh particle size, Sigma-Aldrich) was used to adjust the pH and conductivity of the ultrapure CNC aqueous suspension to the acidic form (CNC-H^+, pH 2.3) followed by filtration. CNC suspensions were stored at 4 °C until further use. The typical dimensions of CNC spindles were determined by transmission electron microscopy to be 384 ± 89 nm by 14 ± 4 nm (**Figure A.3.1**). Elemental analysis (EA) of 4 wt% CNC-H^+ was performed at the UBC Mass Spectrometry and Microanalytical Laboratory on a Fisons Instruments elemental analyzer EA 1108 using flash combustion. The sulfur, hydrogen, and carbon elemental compositions were found to be 0.77 wt% sulfur, 5.97 wt% hydrogen, and 41.01 wt% carbon.

3.2.2 Preparation of Reversible CNC Hydrogels

An imidazole solution (0.1 M) was added to an aqueous suspension of CNC-H^+ (4 wt%, 4.5 mL) and sparged with CO_2 for 5 min. The amount of imidazole was varied from 0.5 to 2 mL of the 0.1 M imidazole solution (1:9, 1:4.5, 1:3, and 1:2.25 imidazole to CNC-H^+ volume ratio). Samples were stored in sealed glass vials until further characterization was performed. To reverse the gelation, the hydrogels were sparged with N_2 for 45 min and stored in sealed glass vials. No sonication, vortex, magnetic stirring, or filtration was applied to samples during the CO_2 and N_2 sparging processes or prior to any measurements.

3.2.3 Rheology

Rheological measurements were performed by a stress-controlled rotational rheometer (Anton Paar MCR501) in strain-controlled or oscillatory mode using a cone–plate geometry (diameter 25 mm, angle 4°). All measurements were performed at 25 °C, and the sample periphery was covered with a thin film of low-viscosity mineral oil to prevent evaporation of water during the experiments. The viscoelastic moduli (storage modulus G′ and the loss modulus G″) were determined by frequency sweep experiments from 0.1 to 100 rad s^{-1} within the linear viscoelastic region (5% strain amplitude). Continuous shear ramps were performed using shear rates from 0.01 to 100 s^{-1} to measure the viscosity of the sample.

3.2.4 Zeta Potential Measurements

The zeta potential, ζ, of the samples was measured at room temperature on a Malvern NanoZS particle size analyzer (Malvern Instruments Ltd., Malvern). A suspension of imidazole (0.1 M), CNC-H^+ (4 wt%), and water in a 1:3:1600 volume ratio and a suspension

of CNC-H^+ (4 wt%) and water in a 1:400 volume ratio were measured. Each measurement was performed in triplicate.

3.2.5 Conductivity and pH Measurements

Conductivity and pH measurements were performed using an Omega PHH-7200 microprocessor-based waterproof pH/conductivity/temperature tester. We measured three samples: a suspension of imidazole (0.1 M), CNC-H^+ (4 wt%), and water in a 1:3:12 volume ratio; a solution containing imidazole (0.1 M) and water in a 1:15 volume ratio; and a suspension of CNC-H^+ (4 wt%) and water in a 3:13 volume ratio. CO_2 was sparged through the samples for 5 min followed by sparging of N_2 for 45 min, and the conductivity was recorded simultaneously. The sparging was cycled 5 times for each sample.

3.3 Results and Discussion

3.3.1 Ionic Strength Increase

Herein, we report a CO_2-switchable CNC hydrogel. This responsive hydrogel was produced by mixing imidazole in an aqueous suspension of cellulose nanocrystals (CNCs). **Figure 3.1** shows the CO_2-switchable aggregation and redispersion mechanisms of these imidazole-containing CNC suspensions. The CNCs have an overall negative charge due to sulfate half-ester groups on their surface, which causes electrostatic repulsion and renders them dispersible in water. Sparging the suspension with CO_2 leads to a reaction between water and CO_2 to form carbonic acid (**Scheme 3.1**), resulting in a decrease of the pH of the solution. As the pH decreases, the proportion of protonated imidazole (pK_{aH} 6.95) increases, and charged hydrogen carbonate and imidazolium salts are formed (**Scheme 3.2**). The formation of these charged species causes an increase in the ionic strength, screens the negative surface charge on CNCs, and reduces the electrostatic repulsion between CNCs. The increase in ionic strength causes a decrease in the Debye length, which is a measure of the electrostatic repulsion distance between two particles. CNCs with a shorter Debye length can come closer together whereby hydrogen bonding and van der Waals interactions might dominate, causing aggregation and ultimately gelation. The protonation of the imidazole was investigated by ^{1}H NMR spectroscopy (**Figure A.3.2**). A downfield shift of the peaks assigned to the hydrogen atoms of imidazole occurs when CO_2 is sparged through a diluted imidazole solution (H_a, 7.11–7.35 ppm; H_b, 7.75–8.40 ppm) because the protonation of imidazole leads to a deshielding of the hydrogen nucleus.

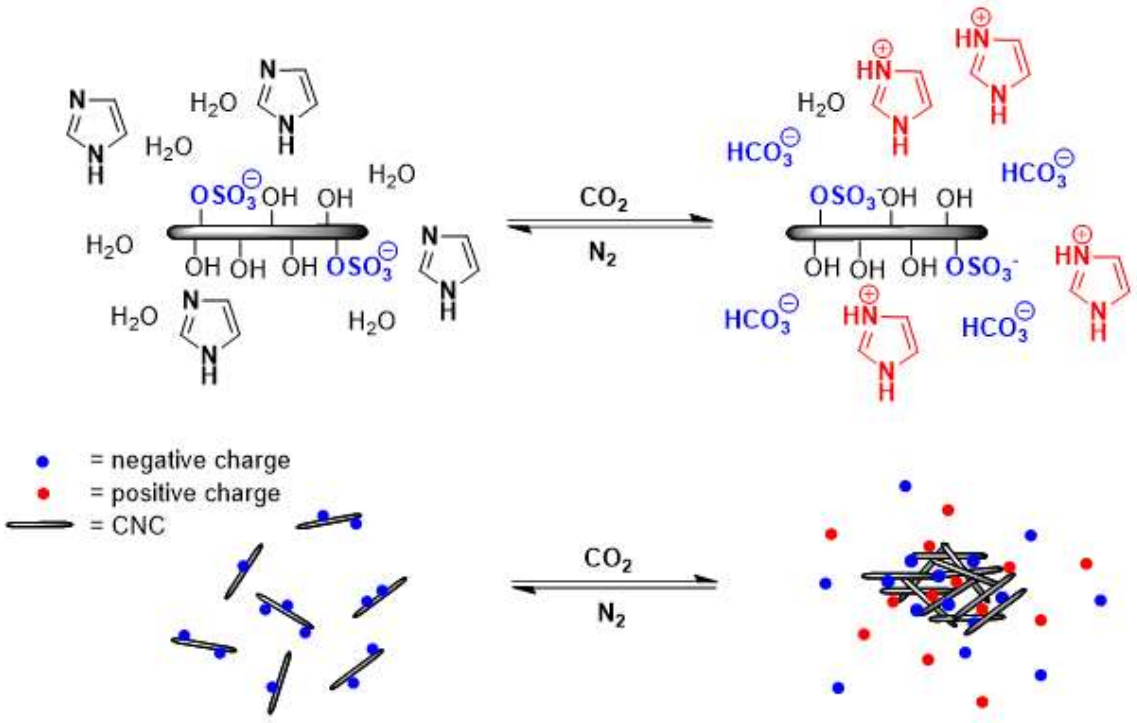

Figure 3.1. Reversible aggregation and redispersion of the CO_2-switchable CNC suspensions containing imidazole in the presence and absence of CO_2.

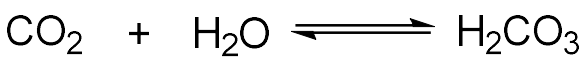

Scheme 3.1. Reaction of CO_2 with water to give carbonic acid.

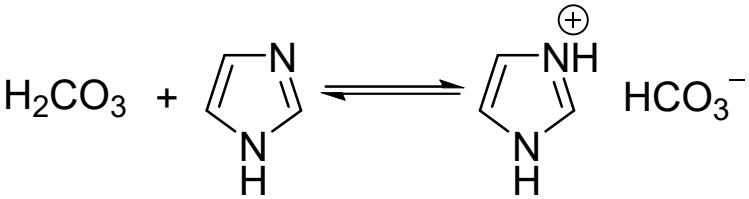

Scheme 3.2. Reaction of imidazole with carbonic acid to give imidazolium hydrogen carbonate.

Both reactions in **Scheme 3.1** and **Scheme 3.2** are reversible. Thus, sparging the hydrogel with N_2 reverses the carbonic acid reaction, expelling CO_2 and increasing the pH of the solution. As the pH increases, a proportion of the imidazolium ion is deprotonated, and the ionic strength decreases, causing CNCs to redisperse and form a stable colloidal suspension. Again, a shift of the hydrogen peaks can be observed in the ^{1}H NMR spectrum (**Figure A.3.2**) when imidazolium is sparged with N_2. Sparging the solution with N_2 results in an upfield shift of the peaks (H_a, 7.35–7.19 ppm; H_b, 8.40–7.96 ppm), due to the deprotonation of the imidazolium and therefore an increase in the shielding of the hydrogen nucleus.

Figure 3.2 shows the CO_2-switchable behavior of our CNC hydrogels. A suspension containing imidazole and CNCs was sparged with CO_2 for 5 min and allowed to stand for 1 h, forming a hydrogel. The gelation could be reversed by sparging with N_2 for 45 min, forming a fluid suspension. The gelation and redispersion of imidazole-containing CNC suspensions using CO_2 and N_2 was repeated five times. Although the focus of this work is on imidazole-containing CNC-H^+ suspensions, we observed similar gelation behavior for imidazole-containing CNC-Na^+ suspensions (**Figure A.3.3**).

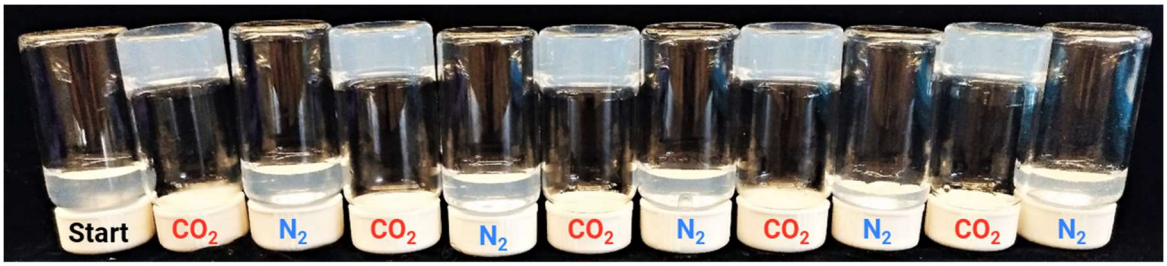

Figure 3.2. Photograph showing the CO_2-switchability of the CNC hydrogel [4.5 mL of CNC-H^+ (4 wt%) and 1.5 mL of 0.1 M imidazole] after alternate CO_2 and N_2 sparging for 5 and 45 min, respectively. Samples were prepared in parallel and cycled individually, with slight volume differences due to solvent loss during cycling.

3.3.2 pH of CNC Hydrogels

To better understand the mechanism of the hydrogel formation, we measured the change in pH and conductivity of the CNC hydrogels while sparging with CO_2 and N_2. **Figure 3.3A** shows a plot of pH as a function of time while sparging CO_2 (5 min), N_2 (45 min), and again with CO_2 (5 min) through suspensions containing CNC-H^+, water, and imidazole at different concentrations. **Figure 3.3B** shows the change in conductivity over five cycles of alternating sparging of the suspension with CO_2 and N_2. As a control experiment, we examined the effect of CO_2 on dilute CNC-H^+ suspensions in the absence of imidazole. The diluted CNC-H^+ suspension has a pH of ~3, which is considerably lower than the pH of pure distilled water (pH ~7), because of the proton counterions of the sulfate half-ester groups on the CNC surface.

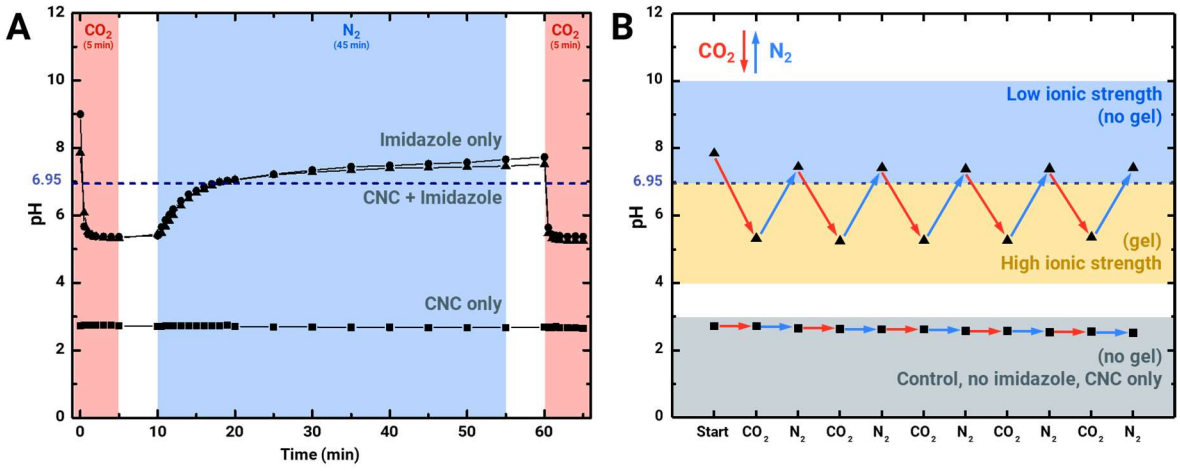

Figure 3.3. pH measurements of switchable CNC hydrogel (▲ 0.1 M imidazole + 4 wt% CNC-H^+ + water, 1:3:12 v/v/v), diluted CNC-H^+ (■ 4 wt% CNC-H^+ + water, 3:13 v/v), and diluted imidazole (● 0.1 M imidazole + water, 1:15 v/v). (A) The pH is plotted as a function of time while alternate CO_2 (red) and N_2 (blue) sparging for 5 or 45 min, respectively. (B) The pH is plotted as a function of alternating CO_2 (red) and N_2 (blue) sparging cycles.

As shown in **Figure 3.3A**, sparging a suspension of imidazole (0.1 M), CNC-H^+ (4 wt%), and water in a 1:3:12 volume ratio with CO_2 for 5 min results in a pH decrease from 7.86 down to 5.3, and therefore below the pK_{aH} of imidazole (pK_{aH} = 6.95). Subsequent sparging of the gel with N_2 for 45 min increases the pH up to 7.46 (above 6.95), consistent with the removal of CO_2. **Figure 3.3B** shows that the pH of this imidazole-containing CNC suspension changes repeatedly between ~5.3 (below pK_{aH} of imidazole) and ~7.4 (above pK_{aH} of imidazole), over five cycles of sparging the suspension with CO_2 and N_2, demonstrating that the reaction to form carbonic acid in the aqueous CNC/imidazole mixture is reversible. The imidazole to CNC volume ratios were determined empirically after testing various volume ratios for CO_2/N_2 switchability (see Experimental 3.2.2). We found that a 1:3 imidazole (0.1 M) to CNC (4 wt%) volume ratio gave consistent CO_2/N_2 switchable mixtures.

In contrast, sparging a suspension of CNC-H^+ (4 wt%) and water (3:13 v/v) with CO_2 or N_2 does not show any change in pH, as shown in **Figure 3.3A**. Furthermore, over the course of five cycles of sparging the imidazole-free CNC suspension with CO_2 (5 min) and N_2 (45 min), the pH does not change significantly, as seen in **Figure 3.3B**. The pH only shows a slight decrease, which we attribute mostly to water evaporation that leads to a slight increase in the concentration of the acidic CNCs.

Figure 3.3A shows that sparging a solution of imidazole (0.1 M) and water in a volume ratio of 1:15 v/v with CO_2 for 5 min decreases the pH from 9 down to 5.36. Sparging the solution with N_2 for 45 min subsequently raises the pH up to 7.66, which is slightly lower than the starting value. This difference in pH after CO_2/N_2 cycling could be due to water evaporation that results in a slight increase in the imidazole concentration, as well as to the presence of unconverted imidazolium species in solution even after N_2 sparging. Imidazole-containing

CNC suspensions show a change in pH whilst sparging with CO_2 and N_2, while CNC suspensions without imidazole do not show a change in pH. Therefore, the protonation of imidazole during sparging of the suspension with CO_2 is implicated in the observed gelation of imidazole-containing CNC suspensions.

3.3.3 Conductivity of CNC Hydrogels

The conductivity of a solution is dependent on ionic strength.[178] We carried out conductivity studies of the imidazole/CNC mixtures to examine the change in ionic strength during cycling between N_2 and CO_2. Although the ionic strength of a solution can be determined from the specific conductance of the solution, we did not quantify this, as the surface charges on the CNCs are difficult to account for.

Figure 3.4A shows the change of conductivity as a function of time while sparging different suspensions containing CNC-H^+, water, and imidazole with CO_2 (5 min), N_2 (45 min), and again with CO_2 (5 min). **Figure 3.4B** shows the change in conductivity over the course of sparging these same suspensions with alternating CO_2 and N_2.

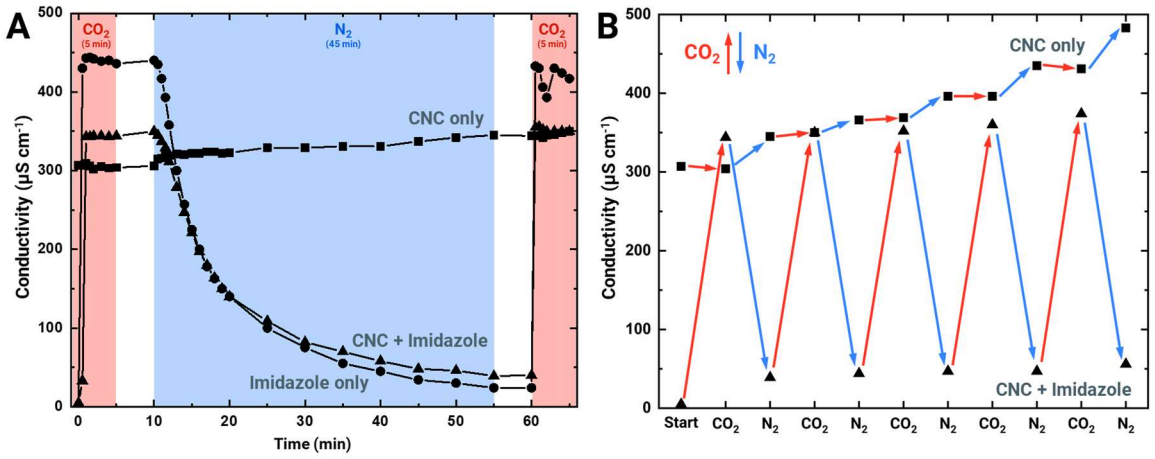

Figure 3.4. Conductivity measurements of switchable CNC hydrogel (▲ 0.1 M imidazole + 4 wt% CNC-H^+ + water, 1:3:12 v/v/v), diluted CNC-H^+ (■ 4 wt% CNC-H^+ + water, 3:13 v/v), and diluted imidazole (● 0.1 M imidazole + water, 1:15 v/v). (A) The conductivity is plotted as a function of time while alternate CO_2 (red) and N_2 (blue) sparging for 5 or 45 min, respectively. (B) The conductivity is plotted as a function of alternate CO_2 (red) and N_2 (blue) sparging cycles.

As shown in **Figure 3.4A**, a suspension of imidazole (0.1 M), CNC-H^+ (4 wt%), and water in a volume ratio of 1:3:12 v/v/v shows an increase in the conductivity from 5 up to 340 μS cm^{-1} upon sparging the suspension with CO_2 for 5 min. Subsequent sparging of the suspension with N_2 for 45 min resulted in a decrease in conductivity to 40 μS cm^{-1}. **Figure 3.4B** shows the changes in conductivity of this imidazole-containing CNC suspension as it is repeatedly sparged, alternating between CO_2 and N_2. The conductivity typically alternates between 340–380 μS cm^{-1} (high ionic strength) and 5–56 μS cm^{-1} (low ionic strength) during the sparging cycles, whereby the conductivity is slightly increasing possibly due to water evaporation and the presence of unconverted imidazolium species remaining in solution even after N_2 sparging.

In contrast, sparging a suspension of CNC-H^+ (4 wt%) and water (3:13 v/v) with CO_2 or N_2 shows almost no change in conductivity, as seen in **Figure 3.4A**,**B**. The dilute CNC-H^+ suspension has a conductivity of 310 μS cm^{-1}, which is considerably higher than the conductivity of pure distilled water (about 5 μS cm^{-1}) because of the charged sulfate groups on CNC particles and their counterions. However, over the course of five sparging cycles with CO_2 (5 min) and N_2 (45 min), the conductivity increases, possibly due to water evaporation, the solubility of CO_2, and the increase in CNC concentration.

Figure 3.4A shows that sparging a suspension of imidazole (0.1 M) and water in a volume ratio of 1:15 v/v with CO_2 for 5 min increases the conductivity from 0 up to 440 μS cm^{-1}. Sparging with N_2 for 45 min drops the conductivity down to 24 μS cm^{-1}, which is slightly higher than the starting value, possibly due to water evaporation, and the presence of unconverted imidazolium species remaining in solution even after N_2 sparging.

The conductivity measurements indicate that the reaction of imidazole, not CNCs, generates ions when the suspension is sparged with CO_2. The formation of these ions, consistent with **Scheme 3.2**, increases the ionic strength of the suspension and, consequently, the conductance of the suspension.

3.3.4 Zeta Potential Measurements of CNC Hydrogels

The zeta potential, ζ, of CNCs after alternating CO_2 and N_2 sparging cycles were investigated and are shown in **Figure 3.5**.

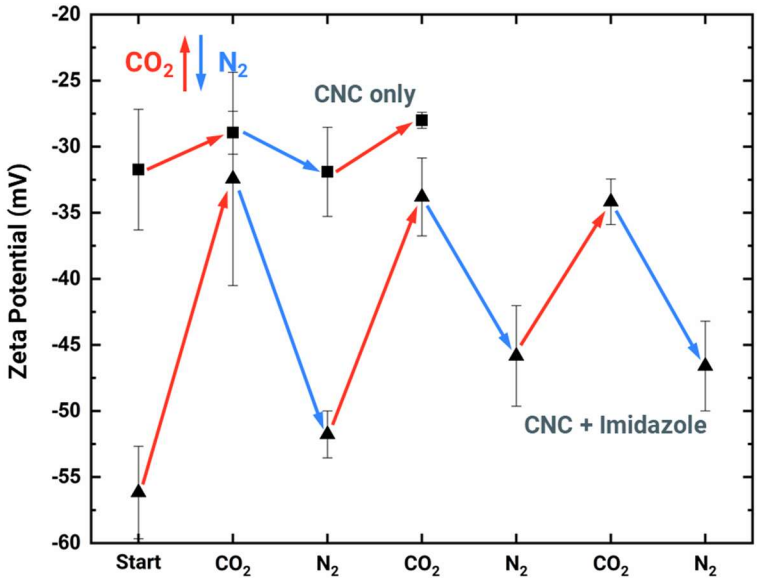

Figure 3.5. Zeta potential of switchable CNC hydrogel (▲ 0.1 M imidazole + 4 wt% CNC-H^+ + water, 1:3:1600 v/v/v) and diluted CNC-H^+ (■ 4 wt% CNC-H^+ + water, 1:400 v/v). The ζ potential is plotted as a function of alternate CO_2 (red) and N_2 (blue) sparging cycles. Error bars correspond to average standard deviation, $n = 3$.

Figure 3.5 shows that the ζ potential of an imidazole-containing CNC suspension (0.1 M imidazole with 4 wt% CNC-H^+ diluted 400 times) shows reversible CO_2-switchable behavior. Sparging the suspension with CO_2 for 5 min increases the ζ potential from −56 to −32 mV because of the formation of imidazolium bicarbonate salts, in agreement with the conductometric measurements. Subsequent sparging of the suspension with N_2 for 45 min decreases the ζ potential back to −52 mV. **Figure 3.5** demonstrates the oscillation of the ζ

potential over three cycles. The ζ potential increases with each N_2 sparging possibly due to water evaporation and the increase in the CNC concentration.

In comparison, a CNC-H^+ (4 wt%) suspension diluted 400 times with water shows only a small ζ potential change between −28 and −32 mV, as seen in **Figure 3.5**. This may be caused by the dissolution of CO_2 in water to form carbonic acid, which slightly impacts the CNC surface charge.

The ζ potential, conductivity, and pH measurements all support the reaction mechanism shown in **Figure 3.1**. Sparging the suspension with CO_2 leads to the formation of carbonic acid which can be seen in **Figure 3.3A** as the pH of the suspension increases. When the pH drops below the pK_{aH} of imidazole (pK_{aH} = 6.95), a larger proportion of the imidazole is protonated. Because of the formation of these charged hydrogen carbonate and imidazolium salts, the conductivity (**Figure 3.4A**) and ζ potential (**Figure 3.5**) increase. The higher ionic strength screens the negative surface charge on CNCs, reduces their electrostatic repulsion, and causes aggregation and ultimately gelation. Sparging the hydrogel with N_2 reverses the carbonic acid reaction, expelling CO_2 whereby the pH of the suspension increases as seen in **Figure 3.3A**. A greater proportion of the imidazolium ion is deprotonated when the pH is higher than the pK_{aH} of imidazole and can be seen in the decreasing conductivity and decreasing ζ potential (**Figure 3.4A** and **Figure 3.5**). Decreasing ionic strength allows the CNCs to redisperse and form a stable colloidal suspension.

3.3.5 Rheological Properties of CNC Hydrogels

We investigated the mechanical properties of the CNC/imidazole hydrogels using rheology. Dynamic frequency sweeps were performed to examine the viscoelastic moduli, storage modulus (G′), loss modulus (G″), and complex modulus (|G*|). In addition, continuous shear ramps were performed to examine the viscosity of the CNC hydrogels.

Figure 3.6 shows that, prior to sparging with CO_2, imidazole-containing CNC suspensions (0.1 M imidazole + 4 wt% CNC-H^+, 1:3 v/v) show liquid-like behavior (G″ > G′ at low frequencies). However, after sparging imidazole-containing CNC suspensions with CO_2 for 5 min, the storage modulus (G′) is greater than the loss modulus (G″), and both properties (G′ and G″) are independent of frequency, which is characteristic of a gel-like (soft solid) material.

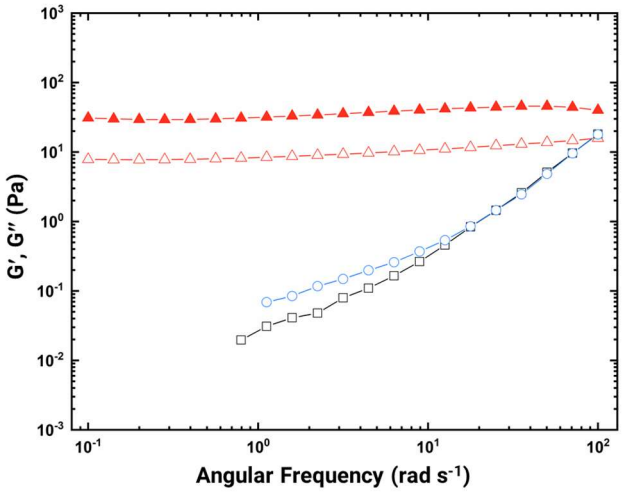

Figure 3.6. Frequency sweep of CO_2-switchable CNC hydrogels (0.1 M imidazole + 4 wt% CNC-H^+, 1:3 v/v) before sparging with CO_2 (black ■), after sparging with CO_2 for 5 min (red ▲), and after sparging with N_2 for 45 min (blue ●). Storage modulus (G′, closed symbol) and loss modulus (G″, open symbol). As the storage modulus (closed symbols) could only be measured for the gel (red), G′ is not shown for the other samples.

In addition, after sparging the treated hydrogel with N_2 for 45 min, we were able to recover the liquid-like properties of the mixture. For these liquid-like samples, the storage modulus (G′) was below the detection limit, and significant instrument noise was observed for the loss modulus (G″) when the angular frequency was less than 1 rad s^{-1} (data not shown in **Figure 3.6**).

Figure 3.7 shows the change in the complex modulus (|G*|) at an angular frequency (ω) of 25.12 rad s^{-1}, for imidazole-containing CNC suspensions (0.1 M imidazole + 4 wt% CNC-H^+, 1:3 v/v) following 5 min of CO_2 and 45 min of N_2 sparging, cycled five times. Sparging the imidazole-containing CNC suspension for 5 min with CO_2 raises the complex modulus from 1.2 to 34.1 Pa while subsequent N_2 sparging drops the complex modulus back down to 1.3 Pa. This change in modulus represents the reversible gelation process and the increasing stiffness of the hydrogel upon the addition of CO_2. However, the complex modulus tends to increase after multiple cycles, likely because of the evaporation of the water concentrating the hydrogel network, as seen in **Figure 3.7**. There may be other phenomena responsible for this trend, such as incomplete redispersion of the CNCs, and the presence of unconverted imidazolium species remaining in solution even after N_2 sparging cycles.

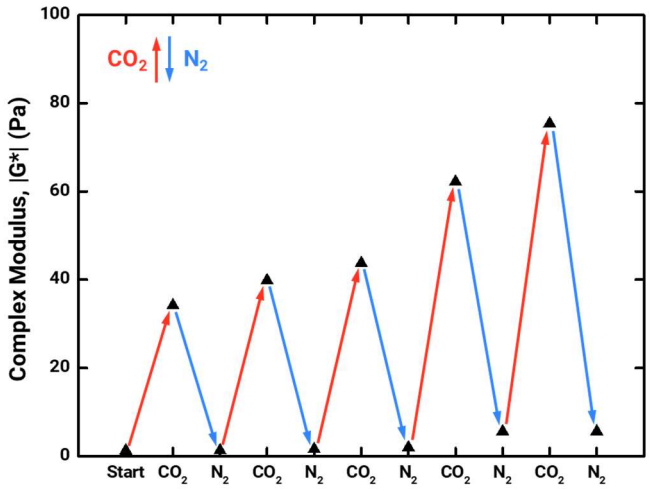

Figure 3.7. Frequency sweep cycling of CO_2-switchable CNC hydrogels (0.1 M imidazole + 4 wt% CNC-H^+, 1:3 v/v) after alternate CO_2 (red) and N_2 (blue) sparging. The change in complex modulus, |G*| (black ▲), is shown over several CO_2 and N_2 sparging cycles. Angular frequency, $\omega = 25.12$ rad s^{-1}.

Figure 3.8 shows the viscosity of CNC hydrogels (0.1 M imidazole + 4 wt% CNC-H^+, 1:3 v/v) as a function of shear rate, before CO_2 treatment, after 5 min of CO_2 sparging, and after 5 min of CO_2 followed by 45 min of N_2 sparging. As the shear rate increases, the viscosity decreases for all samples, demonstrating the hydrogels are shear thinning. **Figure 3.8** depicts the CO_2-switchable behavior of our CNC hydrogels, since the viscosity for the CO_2 treated hydrogel is higher than the untreated imidazole-containing CNC suspension. Sparging the gel with N_2 causes the viscosity to decrease, but it remains slightly higher than before treatment.

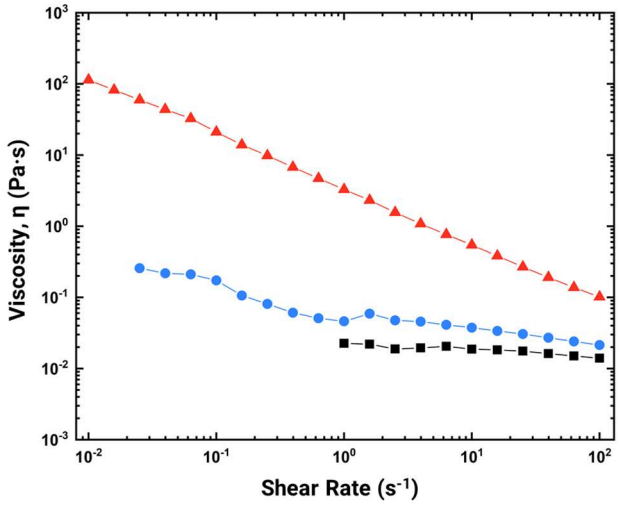

Figure 3.8. Continuous shear ramp of CO_2-switchable CNC hydrogels (0.1 M imidazole + 4 wt% CNC-H^+, 1:3 v/v) showing the viscosity (η) for imidazole-containing CNC suspensions before CO_2 treatment (black ■), after 5 min of CO_2 sparging (red ▲), and after 5 min of CO_2 followed by 45 min of N_2 sparging (blue ●).

Figure 3.9 shows the cycled switching in the viscosity of the imidazole-containing CNC hydrogel (0.1 M imidazole + 4 wt% CNC-H^+, 1:3 v/v) by sparging with CO_2 and N_2 over five cycles at a shear rate of 10 s^{-1}. CO_2 treatment increases the viscosity of the imidazole-containing CNC suspensions by ~0.5 Pa s each cycle, while N_2 sparging significantly reduces the viscosity by at least 0.4 Pa s. **Figure 3.9** shows that the viscosity of the hydrogel increases over time after repeated CO_2 and N_2 sparging cycles, likely due to evaporation of water, a change in the aggregation state of CNCs, and the presence of unconverted imidazolium species remaining in solution even after N_2 sparging cycles.

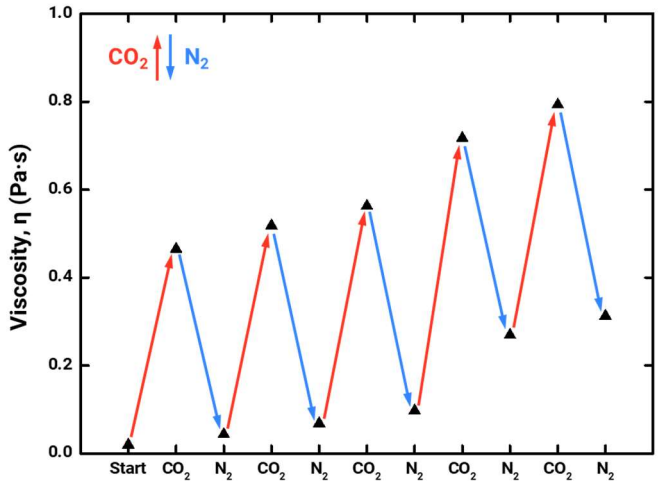

Figure 3.9. Continuous shear ramp cycling of CO_2-switchable CNC hydrogels (0.1 M imidazole + 4 wt% CNC-H^+, 1:3 v/v) after alternate CO_2 (red) and N_2 (blue) sparging. The change in viscosity, η (black ■), is shown over several CO_2 and N_2 sparging cycles. Shear rate = 10 s^{-1}.

3.3.6 Imidazole Concentration

The influence of the imidazole concentration was investigated by preparing four hydrogels with varying volumes of 0.1 M imidazole solution, varying from 0.5 to 2 mL (**Table 3.1**). The time needed for gelation and the rheological properties of the hydrogels were investigated.

Table 3.1. Hydrogels with different imidazole concentration, the imidazole to CNC-H^+ volume ratio, and the corresponding gelation times

	4 wt% CNC-H^+	**0.1 M imidazole**	**Imidazole to CNC-H^+ volume ratio**	**Gelation time after sparging for 5 min with CO_2**
a	4.5 mL	0.5 mL	1:9	no gel observed
b	4.5 mL	1.0 mL	1:4.5	no gel observed
c	4.5 mL	1.5 mL	1:3	gel after 1 h
d	4.5 mL	2.0 mL	1:2.25	gel after 30 min

Table 3.1 shows the different gelation times observed as the imidazole concentration in the CNC suspensions was varied. Faster gelation times were observed for higher imidazole concentrations. The mixtures with 1:9 and 1:4.5 imidazole (0.1 M) to CNC-H^+ (4 wt%) volume ratios do not form gels. The sample with a 1:3 imidazole to CNC-H^+ volume ratio forms a gel after 1 h, while the sample with 1:2.25 imidazole to CNC-H^+ volume ratio forms a hydrogel after 30 min. This gelation behavior can be explained by the higher ionic strength produced

after sparging concentrated imidazole suspensions with CO_2. A higher ionic strength leads to a higher shielding of the surface charge and therefore enables faster aggregation of CNCs.

Figure 3.10 shows photographs of imidazole-containing CNC suspensions that were sparged with CO_2 for 5 min and aged for 24 h. As shown, the two suspensions with a low imidazole concentration (1:9 and 1:4.5, 0.1 M imidazole to 4 wt% CNC-H^+ volume ratio) do not form a gel even after 24 h.

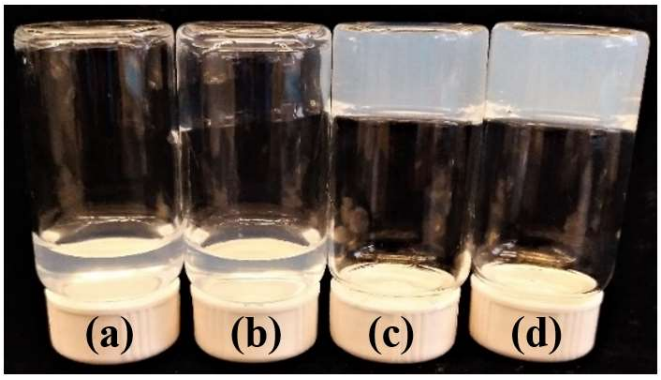

Figure 3.10. Photograph showing the CO_2-switchable CNC hydrogels with different imidazole to CNC-H^+ volume ratios after 5 min of CO_2 sparging followed by aging for 24 h: (a) 1:9, (b) 1:4.5, (c) 1:3, and (d) 1:2.25 imidazole (0.1 M) to CNC-H^+ (4 wt%) volume ratios.

Figure 3.11 shows the viscoelastic moduli, storage modulus G′ and loss modulus G″, of the hydrogels with varying imidazole concentrations. **Figure 3.11** clearly shows that the hydrogels with a higher imidazole concentration (1:2.25 and 1:3, 0.1 M imidazole to 4 wt% CNC-H^+ volume ratio) have gel-like characteristics, since the storage modulus is greater than the loss modulus (G′ > G″), and both are independent of the angular frequency. Furthermore, the larger storage modulus of the hydrogel with 1:2.25 imidazole to CNC-H^+ volume ratio implies that this hydrogel is stronger compared to the hydrogel with 1:3 imidazole to CNC-H^+

volume ratio. The sample with 1:4.5 imidazole to CNC-H^+ volume ratio does not show gel-like behavior. The loss modulus (G″) and the storage modulus (G′) overlap over an extended range of angular frequency, and the slope of both (G′ and G″) is 0.5. This behavior is characteristic of the gelation point of a material.[179] The samples with imidazole to CNC-H^+ volume ratios below 1:4.5 show liquid-like behavior, as seen in **Figure 3.11**. For the 1:9 imidazole to CNC-H^+ volume ratio sample, the storage modulus (G′) is below the detection limit for the instrument and is therefore smaller than the loss modulus (G″), which implies liquid-like behavior. Furthermore, no reliable data for G′ and G″ could be measured for liquid-like samples when the angular frequency was below 1 rad s^{-1}.

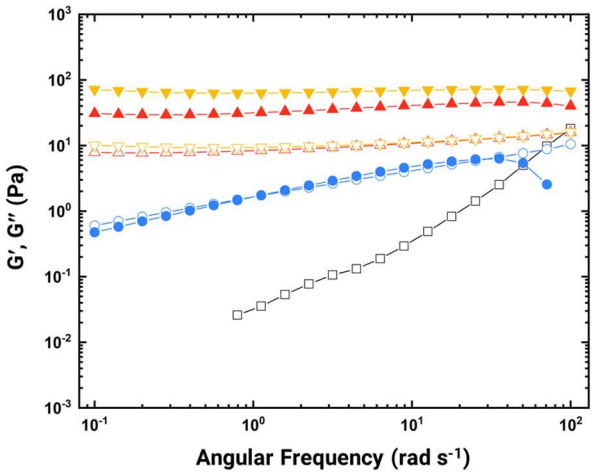

Figure 3.11. Frequency sweep of switchable CNC hydrogels with different imidazole to CNC-H^+ volume ratios after 5 min of CO_2 sparging: 1:9 (black ■), 1:4.5 (blue ●), 1:3 (red ▲), and 1:2.25 (yellow ▼) imidazole (0.1 M) to CNC-H^+ (4 wt%) volume ratios. Storage modulus (G′, closed symbol) and loss modulus (G″, open symbol) as a function of angular frequency measured at a strain of 5%. Some curves are not shown as the data were below the detection limit of the instrument.

Figure 3.12 shows the viscosity of the CNC hydrogels with varying imidazole concentrations as a function of shear rate. With increasing shear rate, the viscosity decreases for all samples, which indicates that the hydrogels are shear thinning. The graph also depicts that when the imidazole concentration is higher, the viscosity of the hydrogel is higher.

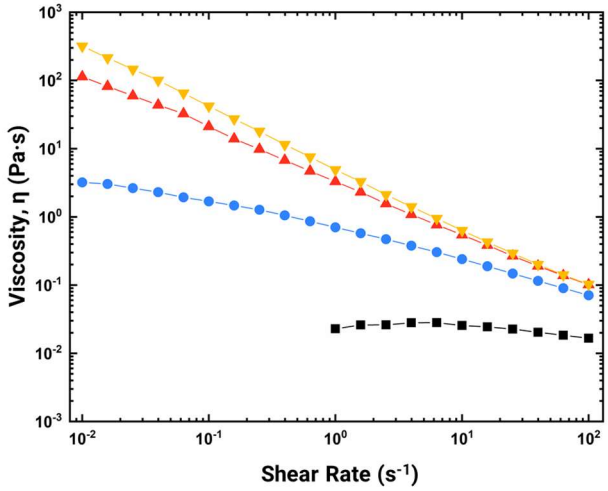

Figure 3.12. Continuous shear ramp of switchable CNC hydrogels after 5 min of CO_2 treatment using rotational rheology. The viscosity η as a function of shear rate is plotted for the different imidazole to CNC-H^+ volume ratios (**Table 3.1**): 1:9 (black ■), 1:4.5 (blue ●), 1:3 (red ▲), and 1:2.25 (yellow ▼) imidazole (0.1 M) to CNC-H^+ (4 wt%) volume ratio.

3.3.7 Other Amines

This chapter has focused on imidazole-containing suspensions. We initially explored a mix of over 30 mono- and poly-amines empirically, with pK_{aH} spanning ~2-11, but found that imidazole was the best candidate we tested for CO_2-switchable CNC hydrogels.

To explore whether other amines would work, we mixed 0.5 mL of different amines dissolved in water (0.1 M) with 4.5 mL of a 4 wt% CNC-H^+ suspension and sparged CO_2 through these suspensions for 5 min. If no gelation was observed after 30 min, additional amine was added (in 0.5 mL aliquots), and the experiment was repeated until a maximum of 2.5 mL of amine solution was added or a gel formed. According to their gelation behavior we categorized the different amines into three groups. All the amines tested, including their amount, pK_{aH}, and gelation behavior, are tabulated in **Table A.3.1**. The amines in group 3 either did not gel or formed very strong gels for which the attractive interactions are too strong to redisperse the CNCs using N_2, making the gelation irreversible. The amines in group 2 formed weak gels, though other factors including foaming, or a color change were observed. Group 1 amines formed weak, colorless gels. These weak gels were sparged with N_2 for 1 h, but only the imidazole CNC-H^+ hydrogel showed a reversible switch between gel and liquid states. pH measurements of diluted group 1 amines during CO_2 and N_2 sparging lead us to conclude that the pK_{aH} of the amine must be carefully chosen to form CO_2-reversible hydrogels. If the pK_{aH} is too low, the proportion of protonated amines is not sufficiently high enough to destabilize the CNCs in suspension when sparged with CO_2, and gelation may not occur. Alternatively, if the pK_{aH} is too high, the proportion of protonated ammonium ions in solution is too high, even after sparging with N_2, limiting the reversibility of gelation for these CNC suspensions. Future studies considering the influence of the pK_{aH}, the number of amine

groups (e.g. diamines, triamines, polymeric amines), the hydrophobicity, the size of the molecule, and the concentration, could help to impose requirements on the amine to achieve reversible protonation and deprotonation with CO_2 and N_2 sparging.

3.4 Conclusion

We have shown that CO_2-switchable CNC hydrogels can be prepared by the addition of imidazole to an aqueous suspension of CNCs. Sparging CO_2 through this suspension forms charged hydrogen carbonate and imidazolium salts, leading to an increase in ionic strength and better screening of the negatively charged CNC particles. Therefore, agglomeration of the CNCs occurs, and a hydrogel is formed. Sparging N_2 through the dispersion reverses the reaction, thereby deprotonating the imidazolium ion, and the ionic strength decrease allows the CNC particles to redisperse and form a stable suspension. Using this approach, we can switch the gelation of CNC hydrogels by simply sparging CO_2 or N_2 gas, without the need for any extensive chemical functionalization, or the addition of acids or bases as a trigger. These reversible CO_2-switchable CNC hydrogels could have potential in various applications, including switchable adsorbents, flocculants, and tissue engineering.

Chapter 4: Freeze-Thaw Gelation of Cellulose Nanocrystals

4.1 Introduction

Gels are three-dimensional (3D) networks that typically consist of more than 90 vol% solvent. Gels can be formed through covalent crosslinking of networked components (chemical gels) or through non-covalent interactions, including hydrogen bonding, ionic interactions, and hydrophobic interactions, of network components (physical gels).[11] Physical gels are of interest owing to their reversible aggregation mechanisms, which can allow tuning of the network structure in response to various stimuli including temperature, light, CO_2, and pH.[180–182] The dynamic nature of physical gels makes them attractive for applications in 3D printing, tissue engineering, and controlled drug release.[90,105,183–187]

There has been extensive research into gels formed from molecules and polymers,[22,128,188,189] but gels formed from colloids are equally interesting.[28,190] Colloidal gels are a self-supporting physically percolated network of nanoparticles. They have been prepared using various materials, including metal and metal oxide nanowires, carbon nanotubes, and graphene oxide.[18,31,35] Doi and Edwards developed a theory for the phase behavior of rod-like particles transitioning between dilute, semi-dilute, and concentrated regimes, which can be used to predict the concentration for gel formation depending on the length and aspect ratio of the components.[18] However, these colloidal systems tend to rely on entanglement rather than a percolation mechanism, where the particles bend and wrap around each other to form an entangled mesh network.

The Derjaguin and Landau, Verwey and Overbeek (DLVO) theory is used as a foundation for our current understanding of colloidal stability. The DLVO theory takes into account attractive van der Waals forces and repulsive electrostatic double layer forces that act

between charged particles in suspension. Thermodynamically, colloidal suspensions are unstable, but exist due to the kinetic stability provided by the electrostatic repulsion between charged particles.[191]

Cellulose nanocrystals (CNCs) are biocompatible materials made from the most abundant biopolymer on earth, cellulose. CNCs are rod-shaped particles with dimensions of ~100-500 nm by ~5-20 nm, and are produced by treating wood pulp, or other biomass, in sulfuric acid.[50,94,157] The sulfuric acid treatment introduces negatively charged sulfate half-ester groups onto the surface of CNCs, and electrostatic repulsion between particles stabilizes CNCs in suspension. CNCs have attracted interest due to a number of their physicochemical properties including high degree of crystallinity, low density, high specific surface area, liquid crystallinity, and robust mechanical properties.[43,50,73,177] As well, the photonic properties of CNCs that arise from their organization into a cholesteric liquid crystal have been widely explored.[98,100,101,192]

Previous work on colloidal gels used particles that are typically less than 100 nm in width and greater than 1 μm in length and are relatively flexible. CNCs, on the other hand, are rigid rod-shaped particles that are not susceptible to bending or entanglement but are able to form self-supporting percolated networks due to hydrogen bonding interactions between individual particles. The differences in network formation between entanglement and rigid percolation is not well understood for colloidal systems.

CNC can aggregate to form colloidal gels by disrupting the subtle balance of forces between the CNCs through increased concentration, chemical modification, covalent crosslinking, changing ionic strength, or heating.[64,71,194,76,79,81,82,112,114,170,193] Previous reports have also demonstrated the production of cellulose-based aerogel materials by freeze-drying

suspensions of cellulose nanofibrils (CNFs)[195] and cellulose nanocrystals (CNCs).[193,196,197] Freezing of various colloidal systems has been explored,[198,199] however, the structural or rheological properties of freeze-thaw (FT) casted CNC gels have not been investigated. Typically, anisotropic freezing, covalent crosslinking, or high concentrations are required for FT gelation of CNC suspensions.

Here, we show the versatile preparation of physical colloidal gels from CNCs by a simple freeze-thaw cycling procedure. In this process, the CNC colloids are destabilized in suspension and undergo aggregation and network formation to give gels. We show that this simple freeze-thaw procedure can be used to gel CNCs in water and polar organic solvents, giving hydrogels and organogels, respectively.

4.2 Experimental

4.2.1 Materials and Instrumentation

All chemicals were used as received without any further purification. Cellulose nanocrystals (CNCs) were provided by FPInnovations as either a powder, or an aqueous suspension with a sodium counterion (CNC-Na^+, 4 wt%, pH 6.5, conductivity 400 μS cm^{-1}). CNC powders and suspensions were obtained using previously described procedures.[81,177] Elemental analysis (EA) was performed at the UBC Mass Spectrometry and Microanalytical Laboratory on a Fisons Instruments Elemental Analyzer EA 1108 using flash combustion. Samples were freeze-dried and rinsed with double-distilled H_2O to remove any unbound sulfate ions by vacuum filtration and freeze-dried again prior to elemental analysis. Zeta potential and dynamic light scattering experiments were measured at room temperature on a NanoBrook Omni (Brookhaven Instruments). A suspension of CNC-Na^+ (4 wt%) at various freeze-thaw cycling stages was diluted 1:100 with water and each sample was measured in triplicate. Scanning electron microscopy (SEM) was performed at the UBC Bioimaging Facility on a Hitachi S4700 electron microscope with samples sputter-coated with platinum/palladium alloy. Powder X-ray diffraction (PXRD) patterns were recorded on a Bruker D8 Advance diffractometer equipped with a Cu Kα sealed tube X-ray source and a NaI scintillation detector. 2D X-ray diffraction patterns were recorded on a Bruker APEX DUO with an APEX II CCD detector in transmission mode using a Cu Kα sealed tube X-ray source. Samples were placed 40 mm away from the detector in a 0.7 mm glass capillary and measured at room temperature.

4.2.2 Preparation of Freeze-Thaw CNC Hydrogels

An aqueous suspension of CNC-Na^+ (5 mL, 4 wt%) was added to a 20 mL glass scintillation vial (27 mm diameter, 55 mm height) and sealed. The vial was rapidly placed into a dewar containing liquid nitrogen (LN2) for 5 min, such that the meniscus of the CNC suspension was below the LN2 level. The frozen sample was thawed at room temperature for at least 2 h. Successive freeze-thaw (FT) cycling was performed by freezing the sample for 5 min in LN2, followed by 2 h of thawing at room temperature. Unless otherwise noted, the freezing time was 5 min in LN2, and the thaw time was at least 2 h.

4.2.3 Preparation of Freeze-Thaw CNC Organogels

CNC powder (spray-dried CNC-Na^+) was dispersed in 10 mL of solvent, either H_2O, dimethylsulfoxide (DMSO), or dimethylformamide (DMF). The sample was then sonicated using a probe sonicator (QSonica Sonicator Q700) for 10 min at 50% amplitude (~10 kJ). The suspension was submerged in LN2 for 5 min, followed by at least 2 h of thawing at room temperature. Successive freeze-thaw (FT) cycling was performed as described above by freezing for 5 min in LN2 followed by thawing to room temperature for at least 2 h.

4.2.4 Rheology

Rheological properties were characterized using a MCR501 rheometer (Anton Paar) with a cone-plate geometry (diameter 25 mm, angle 4°, gap 0.57 mm) in strain-controlled and oscillatory shear modes. All measurements were conducted at 25 °C. A thin film of polydimethylsiloxane oil was applied to the sample periphery to suppress solvent evaporation during the experiments. Frequency sweeps were performed over the frequency range from 0.01

to 100 rad s^{-1} with a 5% strain amplitude. The complex modulus at the frequency of 8.9 rad s^{-1} was used to compare changes in rheological properties between FT cycles.

4.3 Results and Discussion

The CNCs used in this work were obtained from sulfuric acid treatment of kraft pulp and had dimensions of 384 ± 89 nm by 14 ± 4 nm.[82] We noticed that suspensions of CNCs in water that were frozen formed gels when thawed and the CNCs in the gels were difficult to redisperse. To explore the controlled gelation of CNCs through this approach, we first investigated the freezing of 4 wt% CNC suspensions for variable lengths of time. Samples were immersed in liquid nitrogen (LN2) for times ranging from 30 s to 10 min then subsequently warmed to room temperature over a period of 2 h. When placed upside down (inverted), all of the samples that were frozen for longer than 1 min retained their shape (**Figure 4.1A**), but none were able to pass the inversion test after 5 min, **Figure 4.1B**. Qualitatively, the viscosity of the thawed samples increased the longer they had been submerged in LN2, suggesting the aggregation of CNCs into larger clusters forming interconnected networks. However, the samples did not pass the inversion test after 5 min for all freezing times tested, as the networks formed were relatively weak and could not support their weight after only one FT cycle. After approximately 2 min of LN2 treatment, the sample properties did not change significantly so a freezing time of 5 min in LN2 was used for all subsequent FT cycling experiments.

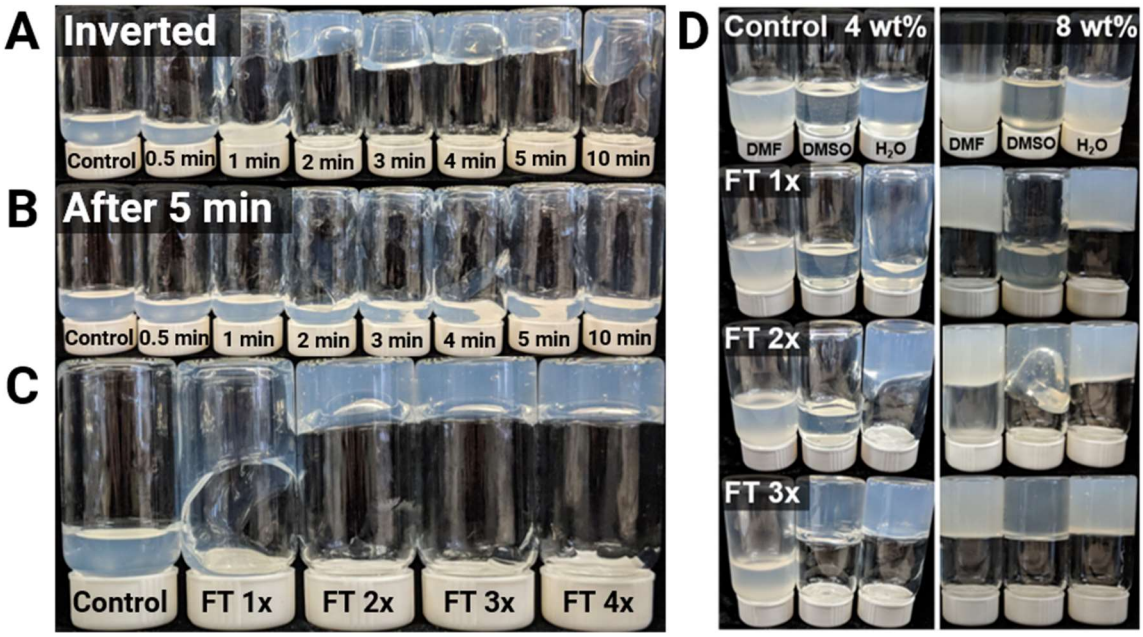

Figure 4.1. Optical photographs of freeze-thawed CNC suspensions. (A) 4 wt% CNC-Na^+ suspensions showing the effect of freezing time in liquid nitrogen (LN2) on the gel properties. Sample vials were immersed in LN2 for the time indicated followed by 2 h of thawing at room temperature. The samples become more viscous as the freezing time in LN2 is extended. (B) The samples are weak gels and cannot support their weight while inverted after 5 min. (C) Freeze-thaw (FT) cycling of 4 wt% CNC-Na^+ suspensions in liquid nitrogen. Sample vials were immersed in liquid nitrogen for 5 min followed by 2 h of thawing at room temperature. Subsequent cycling of the FT process (1, 2, 3, or 4 times) yielded gels with self-supporting structures. (D) FT cycling of 4 wt% and 8 wt% CNC-Na^+ suspensions in DMF, DMSO, and water. The gelation characteristics depend on the chosen solvent and concentration of CNCs. Control sample represents a 4 wt% CNC-Na^+ suspension before FT cycling.

We next investigated the successive FT cycling of 4 wt% CNC suspensions. As shown in **Figure 4.1C**, the samples form self-supporting hydrogels after successive FT cycling. Furthermore, FT cycling can be used to gel CNCs in polar organic solvents, including dimethylformamide (DMF) and dimethylsulfoxide (DMSO), **Figure 4.1D**. Non-polar solvents

did not show this behavior as CNCs have limited dispersibility in non-polar or weakly polar solvents (acetone, ethanol, toluene, hexanes; data not shown).

Elemental analysis of the gels shows that there is no significant change in sulfur content after FT cycling, **Table A.4.1**. A decrease in sulfur content would suggest a loss of negatively charged sulfate groups from the surface of CNCs, which is known to destabilize CNCs in suspension.[81,122] Therefore, we attribute the mechanism of gelation to aggregation, caused by physical confinement of CNCs between growing ice crystals.

To better understand the structural properties of the gels, we prepared a CNC hydrogel by 4x FT cycles in water then freeze-dried it to form an aerogel. The aerogel was analyzed by scanning electron microscopy (SEM) and powder X-ray diffraction (PXRD). SEM of the CNC aerogel shows the formation of an interconnected, porous cellulosic sheet network, **Figure 4.2A-C**. The formation of sheets is consistent with the physical confinement of CNCs between growing ice crystals, paralleling the observed arrest of colloids in confined spaces.[200] CNCs sandwiched between growing ice crystals then aggregate into sheets to form the porous aerogel network.

PXRD was performed on freeze-dried CNC samples (control) and the aerogel, **Figure 4.2D**. There is no significant change in the diffraction patterns between the two samples, which suggests that FT cycling does not disrupt the crystallinity of the CNCs. Therefore, it is not the amorphous cellulose that contributes to the gelation of these systems, rather gelation is largely driven by CNC aggregation due to physical confinement upon freezing. Although there have been reports of directional freezing of CNC suspensions to produce aerogels with ordered networks,[196,197,201] we did not see evidence of ordered CNC alignment after FT cycling from 2D X-ray diffraction, **Figure A.4.1**.

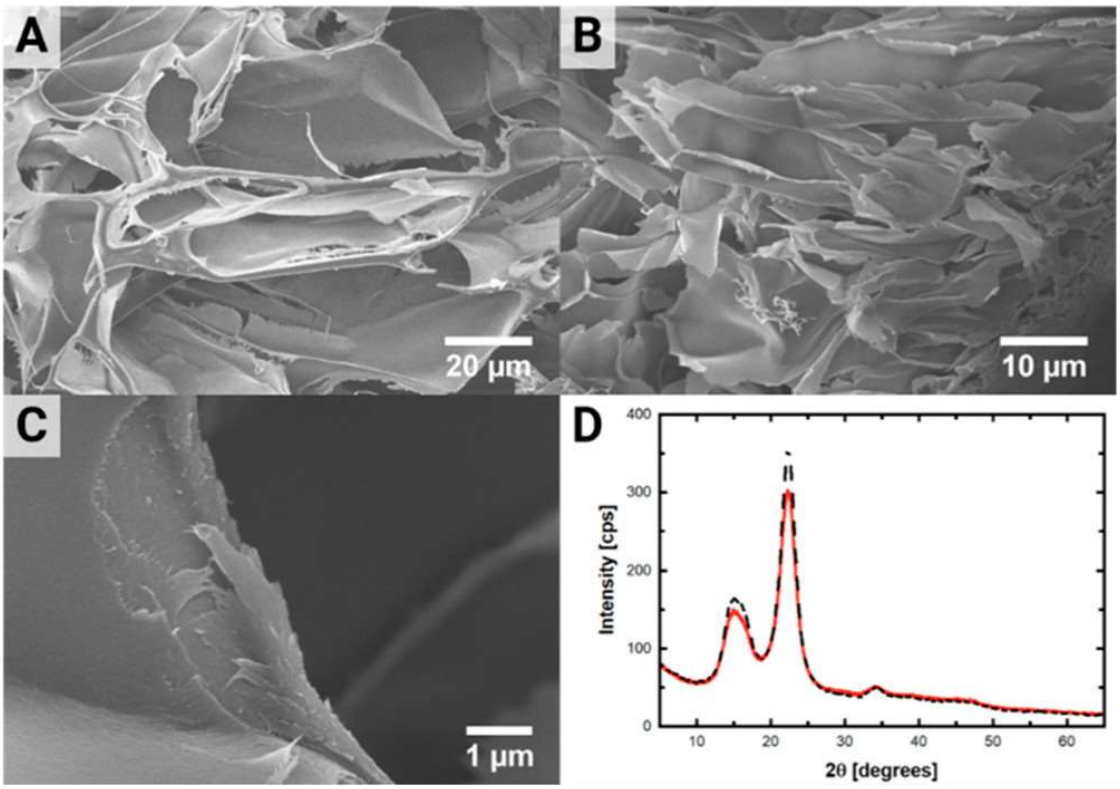

Figure 4.2. Microstructure of freeze-thawed CNC hydrogel. (A-C) Scanning electron micrographs of freeze-dried 4 wt% CNC-Na^+ suspensions after 4x FT cycles. (D) Powder X-ray diffraction pattern for 4 wt% CNC-Na^+ suspension before (black dashed line) and after 4x FT cycles (red solid line).

Zeta potential and dynamic light scattering measurements were performed to investigate changes in the colloidal stability and aggregate size of CNCs in suspension, **Figure 4.3**. The data confirm that FT cycling induces aggregation of CNCs. The zeta potential of CNC aggregates shows a gradual increase in absolute value, suggesting the aggregation of negatively charged CNCs into larger clusters with a more negative zeta potential, **Figure 4.3A**. Similarly, the effective diameter of the colloids in suspension increases from 120 nm to 440 nm after 4x FT cycles, indicating that larger aggregated clusters of CNCs form after each FT

cycle, **Figure 4.3B**. **Figure A.4.2** shows representative lognormal size distributions for each FT cycle. The mode of lognormal distribution was used to compare the change in effective diameter of CNC samples after each FT cycle.

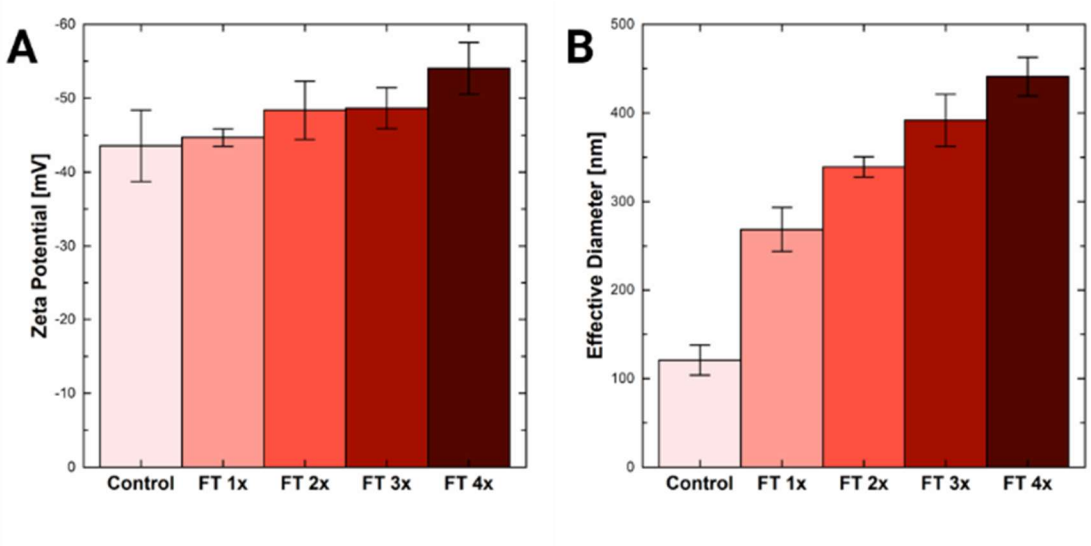

Figure 4.3. Zeta potential (A) and dynamic light scattering effective diameter (B) of 4 wt% CNC-Na^+ suspensions after FT cycling. Error bars represent standard deviation of each sample measured in triplicate. Control sample represents a 4 wt% CNC-Na^+ suspension before FT cycling.

The rheology of the CNC hydrogels was investigated using a rotational rheometer equipped with a cone-and-plate geometry. Dynamic frequency sweeps were performed to compare the rheological properties of CNC hydrogels prepared under various conditions, **Figure A.4.3**. We found that successive FT cycling can increase the complex modulus of CNC suspensions by more than two orders of magnitude, from 0.4 to 150 Pa (at the frequency of 8.9 rad s^{-1}). We found that the complex modulus of CNC samples plateaued or saturated after approximately 2 min of freezing in LN2, **Figure 4.4A**. Suspensions frozen at −12 °C required

significantly longer freezing times (more than 2 weeks) for the complex modulus of the resultant hydrogel to plateau, **Figure A.4.4**.

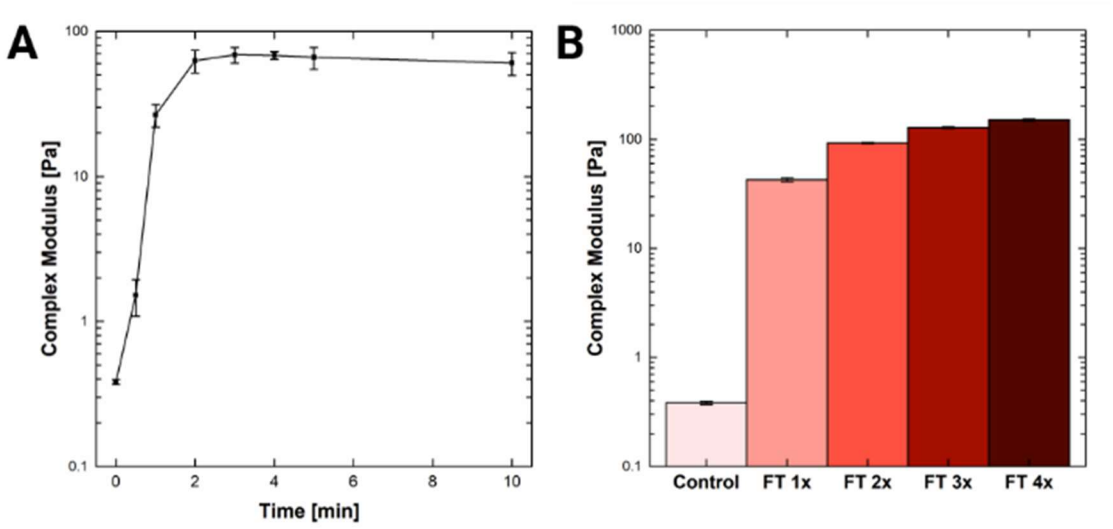

Figure 4.4. Rheological properties of freeze-thawed CNC hydrogels. (A) Complex modulus (at the frequency of 8.9 rad s^{-1}) of 4 wt% CNC-Na^+ suspensions after freezing in liquid nitrogen for various times between 0 and 10 min. Error bars represent standard deviation of three independent samples. (B) Complex modulus (at the frequency of 8.9 rad s^{-1}) of 4 wt% CNC-Na^+ suspensions after FT cycling in liquid nitrogen. Error bars represent standard deviation of three independent samples. Control sample represents a 4 wt% CNC-Na^+ suspension before FT cycling.

The rheology of CNC suspensions can be tuned by FT cycling. The complex modulus of 4 wt% CNC suspensions after each FT cycle shows a significant increase of over two orders of magnitude followed by incremental increases, reaching a plateau at approximately 100 Pa, **Figure 4.4B**. The use of FT cycling demonstrates our ability to control the final rheological properties of the hydrogel by changing the number of FT cycles.

The concentration of the starting suspension is important for the formation of hydrogels by FT cycling. Suspensions of 1 wt%, 2 wt%, and 3 wt% CNCs do not form hydrogels even after 4x FT cycles, **Figure 4.5A**. The complex modulus of all suspensions increases after each FT cycle, but this is not sufficient to form a self-supporting hydrogel for concentrations below 4 wt%, **Figure 4.5B**. The 4 wt% suspensions can form self-supporting hydrogels after just 2x FT cycles, and gelation can be achieved at significantly lower concentrations than those reported previously using 10 wt% CNC suspensions and anisotropic freezing to form hydrogels.[196] FT cycling provides greater control over the stability and rheological properties of the resultant hydrogel at lower concentrations.

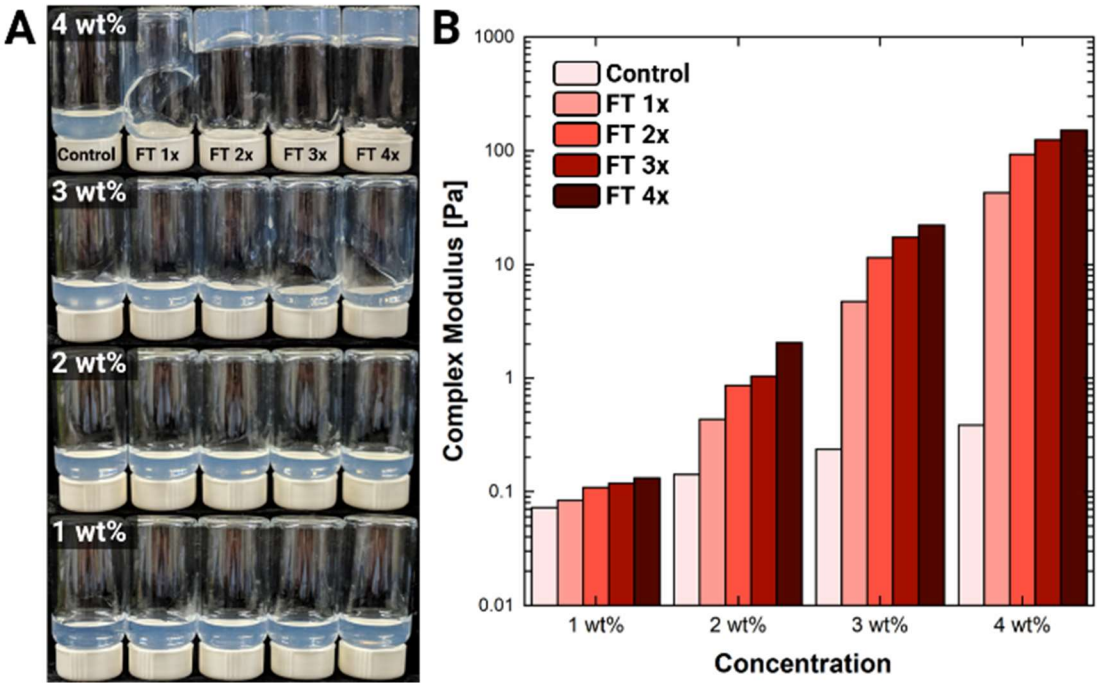

Figure 4.5. Freeze-thaw gelation of CNC suspensions with varying concentration. (A) FT cycling of CNC suspensions with varying concentrations in water. The concentration of CNCs needs to be greater than 3 wt% to produce self-supporting hydrogels after repeated FT cycling. (B) Complex modulus (at the frequency of 8.9 rad

s^{-1}) of CNC suspensions with varying concentrations in water after repeated FT cycling. Control sample represents a 4 wt% CNC-Na^+ suspension before FT cycling.

We believe that gelation of CNC suspensions by FT cycling occurs due to irreversible aggregation of physically confined CNCs upon freezing, **Figure 4.6**. Electrostatic repulsion of negatively charged sulfate half-ester groups on the surface of CNCs stabilize the particles in suspension. However, ice crystals formed during freezing excludes CNCs in suspension and forces the colloids into the inter-crystalline grain boundaries between growing ice crystals. The physical confinement of CNCs during freezing causes attractive van der Waals forces to dominate and results in CNCs aggregating into clusters and lamellar sheets, which inhibits redispersion even after thawing. CNCs aggregate into larger extended clusters after each FT cycle and can form three-dimensional self-supporting hydrogel networks.

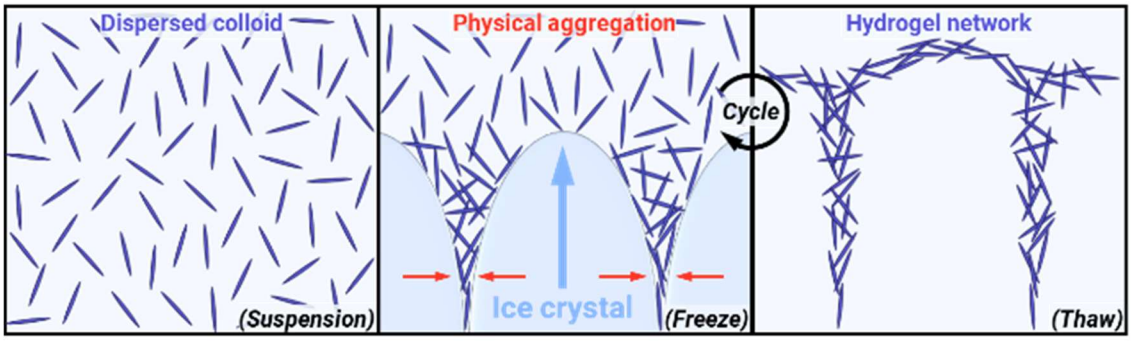

Figure 4.6. Schematic showing freeze-thaw gelation caused by physically confined aggregation of CNCs between growing ice crystals. The CNCs do not fully redisperse when thawed.

4.4 Conclusions

In summary, we have shown that physical colloidal gel networks can be formed by a simple freeze-thaw cycling procedure of CNC suspensions in liquid nitrogen at relatively low concentrations of 4 wt%. Moreover, FT cycling of CNC suspensions in LN2 can produce hydrogels with tunable rheological properties by varying the concentration, freezing time, freezing temperature, and number of FT cycles. The destabilization of CNCs by physical confinement allows for the preparation of hydrogels with tunable properties without the need for chemical modification, addition of salts, or other additives.

Chapter 5: Conclusion and Future Directions

5.1 Conclusions

In 2017, the forest products industry contributed nearly $25 billion (1.6%) to Canada's nominal gross domestic product (GDP).[202] However, the forest products market is undergoing a continued decline due to changes in the world markets towards electronic media and away from paper-based communications.[44,203] Therefore, continued development in nanocellulose-based technologies is needed to boost the growth of the forest products industry in Canada. In 2018, the global market for nanocellulose was estimated at approximately $380 million and projected to grow to nearly $880 million by 2023.[204,205] There remains an interest in developing high value materials using CNCs, so developing transformative platforms to expand their scope is essential.

The goal of this thesis was achieved by demonstrating various ways in which we can gel CNCs. A conceptual foundation was provided to describe the colloidal stability of CNCs highlighting the importance of surface charge, ionic strength, and kinetic stabilization.

In **Chapter 2** we found that hydrothermally treating CNC suspensions causes them to gel at elevated temperatures. Desulfation of the surface of CNCs was found to be the cause of gelation due to a destabilization of their surface charge. The loss of sulfate groups from the surface of CNCs caused a decrease in the magnitude of negative charge on their surface, reducing the electrostatic repulsion between particles, causing them to aggregate. These aggregated CNC networks were able to form robust 3D hydrogels. We found that by varying the preparation conditions we could prepare hydrogels and aerogels with differing properties, including hydrogels that were self-recovering and shear thinning, and aerogels with tunable

porosity and density. This chapter lays the foundation for subsequent work to prepare colloidal gels using CNCs using various stimuli by controllably disrupting their colloidal stability.

In **Chapter 3** we showed that we can reversibly trigger the gelation of imidazole-containing CNC suspensions using CO_2. The ionic strength of the system could be drastically increased by bubbling CO_2 into the system due to the formation of charged imidazolium salts. The increased ionic strength was effective at charge shielding the negatively charged CNCs, resulting in gelation. We found that the gelation can be reversed by bubbling with N_2 to remove CO_2, and revert the system back to a low ionic strength liquid as the imidazolium deprotonated and returned to its neutral form. We showed that this reversible switching between gel and liquid states could be cycled five times without the need for extensive chemical functionalization.

In **Chapter 4** a simple freeze-thaw cycling process was used to gel CNC suspensions using liquid nitrogen at relatively low concentrations of 4 wt%. The rheological properties of the CNC hydrogels could be tuned by varying the concentration, freezing time, and number of cycles. We found that we could destabilize the system by physically confining CNCs between growing ice crystals to form 3D gel networks in several solvents. The ability to gel CNC suspensions without the need for chemical modification, addition of salts, or other additives is attractive as a general strategy to prepare colloidal gels with varying composition.

In summary, each chapter in this thesis explores a mechanistically different way to destabilize colloidal CNC suspension, from a decrease in surface charge due to desulfation, to switching the ionic strength using CO_2/N_2, and irreversible aggregation due to physically confinement. These strategies exploit various properties of colloidal systems to manipulate their stability and form new soft colloidal gel materials.

However, there remain limitations in our understanding of the precise mechanism of aggregation and redispersion that occur in these dynamic colloidal gels. It is unclear why our systems show reversible liquid to gel transitions considering the thermodynamic sink predicted by DLVO theory for particles to aggregate. Thermodynamically, the redispersion of particles once they have aggregated seems counterintuitive. Similarly, the preference for these systems to form 3D gel networks rather than precipitate was surprising. The combination of strong interparticle interactions through hydrogen bonding and the mechanical rigidity of the individual CNC particles may contribute to the formation of percolated colloidal gel networks. Future studies using small-angle X-ray scattering or small-angle neutron scattering may provide further insight into the aggregation dynamics during colloidal gel formation similar to those performed on clay suspensions.[206]

Ultimately, the goal of this thesis was achieved and has highlighted the key conceptual factors in controlling colloidal stability. This work has laid a foundation for preparing colloidal gels using various triggers for applications in catalysis, tissue engineering, environmental remediation, filtration, and 3D printing.[50,64,73,207–209]

5.2 Future Directions

5.2.1 Light-Responsive Gelation of Cellulose Nanocrystals

A long-standing challenge that we hoped to tackle was the light-responsive gelation of CNC suspensions. Our strategy was to use a sulfonated spiropyran, a reversible photochromic molecule that can ring-close upon irradiation and ring-open spontaneously over time in the dark, to destabilize the surface charge of CNCs by triggering a change in pH. Ultimately, we were not able to decrease the pH drastically enough to disrupt the charge of the sulfate half-ester groups on the surface of CNCs to cause gelation, but we did see a change in the rheological properties of the system in response to irradiation, **Figure 5.1**.

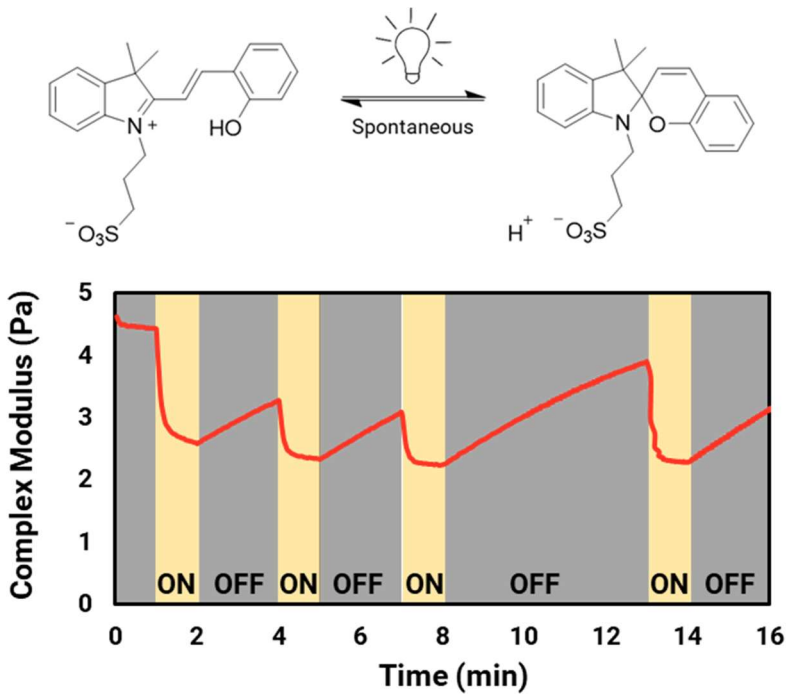

Figure 5.1. The reversible ring-closing and ring-opening of spiropyran in response to light (405 nm). A spiropyran-containing CNC suspension was irradiated during rheological analysis. The complex modulus is plotted as a function of time as the system was irradiated in 1 min intervals, followed by a slow recovery in the dark for 2 or 5 min.

The complex modulus varied in direct response to irradiation and recovered slowly in the absence of light. However, the absolute change in modulus was only 1-2 Pa, which was not a large enough difference to observe gelation macroscopically. We believe the change in complex modulus is due to a change in the effective ionic strength of the system due to the formation of the ring-opened spiropyran zwitterion. The localization of positive charge in the ring-opened form may act to destabilize CNCs in suspension and vary their rheological properties. This system would be of interest for 3D printing applications as it would provide spatial and temporal control over gelation. Further work is required to identify the broader mechanism of destabilization and amplify its effect to achieve reversible light-responsive gelation.

5.2.2 Redox-Switchable Gelation of Cellulose Nanocrystals

Electrochemically triggering the gelation of CNC suspensions using electrodes, or reducing/oxidizing agents, is of interest to prepare gel coatings, electrolytes, and filters. A judicious choice of reducing and oxidizing agents needs to be made to prevent undesirable side-products that may interfere with the colloidal stability of the gel after repeated cycling.

We found that ferrocene-containing CNC suspensions in DMSO can gel upon oxidization with hydrogen peroxide, **Figure 5.2**. Neutral ferrocene can be oxidized, using hydrogen peroxide (H_2O_2), to positively charged ferrocenium, causing a significant increase in the ionic strength of the system. The increase in ionic strength results in gelation of CNCs in suspension. The process may be reversed by reducing the positively charged ferrocenium (high ionic strength system) back to the neutral ferrocene species (low ionic strength system).

Efforts to reduce ferrocenium using hydrazine and return the system back to its liquid state proved unsuccessful so far.

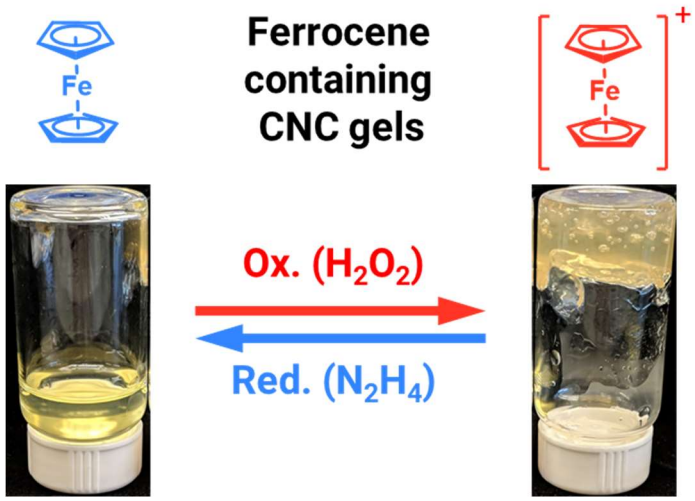

Figure 5.2. Redox-responsive gelation of ferrocene-containing CNC gels.

5.2.3 Anisotropic Cellulose Nanocrystal Gels and Aerogels

CNCs can self-assemble into a chiral nematic structure where the particles adopt a layered helical arrangement. Over time, CNCs above a critical concentration separate into an isotropic phase and chiral nematic (anisotropic) phase. Capturing the anisotropic phase of self-assembled CNCs has been a long-standing theme in our research group for potential applications in catalysis, energy storage, sensors, and chiral separations.[201,210,211] We found that the chiral nematic phase of CNCs could be captured as a hydrogel by hydrothermally treating CNC suspensions after allowing them to phase separate for 5 days, **Figure 5.3**.

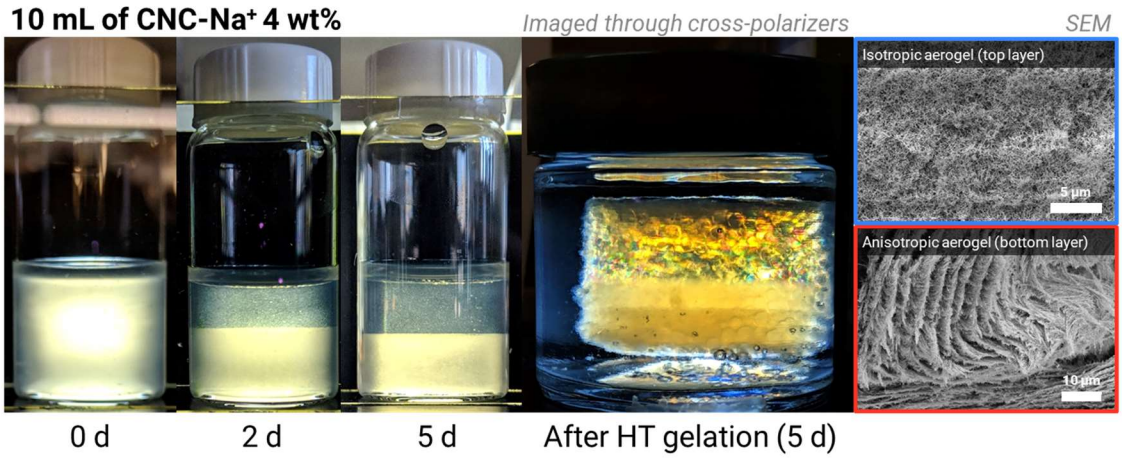

Figure 5.3. Hydrothermal gelation of phase-separated CNC suspensions. Optical photographs of phase separated CNC suspensions after 0, 2, and 5 days imaged through cross-polarizers. Scanning electron micrographs of the critical point dried porous CNC aerogel showing the isotropic (top layer) and anisotropic (bottom layer).

These anisotropic hydrothermally treated CNC hydrogels can be dried by critical point drying from CO_2 to produce highly porous anisotropic aerogels that retain the original chiral nematic structure in the bottom anisotropic layer. Combining CNC suspensions with polymeric precursors during hydrothermal treatment may produce elastic hydrogel networks that may show color changing behavior as the chiral nematic pitch of the hydrogel is compressed. Furthermore, removing the solvent to prepare highly porous isotropic and anisotropic aerogels could be of interest as a scaffold for high surface area post-functionalization for applications in filtration, templating, and catalysis.

5.2.4 Colloidal Gels with Varying Composition, Size, and Shape

We would like to see these strategies extended to other colloidal systems to broaden the applicability of colloidal gels. For example, making conductive gold nanorods, or graphene oxide nanosheets, that can percolate reversibly or in response to a stimulus would be of interest as soft electronic switches. As a liquid, the colloidal particles do not percolate and there is no continuous connected path of touching particles from one side of the liquid to the other, **Figure 5.4A**. In the colloidal gel, however, there may be extended percolation of the colloids in the system, **Figure 5.4B**. The percolation of the gold nanorods, for example, means there is a continuous connected path of interacting particles from one side of the system to the other. This gelation event may result in a drastic increase of the bulk conductivity of the system and may have applications in soft electronic devices and sensors. Factors such as the flexibility and hydrogen bonding between particles would be of interest to evaluate the degree of percolation and the formation of a colloidal gel.

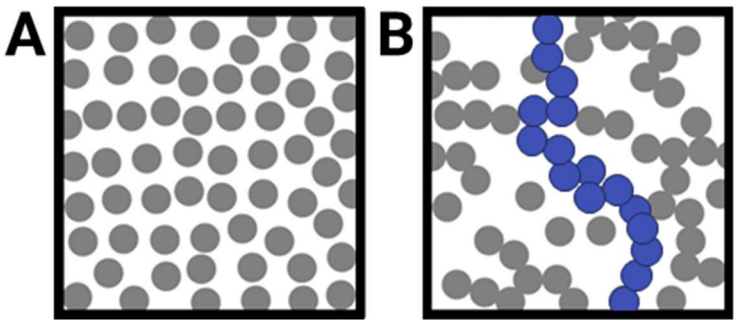

Figure 5.4. Schematic representation of a percolating network forming a connected path through the system. (A) Dense dispersion of particles that do not percolate. (B) Percolated particles forming a continuous path from one side of the system to the other. Adapted from reference 210 licensed under CC BY-NC 4.0.[212]

Alternatively, using colloids with intrinsic magnetic, piezoelectric, photophysical, or electronic properties, could broaden the scope of the potential material properties between dispersed and gelled states. Ultimately, a deeper understanding of how colloids can be manipulated to form gels is needed to expand their material properties before researchers can begin using them as functional soft materials.

References

(1) Alemán, J. V.; Chadwick, A. V.; He, J.; Hess, M.; Horie, K.; Jones, R. G.; Kratochvíl, P.; Meisel, I.; Mita, I.; Moad, G.; Penczek, S.; Stepto, R. F. T. Definitions of Terms Relating to the Structure and Processing of Sols, Gels, Networks, and Inorganic-Organic Hybrid Materials (IUPAC Recommendations 2007). *Pure Appl. Chem.* **2007**, *79*, 1801–1829.

(2) *Molecular Gels: Materials with Self-Assembled Fibrillar Networks*; Weiss, R. G., Térech, P., Eds.; Springer-Verlag: Berlin/Heidelberg, 2006.

(3) Nandakumar, D. K.; Zhang, Y.; Ravi, S. K.; Guo, N.; Zhang, C.; Tan, S. C. Solar Energy Triggered Clean Water Harvesting from Humid Air Existing above Sea Surface Enabled by a Hydrogel with Ultrahigh Hygroscopicity. *Adv. Mater.* **2019**, *31*, 1806730.

(4) Chivers, P. R. A.; Smith, D. K. Shaping and Structuring Supramolecular Gels. *Nat. Rev. Mater.* **2019**, *4*, 463–478.

(5) Peppas, N. A. N. A.; Hilt, J. Z. Z.; Khademhosseini, A.; Langer, R. Hydrogels in Biology and Medicine: From Molecular Principles to Bionanotechnology. *Adv. Mater.* **2006**, *18*, 1345–1360.

(6) Annabi, N.; Tamayol, A.; Uquillas, J. A.; Akbari, M.; Bertassoni, L. E.; Cha, C.; Camci-Unal, G.; Dokmeci, M. R.; Peppas, N. A.; Khademhosseini, A. 25th Anniversary Article: Rational Design and Applications of Hydrogels in Regenerative Medicine. *Adv. Mater.* **2014**, *26*, 85–124.

(7) Gaharwar, A. K.; Peppas, N. A.; Khademhosseini, A. Nanocomposite Hydrogels for Biomedical Applications. *Biotechnol. Bioeng.* **2014**, *111*, 441–453.

(8) Yuk, H.; Zhang, T.; Lin, S.; Parada, G. A.; Zhao, X. Tough Bonding of Hydrogels to

Diverse Non-Porous Surfaces. *Nat. Mater.* **2016**, *15*, 190–196.

(9) Lin, S.; Yuk, H.; Zhang, T.; Parada, G. A.; Koo, H.; Yu, C.; Zhao, X. Stretchable Hydrogel Electronics and Devices. *Adv. Mater.* **2016**, *28*, 4497–4505.

(10) Pierre, A. C.; Pajonk, G. M. Chemistry of Aerogels and Their Applications. *Chem. Rev.* **2002**, *102*, 4243–4266.

(11) Draper, E. R.; Adams, D. J. Low-Molecular-Weight Gels: The State of the Art. *Chem* **2017**, *3*, 390–410.

(12) Cornwell, D. J.; Smith, D. K. Expanding the Scope of Gels – Combining Polymers with Low-Molecular-Weight Gelators to Yield Modified Self-Assembling Smart Materials with High-Tech Applications. *Mater. Horizons* **2015**, *2*, 279–293.

(13) Colquhoun, C.; Draper, E. R.; Schweins, R.; Marcello, M.; Vadukul, D.; Serpell, L. C.; Adams, D. J. Controlling the Network Type in Self-Assembled Dipeptide Hydrogels. *Soft Matter* **2017**, *13*, 1914–1919.

(14) Raeburn, J.; McDonald, T. O.; Adams, D. J. Dipeptide Hydrogelation Triggered via Ultraviolet Light. *Chem. Commun.* **2012**, *48*, 9355–9357.

(15) Levine, I. N. *Physical Chemistry*; McGraw-Hill, 2009.

(16) Cangialosi, A.; Yoon, C.; Liu, J.; Huang, Q.; Guo, J.; Nguyen, T. D.; Gracias, D. H.; Schulman, R. DNA Sequence–Directed Shape Change of Photopatterned Hydrogels via High-Degree Swelling. *Science* **2017**, *357*, 1126–1130.

(17) Lee, S.; Oh, S.; Lee, J.; Malpani, Y.; Jung, Y.-S.; Kang, B.; Lee, J. Y.; Ozasa, K.; Isoshima, T.; Lee, S. Y.; Hara, M.; Hashizume, D.; Kim, J.-M. Stimulus-Responsive Azobenzene Supramolecules: Fibers, Gels, and Hollow Spheres. *Langmuir* **2013**, *29*, 5869–5877.

(18) Jung, S. M.; Jung, H. Y.; Dresselhaus, M. S.; Jung, Y. J.; Kong, J. A Facile Route for 3D Aerogels from Nanostructured 1D and 2D Materials. *Sci. Rep.* **2012**, *2*, 849.

(19) Engler, A. J.; Sen, S.; Sweeney, H. L.; Discher, D. E. Matrix Elasticity Directs Stem Cell Lineage Specification. *Cell* **2006**, *126*, 677–689.

(20) Matsuda, T.; Kawakami, R.; Namba, R.; Nakajima, T.; Gong, J. P. Mechanoresponsive Self-Growing Hydrogels Inspired by Muscle Training. *Science* **2019**, *363*, 504–508.

(21) Lin, S.; Liu, J.; Liu, X.; Zhao, X. Muscle-like Fatigue-Resistant Hydrogels by Mechanical Training. *Proc. Natl. Acad. Sci. U.S.A.* **2019**, *116*, 10244–10249.

(22) Zweep, N.; van Esch, J. H. The Design of Molecular Gelators. In *Functional Molecular Gels*; Royal Society of Chemistry: Cambridge, U.K., 2014; pp 1–29.

(23) Meyers, M. A.; Chawla, K. K. *Mechanical Behavior of Materials : Engineering Methods for Deformation, Fracture, and Fatigue*; Pearson, 2013.

(24) Russel, W. B.; Saville, D. A.; Schowalter, W. R. *Colloidal Dispersions*; Cambridge University Press, 1989.

(25) Bergna, H. E.; Roberts, W. O. *Colloidal Silica*; CRC Press, 2005.

(26) Wright, J. D.; Nico A.J.M., S. *Sol-Gel Materials*; CRC Press, 2018.

(27) Evans, D. F.; Wennerström, H. *The Colloidal Domain : Where Physics, Chemistry, Biology, and Technology Meet*; Wiley-VCH, 1999.

(28) Solomon, M. J.; Spicer, P. T. Microstructural Regimes of Colloidal Rod Suspensions, Gels, and Glasses. *Soft Matter* **2010**, *6*, 1391–1400.

(29) Ditte, A. Vanadium Research; Properties of Vanadic Acid. *C. R. Acad. Sci. Paris* **1885**, *101*, 698–702.

(30) Livage, J. Vanadium Pentoxide Gels. *Chem. Mater.* **1991**, *3*, 578–593.

(31) Xu, Y.; Sheng, K.; Li, C.; Shi, G. Self-Assembled Graphene Hydrogel *via* a One-Step Hydrothermal Process. *ACS Nano* **2010**, *4*, 4324–4330.

(32) Tsurusawa, H.; Leocmach, M.; Russo, J.; Tanaka, H. Gelation as Condensation Frustrated by Hydrodynamics and Mechanical Isostaticity. **2018**, arXiv:1804.04370 [cond-mat.soft].

(33) Kohl, M.; Capellmann, R. F.; Laurati, M.; Egelhaaf, S. U.; Schmiedeberg, M. Directed Percolation Identified as Equilibrium Pre-Transition towards Non-Equilibrium Arrested Gel States. *Nat. Commun.* **2016**, *7*, 11817.

(34) Tsurusawa, H.; Russo, J.; Leocmach, M.; Tanaka, H. Formation of Porous Crystals via Viscoelastic Phase Separation. *Nat. Mater.* **2017**, *16*, 1022–1028.

(35) Kovtyukhova, N. I.; Mallouk, T. E.; Ling Pan, A.; Dickey, E. C. Individual Single-Walled Nanotubes and Hydrogels Made by Oxidative Exfoliation of Carbon Nanotube Ropes. *J. Am. Chem. Soc.* **2003**, *125*, 9761–9769.

(36) Cummins, H. Z. Liquid, Glass, Gel: The Phases of Colloidal Laponite. *J. Non. Cryst. Solids* **2007**, *353*, 3891–3905.

(37) Luckham, P. F.; Rossi, S. The Colloidal and Rheological Properties of Bentonite Suspensions. *Adv. Colloid Interface Sci.* **1999**, *82*, 43–92.

(38) Ruzicka, B.; Zaccarelli, E.; Zulian, L.; Angelini, R.; Sztucki, M.; Moussaïd, A.; Narayanan, T.; Sciortino, F. Observation of Empty Liquids and Equilibrium Gels in a Colloidal Clay. *Nat. Mater.* **2011**, *10*, 56–60.

(39) Ureña-Benavides, E. E.; Ao, G.; Davis, V. A.; Kitchens, C. L. Rheology and Phase Behavior of Lyotropic Cellulose Nanocrystal Suspensions. *Macromolecules* **2011**, *44*, 8990–8998.

(40) Burey, P.; Bhandari, B. R.; Howes, T.; Gidley, M. J. Hydrocolloid Gel Particles: Formation, Characterization, and Application. *Crit. Rev. Food Sci. Nutr.* **2008**, *48*, 361–377.

(41) Zaccarelli, E. Colloidal Gels: Equilibrium and Non-Equilibrium Routes. *J. Phys. Condens. Matter* **2007**, *19*, 323101.

(42) Isikgor, F. H.; Becer, C. R. Lignocellulosic Biomass: A Sustainable Platform for the Production of Bio-Based Chemicals and Polymers. *Polym. Chem.* **2015**, *6*, 4497–4559.

(43) Foster, E. J.; Moon, R. J.; Agarwal, U. P.; Bortner, M. J.; Bras, J.; Camarero-Espinosa, S.; Chan, K. J.; Clift, M. J. D.; Cranston, E. D.; Eichhorn, S. J.; et al. Current Characterization Methods for Cellulose Nanomaterials. *Chem. Soc. Rev.* **2018**, *47*, 2609–2679.

(44) Natural Resources Canada. Overview of Canada's forest industry https://www.nrcan.gc.ca/forests/industry/overview/13311 (accessed Apr 15, 2019).

(45) Natural Resources Canada. Cellulose nanocrystals http://www.nrcan.gc.ca/forests/industry/products-applications/13349 (accessed Apr 15, 2019).

(46) Eichhorn, S. J.; Dufresne, A.; Aranguren, M.; Marcovich, N. E.; Capadona, J. R.; Rowan, S. J.; Weder, C.; Thielemans, W.; Roman, M.; Renneckar, S.; et al. Review: Current International Research into Cellulose Nanofibres and Nanocomposites. *J. Mater. Sci.* **2010**, *45*, 1–33.

(47) Xu, X.; Liu, F.; Jiang, L.; Zhu, J. Y.; Haagenson, D.; Wiesenborn, D. P. Cellulose Nanocrystals vs. Cellulose Nanofibrils: A Comparative Study on Their Microstructures and Effects as Polymer Reinforcing Agents. *ACS Appl. Mater. Interfaces* **2013**, *5*, 2999–

3009.

(48) Siró, I.; Plackett, D. Microfibrillated Cellulose and New Nanocomposite Materials: A Review. *Cellulose* **2010**, *17*, 459–494.

(49) Lavoine, N.; Desloges, I.; Dufresne, A.; Bras, J. Microfibrillated Cellulose – Its Barrier Properties and Applications in Cellulosic Materials: A Review. *Carbohydr. Polym.* **2012**, *90*, 735–764.

(50) Klemm, D.; Kramer, F.; Moritz, S.; Lindstroem, T.; Ankerfors, M.; Gray, D.; Dorris, A.; Lindström, T.; Ankerfors, M.; Gray, D.; Dorris, A. Nanocelluloses: A New Family of Nature-Based Materials. *Angew. Chem., Int. Ed.* **2011**, *50*, 5438–5466.

(51) Fatona, A.; Berry, R. M.; Brook, M. A.; Moran-Mirabal, J. M. Versatile Surface Modification of Cellulose Fibers and Cellulose Nanocrystals through Modular Triazinyl Chemistry. *Chem. Mater.* **2018**, *30*, 2424–2435.

(52) Ferreira, F. V.; Pinheiro, I. F.; Gouveia, R. F.; Thim, G. P.; Lona, L. M. F. Functionalized Cellulose Nanocrystals as Reinforcement in Biodegradable Polymer Nanocomposites. *Polym. Compos.* **2018**, *39*, E9–E29.

(53) Mariano, M.; El Kissi, N.; Dufresne, A. Cellulose Nanocrystals and Related Nanocomposites: Review of Some Properties and Challenges. *J. Polym. Sci. Part B Polym. Phys.* **2014**, *52*, 791–806.

(54) Cao, Y.; Zavaterri, P.; Youngblood, J.; Moon, R.; Weiss, J. The Influence of Cellulose Nanocrystal Additions on the Performance of Cement Paste. *Cem. Concr. Compos.* **2015**, *56*, 73–83.

(55) Moon, R. J.; Schueneman, G. T.; Simonsen, J. Overview of Cellulose Nanomaterials, Their Capabilities and Applications. *JOM* **2016**, *68*, 2383–2394.

(56) Klemm, D.; Cranston, E. D.; Fischer, D.; Gama, M.; Kedzior, S. A.; Kralisch, D.; Kramer, F.; Kondo, T.; Lindström, T.; Nietzsche, S.; Petzold-Welcke, K.; Rauchfuß, F. Nanocellulose as a Natural Source for Groundbreaking Applications in Materials Science: Today's State. *Mater. Today* **2018**, *21*, 720–748.

(57) Bhattacharjee, S. DLS and Zeta Potential – What They Are and What They Are Not? *J. Control. Release* **2016**, *235*, 337–351.

(58) J N Israelachvili. *Intermolecular and Surface Forces*; Academic Press, 2011.

(59) Derjaguin, B.; Landau, L. Theory of the Stability of Strongly Charged Lyophobic Sols and of the Adhesion of Strongly Charged Particles in Solutions of Electrolytes. *Prog. Surf. Sci.* **1993**, *43*, 30–59.

(60) Verwey, E. J. W. Theory of the Stability of Lyophobic Colloids. *J. Phys. Colloid Chem.* **1947**, *51*, 631–636.

(61) Verwey, E. J. W.; Overbeek, J. T. G.; van Nes, K. *Theory of the Stability of Lyophobic Colloids; the Interaction of Sol Particles Having an Electric Double Layer*; Elsevier Publishing Company Inc.: New York, 1948.

(62) Overbeek, J. T. G. The Rule of Schulze and Hardy. *Pure Appl. Chem.* **1980**, *52*, 1151–1161.

(63) Trefalt, G.; Szilagyi, I.; Téllez, G.; Borkovec, M. Colloidal Stability in Asymmetric Electrolytes: Modifications of the Schulze–Hardy Rule. *Langmuir* **2017**, *33*, 1695–1704.

(64) De France, K. J.; Hoare, T.; Cranston, E. D. Review of Hydrogels and Aerogels Containing Nanocellulose. *Chem. Mater.* **2017**, *29*, 4609–4631.

(65) Alizadehgiashi, M.; Khuu, N.; Khabibullin, A.; Henry, A.; Tebbe, M.; Suzuki, T.;

Kumacheva, E. Nanocolloidal Hydrogel for Heavy Metal Scavenging. *ACS Nano* **2018**, *12*, 8160–8168.

(66) Le Goff, K. J.; Gaillard, C.; Helbert, W.; Garnier, C.; Aubry, T. Rheological Study of Reinforcement of Agarose Hydrogels by Cellulose Nanowhiskers. *Carbohydr. Polym.* **2015**, *116*, 117–123.

(67) Yin, O. S.; Ahmad, I.; Mohd Amin, M. C. I. Effect of Cellulose Nanocrystals Content and PH on Swelling Behaviour of Gelatin Based Hydrogel. *Sains Malaysiana* **2015**, *44*, 793–799.

(68) The Functional Response of Alginate-Gelatin-Nanocrystalline Cellulose Injectable Hydrogels toward Delivery of Cells and Bioactive Molecules. *Acta Biomater.* **2016**, *36*, 143–151.

(69) Abitbol, T.; Johnstone, T.; Quinn, T. M.; Gray, D. G. Reinforcement with Cellulose Nanocrystals of Poly(Vinyl Alcohol) Hydrogels Prepared by Cyclic Freezing and Thawing. *Soft Matter* **2011**, *7*, 2373–2379.

(70) Kelly, J. A.; Shukaliak, A. M.; Cheung, C. C. Y.; Shopsowitz, K. E.; Hamad, W. Y.; MacLachlan, M. J. Responsive Photonic Hydrogels Based on Nanocrystalline Cellulose. *Angew. Chem., Int. Ed.* **2013**, *52*, 8912–8916.

(71) Capadona, J. R.; Shanmuganathan, K.; Tyler, D. J.; Rowan, S. J.; Weder, C. Stimuli-Responsive Polymer Nanocomposites Inspired by the Sea Cucumber Dermis. *Science* **2008**, *319*, 1370–1374.

(72) Favier, V.; Cavaille, J. Y.; Canova, G. R.; Shrivastava, S. C. Mechanical Percolation in Cellulose Whisker Nanocomposites. *Polym. Eng. Sci.* **1997**, *37*, 1732–1739.

(73) Moon, R. J.; Martini, A.; Nairn, J.; Simonsen, J.; Youngblood, J. Cellulose

Nanomaterials Review: Structure, Properties and Nanocomposites. *Chem. Soc. Rev.* **2011**, *40*, 3941–3994.

(74) Filipe, V.; Hawe, A.; Jiskoot, W. Critical Evaluation of Nanoparticle Tracking Analysis (NTA) by NanoSight for the Measurement of Nanoparticles and Protein Aggregates. *Pharm. Res.* **2010**, *27*, 796–810.

(75) Giese, M.; Khan, M. K.; Hamad, W. Y.; MacLachlan, M. J. Imprinting of Photonic Patterns with Thermosetting Amino-Formaldehyde-Cellulose Composites. *ACS Macro Lett.* **2013**, *2*, 818–821.

(76) Shafiei-Sabet, S.; Hamad, W. Y.; Hatzikiriakos, S. G. Rheology of Nanocrystalline Cellulose Aqueous Suspensions. *Langmuir* **2012**, *28*, 17124–17133.

(77) Heath, L.; Thielemans, W. Cellulose Nanowhisker Aerogels. *Green Chem.* **2010**, *12*, 1448–1453.

(78) Bertsch, P.; Isabettini, S.; Fischer, P. Ion-Induced Hydrogel Formation and Nematic Ordering of Nanocrystalline Cellulose Suspensions. *Biomacromolecules* **2017**, *18*, 4060–4066.

(79) Shafiei-Sabet, S.; Hamad, W. Y.; Hatzikiriakos, S. G. Ionic Strength Effects on the Microstructure and Shear Rheology of Cellulose Nanocrystal Suspensions. *Cellulose* **2014**, *21*, 3347–3359.

(80) Yang, X.; Cranston, E. D. Chemically Cross-Linked Cellulose Nanocrystal Aerogels with Shape Recovery and Superabsorbent Properties. *Chem. Mater.* **2014**, *26*, 6016–6025.

(81) Lewis, L.; Derakhshandeh, M.; Hatzikiriakos, S. G.; Hamad, W. Y.; MacLachlan, M. J. Hydrothermal Gelation of Aqueous Cellulose Nanocrystal Suspensions.

Biomacromolecules **2016**, *17*, 2747–2754.

(82) Oechsle, A. L.; Lewis, L.; Hamad, W. Y.; Hatzikiriakos, S. G.; MacLachlan, M. J. CO_2-Switchable Cellulose Nanocrystal Hydrogels. *Chem. Mater.* **2018**, *30*, 376–385.

(83) Lewis, L.; Hatzikiriakos, S. G.; Hamad, W. Y.; MacLachlan, M. J. Freeze–Thaw Gelation of Cellulose Nanocrystals. *ACS Macro Lett.* **2019**, *8*, 486–491.

(84) Hu, Z.; Cranston, E. D.; Ng, R.; Pelton, R. Tuning Cellulose Nanocrystal Gelation with Polysaccharides and Surfactants. *Langmuir* **2014**, *30*, 2684–2692.

(85) Chen, W.; Yu, H.; Li, Q.; Liu, Y.; Li, J. Ultralight and Highly Flexible Aerogels with Long Cellulose I Nanofibers. *Soft Matter* **2011**, *7*, 10360–10368.

(86) Wu, Z.-Y.; Li, C.; Liang, H.-W.; Chen, J.-F.; Yu, S.-H. Ultralight, Flexible, and Fire-Resistant Carbon Nanofiber Aerogels from Bacterial Cellulose. *Angew. Chem., Int. Ed.* **2013**, *52*, 2925–2929.

(87) Zhang, Z.; Sèbe, G.; Rentsch, D.; Zimmermann, T.; Tingaut, P. Ultralightweight and Flexible Silylated Nanocellulose Sponges for the Selective Removal of Oil from Water. *Chem. Mater.* **2014**, *26*, 2659–2668.

(88) Wang, S.; Peng, X.; Zhong, L.; Tan, J.; Jing, S.; Cao, X.; Chen, W.; Liu, C.; Sun, R. Ultralight, Elastic, Cost-Effective, and Highly Recyclable Superabsorbent from Microfibrillated Cellulose Fiber for Oil Spillage Cleanup. *J. Mater. Chem. A* **2015**, *3*, 8772–8781.

(89) Jiang, F.; Hsieh, Y.-L. Amphiphilic Superabsorbent Cellulose Nanofibril Aerogels. *J. Mater. Chem. A* **2014**, *2*, 6337–6342.

(90) Domingues, R. M. A.; Gomes, M. E.; Reis, R. L. The Potential of Cellulose Nanocrystals in Tissue Engineering Strategies. *Biomacromolecules* **2014**, *15*, 2327–

2346.

(91) Hamad, W. Y. Development and Properties of Nanocrystalline Cellulose. In *Sustainable Production of Fuels, Chemicals, and Fibers from Forest Biomass*; Zhu, J., Zhang, X., Pan, X., Eds.; American Chemical Society: Washington, DC, 2011; pp 301–321.

(92) Rånby, B. G. Aqueous Colloidal Solutions of Cellulose Micelles. *Acta Chem. Scand.* **1949**, *3*, 649–650.

(93) Peng, B. L.; Dhar, N.; Liu, H. L.; Tam, K. C. Chemistry and Applications of Nanocrystalline Cellulose and Its Derivatives: A Nanotechnology Perspective. *Can. J. Chem. Eng.* **2011**, *89*, 1191–1206.

(94) Siqueira, G.; Bras, J.; Dufresne, A. Cellulosic Bionanocomposites: A Review of Preparation, Properties and Applications. *Polymers* **2010**, *2*, 728–765.

(95) Habibi, Y.; Lucia, L. A.; Rojas, O. J. Cellulose Nanocrystals: Chemistry, Self-Assembly, and Applications. *Chem. Rev.* **2010**, *110*, 3479–3500.

(96) Kloser, E.; Gray, D. G. Surface Grafting of Cellulose Nanocrystals with Poly(Ethylene Oxide) in Aqueous Media. *Langmuir* **2010**, *26*, 13450–13456.

(97) Quennouz, N.; Hashmi, S. M.; Choi, H. S.; Kim, J. W.; Osuji, C. O. Rheology of Cellulose Nanofibrils in the Presence of Surfactants. *Soft Matter* **2016**, *12*, 157–164.

(98) Shopsowitz, K. E.; Qi, H.; Hamad, W. Y.; Maclachlan, M. J. Free-Standing Mesoporous Silica Films with Tunable Chiral Nematic Structures. *Nature* **2010**, *468*, 422–425.

(99) Kelly, J. A.; Giese, M.; Shopsowitz, K. E.; Hamad, W. Y.; MacLachlan, M. J. The Development of Chiral Nematic Mesoporous Materials. *Acc Chem Res* **2014**, *47*, 1088–1096.

(100) Dumanli, A. G.; Kamita, G.; Landman, J.; van der Kooij, H.; Glover, B. J.; Baumberg,

J. J.; Steiner, U.; Vignolini, S. Controlled, Bio-Inspired Self-Assembly of Cellulose-Based Chiral Reflectors. *Adv. Opt. Mater.* **2014**, *2*, 646–650.

(101) Majoinen, J.; Kontturi, E.; Ikkala, O.; Gray, D. G. SEM Imaging of Chiral Nematic Films Cast from Cellulose Nanocrystal Suspensions. *Cellulose* **2012**, *19*, 1599–1605.

(102) Revol, J.-F.; Bradford, H.; Giasson, J.; Marchessault, R. H.; Gray, D. G. Helicoidal Self-Ordering of Cellulose Microfibrils in Aqueous Suspension. *Int. J. Biol. Macromol.* **1992**, *14*, 170–172.

(103) Giese, M.; Blusch, L. K.; Khan, M. K.; MacLachlan, M. J. Functional Materials from Cellulose-Derived Liquid-Crystal Templates. *Angew. Chem., Int. Ed.* **2015**, *54*, 2888–2910.

(104) Alatalo, S.-M.; Pileidis, F.; Mäkilä, E.; Sevilla, M.; Repo, E.; Salonen, J.; Sillanpää, M.; Titirici, M.-M. Versatile Cellulose-Based Carbon Aerogel for the Removal of Both Cationic and Anionic Metal Contaminants from Water. *ACS Appl Mater Interfaces* **2015**, *7*, 25875–25883.

(105) Lin, N.; Gèze, A.; Wouessidjewe, D.; Huang, J.; Dufresne, A. Biocompatible Double-Membrane Hydrogels from Cationic Cellulose Nanocrystals and Anionic Alginate as Complexing Drugs Codelivery. *ACS Appl. Mater. Interfaces* **2016**, *8*, 6880–6889.

(106) De France, K. J.; Chan, K. J. W.; Cranston, E. D.; Hoare, T. Enhanced Mechanical Properties in Cellulose Nanocrystal–Poly(Oligoethylene Glycol Methacrylate) Injectable Nanocomposite Hydrogels through Control of Physical and Chemical Cross-Linking. *Biomacromolecules* **2016**, *17*, 649–660.

(107) Azzam, F.; Siqueira, E.; Fort, S.; Hassaini, R.; Pignon, F.; Travelet, C.; Putaux, J.-L.; Jean, B. Tunable Aggregation and Gelation of Thermoresponsive Suspensions of

Polymer-Grafted Cellulose Nanocrystals. *Biomacromolecules* **2016**, *17*, 2112–2119.

(108) Su, S.; Hamad, W. Y. Nanocomposite Hydrogel and Method for Preparing It, for Industrial and Medical Applications. US Patent 8828434 B2, 2014.

(109) Yang, X.; Bakaic, E.; Hoare, T.; Cranston, E. D. Injectable Polysaccharide Hydrogels Reinforced with Cellulose Nanocrystals: Morphology, Rheology, Degradation, and Cytotoxicity. *Biomacromolecules* **2013**, *14*, 4447–4455.

(110) Kovacs, T.; Naish, V.; O'Connor, B.; Blaise, C.; Gagné, F.; Hall, L.; Trudeau, V.; Martel, P. An Ecotoxicological Characterization of Nanocrystalline Cellulose (NCC). *Nanotoxicology* **2010**, *4*, 255–270.

(111) Colombo, L.; Zoia, L.; Violatto, M. B.; Previdi, S.; Talamini, L.; Sitia, L.; Nicotra, F.; Orlandi, M.; Salmona, M.; Recordati, C.; Bigini, P.; La Ferla, B. Organ Distribution and Bone Tropism of Cellulose Nanocrystals in Living Mice. *Biomacromolecules* **2015**, *16*, 2862–2871.

(112) Chau, M.; Sriskandha, S. E.; Pichugin, D.; Thérien-Aubin, H.; Nykypanchuk, D.; Chauve, G.; Méthot, M.; Bouchard, J.; Gang, O.; Kumacheva, E. Ion-Mediated Gelation of Aqueous Suspensions of Cellulose Nanocrystals. *Biomacromolecules* **2015**, *16*, 2455–2462.

(113) Shafiei-Sabet, S.; Hamad, W.; Hatzikiriakos, S. Influence of Degree of Sulfation on the Rheology of Cellulose Nanocrystal Suspensions. *Rheol. Acta* **2013**, *52*, 741–751.

(114) Yang, X.; Shi, K.; Zhitomirsky, I.; Cranston, E. D. Cellulose Nanocrystal Aerogels as Universal 3D Lightweight Substrates for Supercapacitor Materials. *Adv. Mater.* **2015**, *27*, 6104–6109.

(115) Dorris, A.; Gray, D. G. Gelation of Cellulose Nanocrystal Suspensions in Glycerol.

Cellulose **2012**, *19*, 687–694.

(116) Wicklein, B.; Kocjan, A.; Salazar-Alvarez, G.; Carosio, F.; Camino, G.; Antonietti, M.; Bergström, L. Thermally Insulating and Fire-Retardant Lightweight Anisotropic Foams Based on Nanocellulose and Graphene Oxide. *Nat. Nanotechnol.* **2014**, *10*, 277–283.

(117) Smith, S. W.; Buesch, C.; Matthews, D. J.; Simonsen, J.; Conley, J. F. Improved Oxidation Resistance of Organic/Inorganic Composite Atomic Layer Deposition Coated Cellulose Nanocrystal Aerogels. *J. Vac. Sci. Technol. A Vacuum, Surfaces, Film.* **2014**, *32*, 041508.

(118) Macosko, C. W. *Rheology : Principles, Measurements, and Applications*; VCH: New York, 1994.

(119) Mewis, J.; Wagner, N. J. *Colloidal Suspension Rheology*; Cambridge University Press: New York, 2012.

(120) Titirici, M.-M.; Thomas, A.; Antonietti, M. Replication and Coating of Silica Templates by Hydrothermal Carbonization. *Adv. Funct. Mater.* **2007**, *17*, 1010–1018.

(121) Titirici, M.-M.; Antonietti, M. Chemistry and Materials Options of Sustainable Carbon Materials Made by Hydrothermal Carbonization. *Chem. Soc. Rev.* **2010**, *39*, 103–116.

(122) Beck, S.; Bouchard, J. Auto-Catalyzed Acidic Desulfation of Cellulose Nanocrystals. *Nord. Pulp Pap. Res. J.* **2014**, *29*, 6–14.

(123) Lin, N.; Dufresne, A. Surface Chemistry, Morphological Analysis and Properties of Cellulose Nanocrystals with Gradiented Sulfation Degrees. *Nanoscale* **2014**, *6*, 5384–5393.

(124) Jiang, F.; Esker, A. R.; Roman, M. Acid-Catalyzed and Solvolytic Desulfation of H2SO4-Hydrolyzed Cellulose Nanocrystals. *Langmuir* **2010**, *26*, 17919–17925.

(125) Wang, N.; Ding, E.; Cheng, R. Thermal Degradation Behaviors of Spherical Cellulose Nanocrystals with Sulfate Groups. *Polymer* **2007**, *48*, 3486–3493.

(126) French, A. D. Idealized Powder Diffraction Patterns for Cellulose Polymorphs. *Cellulose* **2013**, *21*, 885–896.

(127) Annabi, N.; Nichol, J. W.; Zhong, X.; Ji, C.; Koshy, S.; Khademhosseini, A.; Dehghani, F. Controlling the Porosity and Microarchitecture of Hydrogels for Tissue Engineering. *Tissue Eng. Part B. Rev.* **2010**, *16*, 371–383.

(128) Slaughter, B. V; Khurshid, S. S.; Fisher, O. Z.; Khademhosseini, A.; Peppas, N. A. Hydrogels in Regenerative Medicine. *Adv. Mater.* **2009**, *21*, 3307–3329.

(129) Vermonden, T.; Censi, R.; Hennink, W. E. Hydrogels for Protein Delivery. *Chem. Rev.* **2012**, *112*, 2853–2888.

(130) Kikuchi, A.; Okano, T. Pulsatile Drug Release Control Using Hydrogels. *Adv. Drug Deliv. Rev.* **2002**, *54*, 53–77.

(131) Döring, A.; Birnbaum, W.; Kuckling, D. Responsive Hydrogels - Structurally and Dimensionally Optimized Smart Frameworks for Applications in Catalysis, Micro-System Technology and Material Science. *Chem. Soc. Rev.* **2013**, *42*, 7391–7420.

(132) Dong, L.; Agarwal, A. K.; Beebe, D. J.; Jiang, H. Adaptive Liquid Microlenses Activated by Stimuli-Responsive Hydrogels. *Nature* **2006**, *442*, 551–554.

(133) Kim, Y. S.; Liu, M.; Ishida, Y.; Ebina, Y.; Osada, M.; Sasaki, T.; Hikima, T.; Takata, M.; Aida, T. Thermoresponsive Actuation Enabled by Permittivity Switching in an Electrostatically Anisotropic Hydrogel. *Nat. Mater.* **2015**, *14*, 1002–1007.

(134) Liu, M.; Ishida, Y.; Ebina, Y.; Sasaki, T.; Hikima, T.; Takata, M.; Aida, T. An Anisotropic Hydrogel with Electrostatic Repulsion between Cofacially Aligned

Nanosheets. *Nature* **2015**, *517*, 68–72.

(135) Klouda, L.; Mikos, A. G. Thermoresponsive Hydrogels in Biomedical Applications. *Eur. J. Pharm. Biopharm.* **2008**, *68*, 34–45.

(136) Han, C. K.; Bae, Y. H. Inverse Thermally Reversible Gelation of Aqueous N-Isopropylacrylamide Copolymer Solutions. *Polymer* **1998**, *39*, 2809–2814.

(137) Jeong, B.; Bae, Y. H.; Lee, D. S.; Kim, S. W. Biodegradable Block Copolymers as Injectable Drug-Delivery Systems. *Nature* **1997**, *388*, 860–862.

(138) Bell, C. L.; Peppas, N. A. Water, Solute and Protein Diffusion in Physiologically Responsive Hydrogels of Poly(Methacrylic Acid-g-Ethylene Glycol). *Biomaterials* **1996**, *17*, 1203–1218.

(139) Torres-Lugo, M.; Peppas, N. A. Molecular Design and in Vitro Studies of Novel PH-Sensitive Hydrogels for the Oral Delivery of Calcitonin. *Macromolecules* **1999**, *32*, 6646–6651.

(140) Chiu, Y.-L.; Chen, S.-C.; Su, C.-J.; Hsiao, C.-W.; Chen, Y.-M.; Chen, H.-L.; Sung, H.-W. PH-Triggered Injectable Hydrogels Prepared from Aqueous N-Palmitoyl Chitosan: In Vitro Characteristics and in Vivo Biocompatibility. *Biomaterials* **2009**, *30*, 4877–4888.

(141) ter Schiphorst, J.; Coleman, S.; Stumpel, J. E.; Ben Azouz, A.; Diamond, D.; Schenning, A. P. H. J. Molecular Design of Light-Responsive Hydrogels, for in Situ Generation of Fast and Reversible Valves for Microfluidic Applications. *Chem. Mater.* **2015**, *27*, 5925–5931.

(142) Lv, S.-W.; Liu, Y.; Xie, M.; Wang, J.; Yan, X.-W.; Li, Z.; Dong, W.-G.; Huang, W.-H. Near-Infrared Light-Responsive Hydrogel for Specific Recognition and Photothermal

Site-Release of Circulating Tumor Cells. *ACS Nano* **2016**, *10*, 6201–6210.

(143) Zhao, Y.-L.; Stoddart, J. F. Azobenzene-Based Light-Responsive Hydrogel System. *Langmuir* **2009**, *25*, 8442–8446.

(144) Zhao, B.; Moore, J. S. Fast PH- and Ionic Strength-Responsive Hydrogels in Microchannels. *Langmuir* **2001**, *17*, 4758–4763.

(145) Horkay, F.; Tasaki, I.; Basser, P. J. Osmotic Swelling of Polyacrylate Hydrogels in Physiological Salt Solutions. *Biomacromolecules* **2000**, *1*, 84–90.

(146) Jeon, C. H.; Makhaeva, E. E.; Khokhlov, A. R. Swelling Behavior of Polyelectrolyte Gels in the Presence of Salts. *Macromol. Chem. Phys.* **1998**, *199*, 2665–2670.

(147) Traitel, T.; Cohen, Y.; Kost, J. Characterization of Glucose-Sensitive Insulin Release Systems in Simulated in Vivo Conditions. *Biomaterials* **2000**, *21*, 1679–1687.

(148) Kawamura, A.; Kiguchi, T.; Nishihata, T.; Uragami, T.; Miyata, T. Target Molecule-Responsive Hydrogels Designed via Molecular Imprinting Using Bisphenol A as a Template. *Chem. Commun.* **2014**, *50*, 11101–11103.

(149) Shiraki, Y.; Tsuruta, K.; Morimoto, J.; Ohba, C.; Kawamura, A.; Yoshida, R.; Kawano, R.; Uragami, T.; Miyata, T. Preparation of Molecule-Responsive Microsized Hydrogels via Photopolymerization for Smart Microchannel Microvalves. *Macromol. Rapid Commun.* **2015**, *36*, 515–519.

(150) Osada, Y.; Okuzaki, H.; Hori, H. A Polymer Gel with Electrically Driven Motility. *Nature* **1992**, *355*, 242–244.

(151) Murdan, S. Electro-Responsive Drug Delivery from Hydrogels. *J. Control. Release* **2003**, *92*, 1–17.

(152) Zrinyi, M. Intelligent Polymer Gels Controlled by Magnetic Fields. *Colloid Polym. Sci.*

2000, *278*, 98–103.

(153) Reinicke, S.; Doehler, S.; Tea, S.; Krekhova, M.; Messing, R.; Schmidt, A. M.; Schmalz, H. Magneto-Responsive Hydrogels Based on Maghemite/Triblock Terpolymer Hybrid Micelles. *Soft Matter* **2010**, *6*, 2760–2773.

(154) Dufresne, A. *Nanocellulose: From Nature to High Performance Tailored Materials*, 1st ed.; Walter de Gruyter GmbH: Berlin, Boston, 2012.

(155) *Polysaccharides II*; Klemm, D., Ed.; Springer-Verlag: Berlin, 2006.

(156) Rojas, O. J. *Cellulose Chemistry and Properties : Fibers, Nanocelluloses and Advanced Materials*; 2016.

(157) Lam, E.; Male, K. B.; Chong, J. H.; Leung, A. C. W.; Luong, J. H. T. Applications of Functionalized and Nanoparticle-Modified Nanocrystalline Cellulose. *Trends Biotechnol.* **2012**, *30*, 283–290.

(158) Eichhorn, S. J. Cellulose Nanowhiskers: Promising Materials for Advanced Applications. *Soft Matter* **2011**, *7*, 303–315.

(159) Lagerwall, J. P. F.; Schutz, C.; Salajkova, M.; Noh, J. H.; Park, J. H.; Scalia, G.; Bergstrom, L. Cellulose Nanocrystal-Based Materials: From Liquid Crystal Self-Assembly and Glass Formation to Multifunctional Thin Films. *NPG Asia Mater.* **2014**, *6*, e80.

(160) Giese, M.; Blusch, L. K.; Khan, M. K.; Hamad, W. Y.; MacLachlan, M. J. Responsive Mesoporous Photonic Cellulose Films by Supramolecular Cotemplating. *Angew. Chem., Int. Ed.* **2014**, *53*, 8880–8884.

(161) Parker, R. M.; Frka-Petesic, B.; Guidetti, G.; Kamita, G.; Consani, G.; Abell, C.; Vignolini, S. Hierarchical Self-Assembly of Cellulose Nanocrystals in a Confined

Geometry. *ACS Nano* **2016**, *10*, 8443–8449.

(162) Gonzalez, J. S.; Luduena, L. N.; Ponce, A.; Alvarez, V. A. Poly(Vinyl Alcohol)/Cellulose Nanowhiskers Nanocomposite Hydrogels for Potential Wound Dressings. *Mater. Sci. Eng. C Mater. Biol. Appl.* **2014**, *34*, 54–61.

(163) Yang, J.; Han, C.; Xu, F.; Sun, R. Simple Approach to Reinforce Hydrogels with Cellulose Nanocrystals. *Nanoscale* **2014**, *6*, 5934–5943.

(164) Guo, H. L.; Su, P.; Kang, X.; Ning, S. K. Synthesis and Characterization of Nitrogen-Doped Graphene Hydrogels by Hydrothermal Route with Urea as Reducing-Doping Agents. *J. Mater. Chem. A* **2013**, *1*, 2248–2255.

(165) McKee, J. R.; Appel, E. A.; Seitsonen, J.; Kontturi, E.; Scherman, O. A.; Ikkala, O. Healable, Stable and Stiff Hydrogels: Combining Conflicting Properties Using Dynamic and Selective Three-Component Recognition with Reinforcing Cellulose Nanorods. *Adv. Funct. Mater.* **2014**, *24*, 2706–2713.

(166) Garcia-Astrain, C.; Gonzalez, K.; Gurrea, T.; Guaresti, O.; Algar, I.; Eceiza, A.; Gabilondo, N. Maleimide-Grafted Cellulose Nanocrystals as Cross-Linkers for Bionanocomposite Hydrogels. *Carbohydr. Polym.* **2016**, *149*, 94–101.

(167) Habibi, Y. Key Advances in the Chemical Modification of Nanocelluloses. *Chem. Soc. Rev.* **2014**, *43*, 1519–1542.

(168) Dong, X. M.; Revol, J.-F.; Gray, D. G. Effect of Microcrystallite Preparation Conditions on the Formation of Colloid Crystals of Cellulose. *Cellulose* **1998**, *5*, 19–32.

(169) Kan, K. H. M.; Li, J.; Wijesekera, K.; Cranston, E. D. Polymer-Grafted Cellulose Nanocrystals as PH-Responsive Reversible Flocculants. *Biomacromolecules* **2013**, *14*, 3130–3139.

(170) Way, A. E.; Hsu, L.; Shanmuganathan, K.; Weder, C.; Rowan, S. J. PH-Responsive Cellulose Nanocrystal Gels and Nanocomposites. *ACS Macro Lett.* **2012**, *1*, 1001–1006.

(171) Wang, H.-D.; Jessop, P. G.; Bouchard, J.; Champagne, P.; Cunningham, M. F. Cellulose Nanocrystals with CO_2-Switchable Aggregation and Redispersion Properties. *Cellulose* **2015**, *22*, 3105–3116.

(172) Liu, Y.; Jessop, P. G.; Cunningham, M.; Eckert, C. A.; Liotta, C. L. Switchable Surfactants. *Science* **2006**, *313*, 958–960.

(173) Mercer, S. M.; Jessop, P. G. "Switchable Water": Aqueous Solutions of Switchable Ionic Strength. *ChemSusChem* **2010**, *3*, 467–470.

(174) Han, D.; Boissiere, O.; Kumar, S.; Tong, X.; Tremblay, L.; Zhao, Y. Two-Way CO_2-Switchable Triblock Copolymer Hydrogels. *Macromolecules* **2012**, *45*, 7440–7445.

(175) Robert, T.; Mercer, S. M.; Clark, T. J.; Mariampillai, B. E.; Champagne, P.; Cunningham, M. F.; Jessop, P. G. Nitrogen-Containing Polymers as Potent Ionogens for Aqueous Solutions of Switchable Ionic Strength: Application to Separation of Organic Liquids and Clay Particles from Water. *Green Chem.* **2012**, *14*, 3053–3062.

(176) Su, X.; Robert, T.; Mercer, S. M.; Humphries, C.; Cunningham, M. F.; Jessop, P. G. A Conventional Surfactant Becomes CO_2-Responsive in the Presence of Switchable Water Additives. *Chem. Eur. J.* **2013**, *19*, 5595–5601.

(177) Hamad, W. Y.; Hu, T. Q. Structure-Process-Yield Interrelations in Nanocrystalline Cellulose Extraction. *Can. J. Chem. Eng.* **2010**, *88*, 392–402.

(178) Moore, W. J.; Hummel, D. *Physikalische Chemie 4: Auflage*; De Gruyter: Berlin, 1986.

(179) Winter, H. H.; Chambon, F. Analysis of Linear Viscoelasticity of a Crosslinking Polymer at the Gel Point. *J. Rheol.* **1986**, *30*, 367–382.

(180) McKee, J. R.; Hietala, S.; Seitsonen, J.; Laine, J.; Kontturi, E.; Ikkala, O. Thermoresponsive Nanocellulose Hydrogels with Tunable Mechanical Properties. *ACS Macro Lett.* **2014**, *3*, 266–270.

(181) Shikinaka, K.; Kaneda, K.; Mori, S.; Maki, T.; Masunaga, H.; Osada, Y.; Shigehara, K. Direct Evidence for Structural Transition Promoting Shear Thinning in Cylindrical Colloid Assemblies. *Small* **2014**, *10*, 1813–1820.

(182) Jones, C. D.; Steed, J. W. Gels with Sense: Supramolecular Materials That Respond to Heat, Light and Sound. *Chem. Soc. Rev.* **2016**, *136*, 87–94.

(183) Wang, Q.; Gu, Z.; Jamal, S.; Detamore, M. S.; Berkland, C. Hybrid Hydroxyapatite Nanoparticle Colloidal Gels Are Injectable Fillers for Bone Tissue Engineering. *Tissue Eng. Part A* **2013**, *19*, 2586–2593.

(184) Plackett. A Review of Nanocellulose as a Novel Vehicle for Drug Delivery. *Nord. Pulp Pap. Res. J.* **2014**, *29*, 105–118.

(185) Li, Y.; Khuu, N.; Gevorkian, A.; Sarjinsky, S.; Therien-Aubin, H.; Wang, Y.; Cho, S.; Kumacheva, E. Supramolecular Nanofibrillar Thermoreversible Hydrogel for Growth and Release of Cancer Spheroids. *Angew. Chem., Int. Ed.* **2017**, *56*, 6083–6087.

(186) Truong, W. T.; Lewis, L.; Thordarson, P. Biomedical Applications of Molecular Gels. In *Functional Molecular Gels*; Royal Society of Chemistry, 2014; pp 157–194.

(187) Dennis, S. C.; Detamore, M. S.; Kieweg, S. L.; Berkland, C. J. Mapping Glycosaminoglycan–Hydroxyapatite Colloidal Gels as Potential Tissue Defect Fillers. *Langmuir* **2014**, *30*, 3528–3537.

(188) Terech, P.; Weiss, R. G. Low-Molecular Mass Gelators of Organic Liquids and the Properties of Their Gels. *Chem. Rev.* **1997**, *97*, 3133–3159.

(189) Lee, K. Y.; Mooney, D. J. Hydrogels for Tissue Engineering. *Chem. Rev.* **2001**, *101*, 1869–1879.

(190) Slomkowski, S.; Aleman, J. V; Gilbert, R. G.; Hess, M.; Horie, K.; Jones, R. G.; Kubisa, P.; Meisel, I.; Mormann, W.; Penczek, S.; Stepto, R. F. T. Terminology of Polymers and Polymerization Processes in Dispersed Systems (IUPAC Recommendations 2011). *Pure Appl. Chem.* **2011**, *83*, 2229–2259.

(191) Borsos, A.; Gilányi, T. Transition from Thermodynamically Stable Solution to Colloid Dispersion State. *Colloid Polym. Sci.* **2012**, *290*, 473–479.

(192) Tran, A.; Hamad, W. Y.; MacLachlan, M. J. Fabrication of Cellulose Nanocrystal Films through Differential Evaporation for Patterned Coatings. *ACS Appl. Nano Mater.* **2018**, *1*, 3098–3104.

(193) Chau, M.; De France, K. J.; Kopera, B.; Machado, V. R.; Rosenfeldt, S.; Reyes, L.; Chan, K. J. W.; Förster, S.; Cranston, E. D.; Hoare, T.; Kumacheva, E. Composite Hydrogels with Tunable Anisotropic Morphologies and Mechanical Properties. *Chem. Mater.* **2016**, *28*, 3406–3415.

(194) Capadona, J. R.; Van Den Berg, O.; Capadona, L. A.; Schroeter, M.; Rowan, S. J.; Tyler, D. J.; Weder, C. A Versatile Approach for the Processing of Polymer Nanocomposites with Self-Assembled Nanofibre Templates. *Nat. Nanotechnol.* **2007**, *2*, 765–769.

(195) Erlandsson, J.; Françon, H.; Marais, A.; Granberg, H.; Wågberg, L. Cross-Linked and Shapeable Porous 3D Substrates from Freeze-Linked Cellulose Nanofibrils. *Biomacromolecules* **2019**, *20*, 728–737.

(196) Chu, G.; Qu, D.; Zussman, E.; Xu, Y. Ice-Assisted Assembly of Liquid Crystalline Cellulose Nanocrystals for Preparing Anisotropic Aerogels with Ordered Structures.

Chem. Mater. **2017**, *29*, 3980–3988.

(197) Munier, P.; Gordeyeva, K.; Bergström, L.; Fall, A. B. Directional Freezing of Nanocellulose Dispersions Aligns the Rod-Like Particles and Produces Low-Density and Robust Particle Networks. *Biomacromolecules* **2016**, *17*, 1875–1881.

(198) Deville, S. *Freezing Colloids: Observations, Principles, Control, and Use: Applications in Materials Science, Life Science, Earth Science, Food Science, and Engineering*; Springer International Publishing, 2017.

(199) Bouville, F.; Maire, E.; Deville, S. Self-Assembly of Faceted Particles Triggered by a Moving Ice Front. *Langmuir* **2014**, *30*, 8656–8663.

(200) Hug, J. E.; van Swol, F.; Zukoski, C. F. The Freezing of Colloidal Suspensions in Confined Spaces. *Langmuir* **1995**, *11*, 111–118.

(201) Xu, Y.-T.; Dai, Y.; Nguyen, T.-D.; Hamad, W. Y.; MacLachlan, M. J. Aerogel Materials with Periodic Structures Imprinted with Cellulose Nanocrystals. *Nanoscale* **2018**, *10*, 3805–3812.

(202) Natural Resources Canada. Indicator: Gross domestic product https://www.nrcan.gc.ca/forests/report/economy/16556 (accessed Apr 15, 2019).

(203) Natural Resources Canada. Selective Cuttings: Newsprint exports continue long-term decline in 2012 http://cfs.nrcan.gc.ca/selective-cuttings/14 (accessed Apr 15, 2019).

(204) CelluForce. CelluForce restarts production of cellulose nanocrystals at its newly modernized facility https://www.celluforce.com/en/media/latest-news/celluforce-restarts-production-of-cellulose-nanocrystals-at-its-newly-modernized-facility/ (accessed Apr 15, 2019).

(205) Nanocellulose Market Analysis | Recent Market Developments | Industry Forecast to

2023 https://www.marketsandmarkets.com/Market-Reports/nano-cellulose-market-56392090.html (accessed Apr 15, 2019).

(206) Pignon, F.; Magnin, A.; Piau, J.-M.; Cabane, B.; Lindner, P.; Diat, O. Yield Stress Thixotropic Clay Suspension: Investigations of Structure by Light, Neutron, and x-Ray Scattering. *Phys. Rev. E* **1997**, *56*, 3281–3289.

(207) Or, T.; Miettunen, K. E.; Cranston, E. D.; Moran-Mirabal, J. M.; Vapaavuori, J. Cellulose Nanocrystal Aerogels as Electrolyte Scaffolds for Glass and Plastic Dye-Sensitized Solar Cells. *ACS Appl. Energy Mater.* **2019**, acsaem.9b00795.

(208) Khabibullin, A.; Alizadehgiashi, M.; Khuu, N.; Prince, E.; Tebbe, M.; Kumacheva, E. Injectable Shear-Thinning Fluorescent Hydrogel Formed by Cellulose Nanocrystals and Graphene Quantum Dots. *Langmuir* **2017**, *33*, 12344–12350.

(209) Gaponik, N.; Herrmann, A.-K.; Eychmüller, A. Colloidal Nanocrystal-Based Gels and Aerogels: Material Aspects and Application Perspectives. *J. Phys. Chem. Lett.* **2012**, *3*, 8–17.

(210) Kose, O.; Tran, A.; Lewis, L.; Hamad, W. Y.; MacLachlan, M. J. Unwinding a Spiral of Cellulose Nanocrystals for Stimuli-Responsive Stretchable Optics. *Nat. Commun.* **2019**, *10*, 510.

(211) Cao, Y.; Lewis, L.; Hamad, W. Y.; MacLachlan, M. J. Pressure-Responsive Hierarchical Chiral Photonic Aerogels. *Adv. Mater.* **2019**, *31*, 1808186.

(212) Tsurusawa, H.; Leocmach, M.; Russo, J.; Tanaka, H. Direct Link between Mechanical Stability in Gels and Percolation of Isostatic Particles. *Sci. Adv.* **2019**, *5*, eaav6090.

(213) PubChem. Open Chemistry Database: PubChem Compound. https://www.ncbi.nlm.nih.gov/pccompound.

(214) Boncel, S.; Saletra, K.; Hefczyc, B.; Walczak, K. Z. Michael-type addition of azoles of broad-scale acidity to methyl acrylate. *Beilstein Journal of Organic Chemistry* **2011**, *7*, 173–178.

(215) ZirChrom. Dissociation Constants Of Organic Acids And Base. https://www.zirchrom.com/organic.htm.

(216) Kuo, M.-S.; Chang, S.-J.; Hsieh, P.-H.; Huang, Y.-C.; Li, C.-C.; Franks, G. Efficient Dispersants for TiO2 Nanopowder in Organic Suspensions. *J. Am. Ceram. Soc.* **2016**, *99*, 445–451.

(217) Gupta, M.; da Silva, E. F.; Svendsen, H. F. Computational Study of Thermodynamics of Polyamines with Regard to CO_2 Capture. *Energy Procedia* **2012**, *23*, 140–150.

(218) Human Metabolome Database. Metabocard for Norspermidine (HMDB0011634). http://www.hmdb.ca/metabolites/HMDB11634.

Appendix

A.1 Supporting Information for Chapter 1

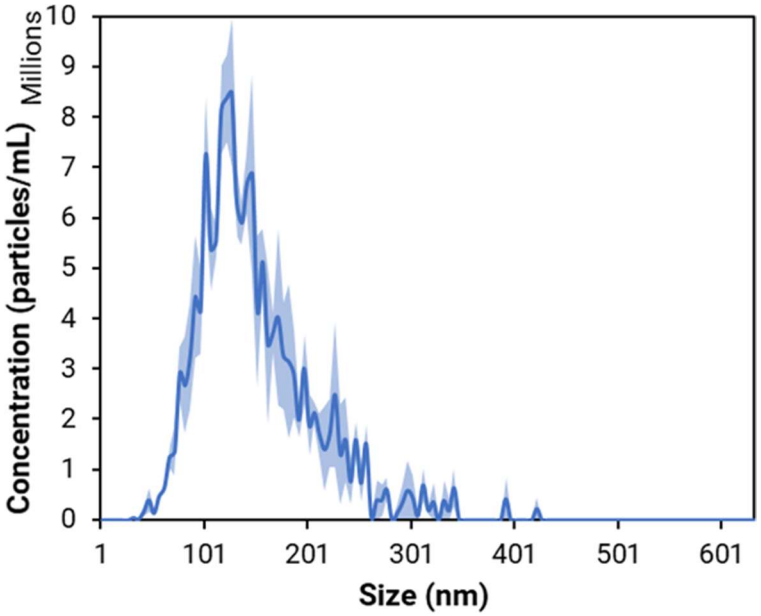

Figure A.1.1. Nanoparticle tracking analysis showing the size distribution and particle concentration of a 4 wt% CNC suspension diluted 1,000,000 times. CNCs measured had an average size of 150 ± 5 nm and a particle concentration of 1.51 ± 0.03 x 10^{15} particles mL^{-1}. Error bars represent standard deviation (n = 3). We acknowledge the assistance of Kelsi Lix and Prof. Russ Algar.

A.2 Supporting Information for Chapter 2

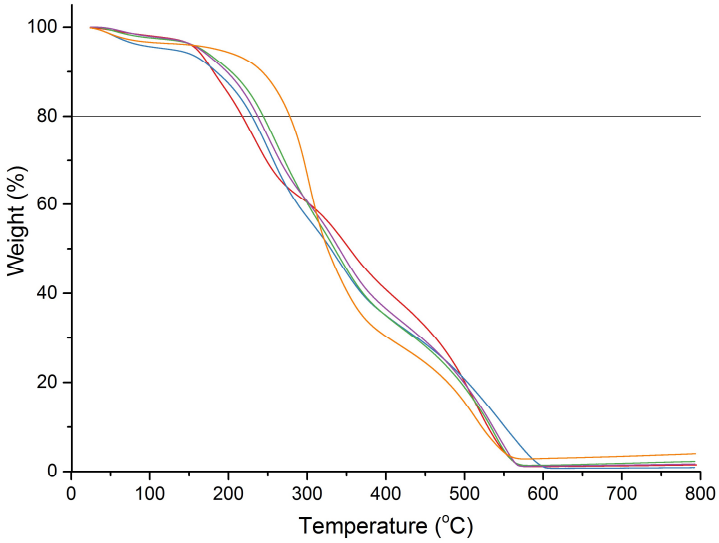

Figure A.2.1. Thermogravimetric analysis curves of 4 wt% CNC-H^+ samples treated at various temperatures for 20 h, showing the determination of the degradation temperature at which the TGA curve intersects at 80 wt% remaining for each sample, represented as T80%. CNC-120 (orange), CNC-100 (purple), CNC-80 (green), CNC-60 (blue), CNC-NT (red).

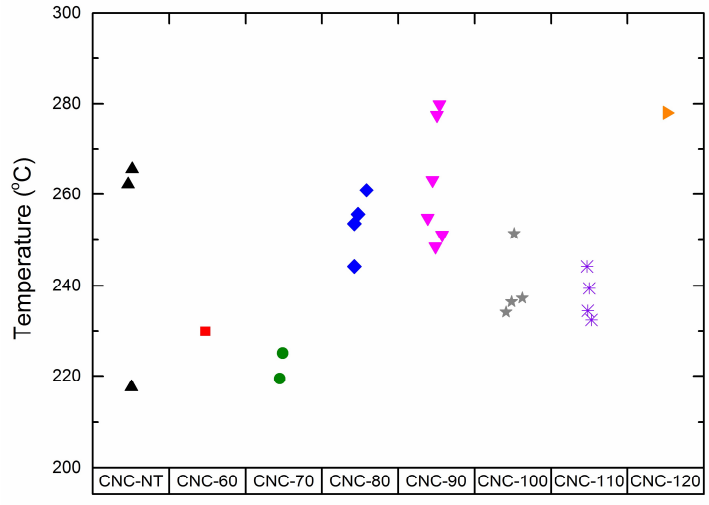

Figure A.2.2. Temperature at which TGA curve is 80 wt%, T80%, for each sample. Samples were heated at a rate of 5 °C min^{-1} under N_2.

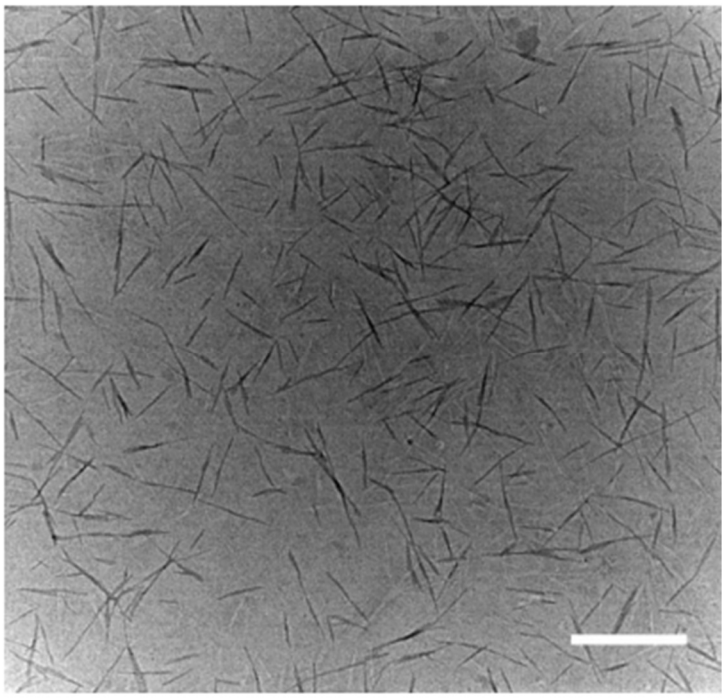

Figure A.2.3. Transmission electron micrograph analysis of CNCs , which are 191 ± 80 by 13 ± 3 nm in dimension. Errors correspond to average standard deviation, n = 335. ImageJ (NIH, http://imagej.nih.gov/ij/) was used to manually measure CNC lengths and widths. Scale bar represents 500 nm.

A.3 Supporting Information for Chapter 3

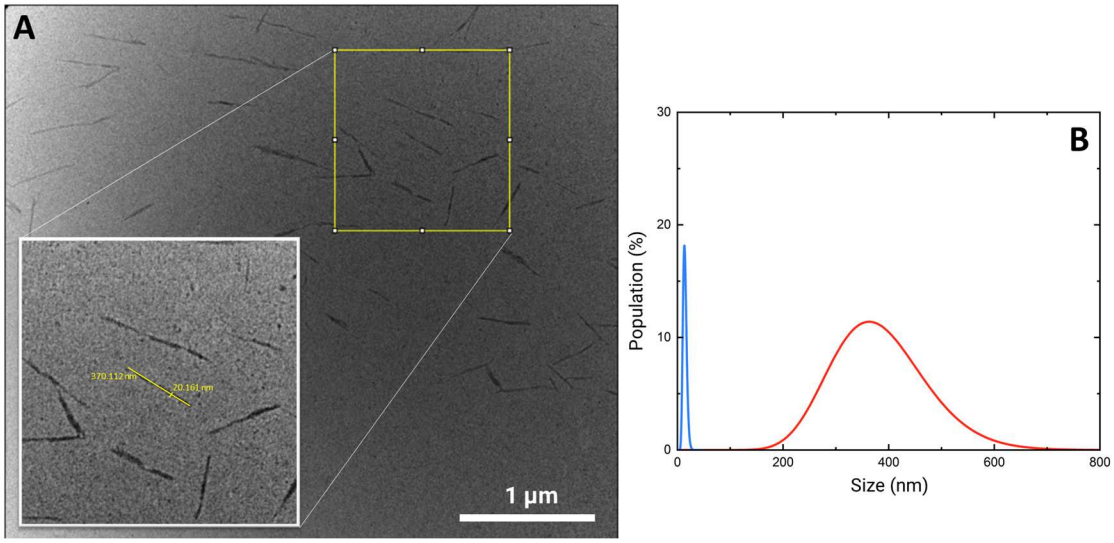

Figure A.3.1. Transmission electron microscopy analysis of CNCs , which are 384 ± 89 nm by 14 ± 4 nm in dimension. Errors correspond to average standard deviation, n = 250. (A) TEM image of CNCs deposited on the grid from their 0.004 wt% suspension. The scale bar is 500 nm. ImageJ (NIH, http://imagej.nih.gov/ij/) was used to manually measure CNC lengths and width. (B) Size distribution of the width (blue) and length (red) of the CNCs, determined by analyzing 250 CNCs.

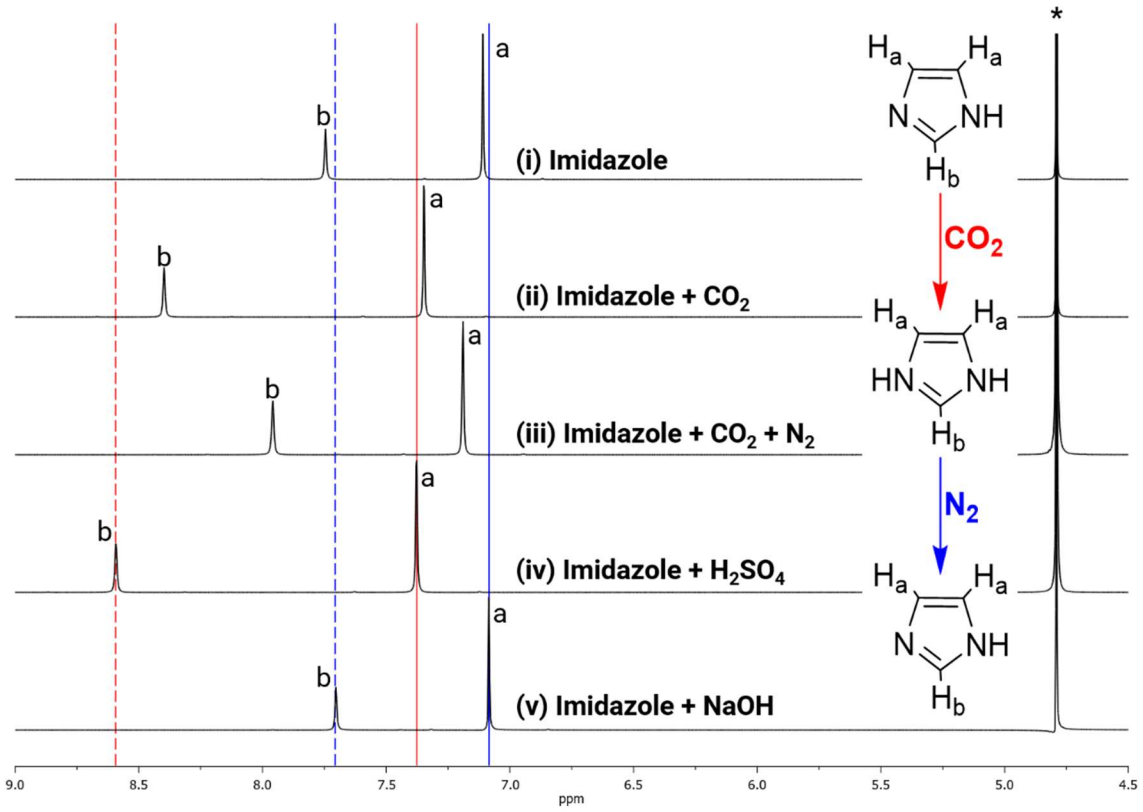

Figure A.3.2. The ^{1}H NMR (400 MHz, D_2O) spectra of imidazole (i) before CO_2 treatment (δ7.11 [H_a, s], δ7.75 [H_b, s]), (ii) after 5 min of CO_2 sparging (δ7.35 [H_a, d], δ8.40 [H_b, s]), (iii) after 5 min of CO_2 followed by 45 min of N_2 sparging (δ7.19 [H_a, s], δ7.96 [H_b, s]), (iv) with H_2SO_4 (δ7.38 [H_a, d], δ8.59 [H_b, s]), and (v) with NaOH (δ7.09 [H_a, d], δ7.70 [H_b, s]).

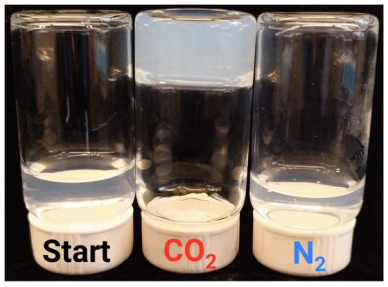

Figure A.3.3. Photograph showing the CO_2-switchability of a CNC-Na^+ (4 wt%, 4.5 mL) and imidazole (0.1 M, 1.5 mL) mixture after sparging for 5 min with CO_2 and then 45 min with N_2, showing similar gelation behavior as CNC-H^+ containing samples.

Table A.3.1. Gelation behavior of different amine-containing CNC-H^+ suspensions.

Amines	Formula	Amine amount [mL of 0.1 M solution]	Behavior after CO_2 sparging	pK_{aH}
Group 1				
imidazole	$C_3H_4N_2$	2.5	**weak gel (reversible)**	6.9[213]
ethanolamine	C_2H_7NO	1.0	weak gel	9.5[213]
isopropylamine	C_3H_9N	2.0	weak gel	10.6[213]
triethylamine	$C_6H_{15}N$	2.0	weak gel	10.8[213]
diethylamine	$C_4H_{11}N$	2.5	weak gel	11.1[213]
diisopropylamine	$C_6H_{15}N$	2.0	weak gel	11.1[213]
dipropylamine	$C_6H_{15}N$	2.0	weak gel	11.0[213]
N,N-diisopropylethylamine	$C_8H_{19}N$	2.5	weak gel	10.8[214]
Group 2				
trimethylamine hydrochloride	$C_3H_9N{\cdot}HCl$	2.0	weak gel (salt)	9.8[213]
methylamine hydrochloride	$CH_5N{\cdot}HCl$	2.5	weak gel (salt)	10.6[213]
n-hexylamine	$C_6H_{15}N$	1.5	weak gel (foamed)	10.6[215]
n-octylamine	$C_8H_{19}N$	2.0	weak gel (foamed)	10.7[215]
n-hexyldecylamine	$C_{16}H_{35}N$	1.5	weak gel (foamed)	10.6[215]
oleylamine	$C_{18}H_{37}N$	1.0	weak gel (foamed)	10.0[216]
4-aminophenol	C_6H_7NO	3.5	weak gel (colored)	10.5[213]
1,2-phenylenediamine	$C_6H_8N_2$	2.5	extremely weak gel (colored)	4.5/<2[213]
Group 3				
2-aminophenol	C_6H_7NO	2.5	no gel	9.7[213]
3-aminophenol	C_6H_7NO	2.5	no gel	9.8[213]
1,3-phenylenediamine	$C_6H_8N_2$	2.5	no gel	4.9/2.6[213]
1,4-phenylenediamine	$C_6H_8N_2$	2.5	strong gel (colored)	6.2/2.7[213]
N,N,N′,N′,N″-pentamethyldiethylenetriamine	$C_9H_{23}N_3$	0.5	strong gel	9.2[217]
N,N,N′,N′-tetramethylethylenediamine	$C_6H_{16}N_2$	0.5	strong gel	9.1[217]
ethylenediamine	$C_2H_8N_2$	0.5	strong gel	10.7/7.5[213]
bis(3-aminopropyl)amine	$C_6H_{17}N_3$	0.5	strong gel	10.9[218]
1,3-diaminopropane	$C_3H_{10}N_2$	0.5	strong gel	10.9/9.0[215]
hexamethylenediamine	$C_6H_{16}N_2$	0.5	strong gel	11.0/10.7[213]

A.4 Supporting Information for Chapter 4

Table A.4.1. Elemental analysis of freeze-dried hydrogel after 4x FT cycling.

	Control (no FT cycling)	FT 4x
wt% sulfur	0.99	0.98
wt% carbon	39.75	39.93
wt% hydrogen	6.04	6.04

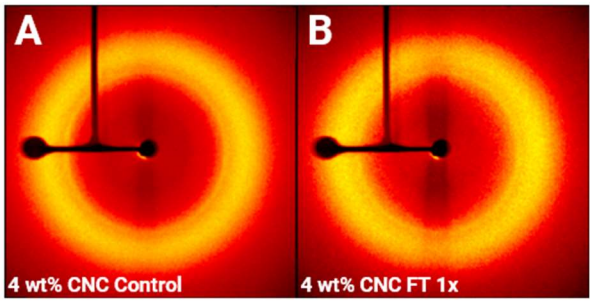

Figure A.4.1. 2D XRD patterns of 4 wt% CNC-Na^+ samples (A) before (control), and (B) after 1x FT cycles. The 2D XRD patterns show uniform radial intensity and do not show any angular anisotropy, suggesting an isotropic arrangement of CNCs. There was no observed alignment of CNCs after FT cycling, which further supports an aggregation-induced gelation mechanism due to physical confinement after repeated FT cycling.

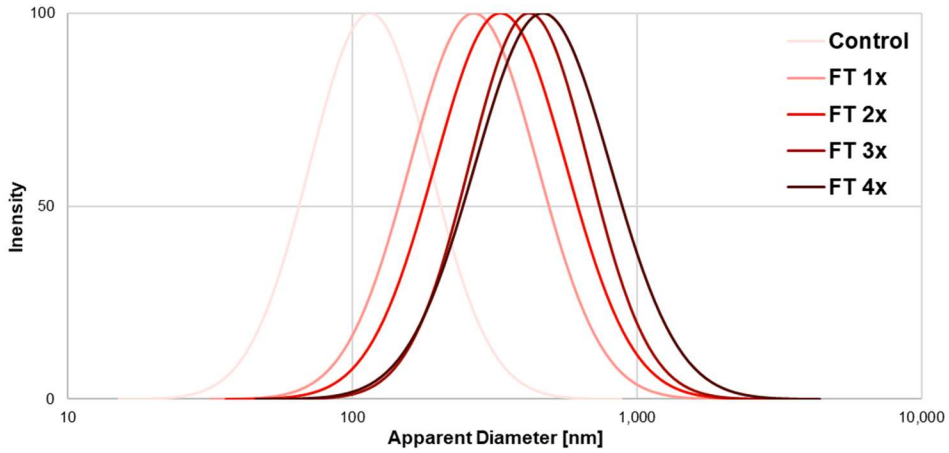

Figure A.4.2. Representative dynamic light scattering lognormal distributions of 4 wt% CNC-Na^+ suspensions showing the increase in apparent diameter as CNCs aggregate after each FT cycle. Control sample represents a 4 wt% CNC-Na^+ suspension before FT cycling.

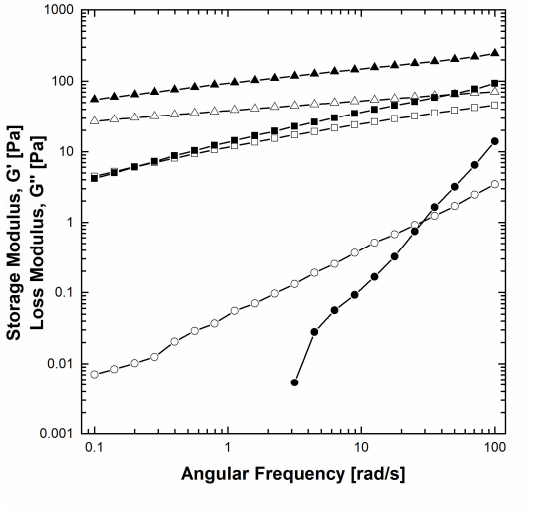

Figure A.4.3. Representative dynamic frequency sweeps of FT CNC samples showing the storage modulus, G' (closed symbols), and the loss modulus, G" (open symbols), for 4 wt% CNC suspensions before FT cycling (circles), after 1x FT cycle (squares), and after 4x FT cycles (triangles). G' is greater than G" over all frequencies tested for 4 wt% CNC suspensions that have undergone at least 2x FT cycles.

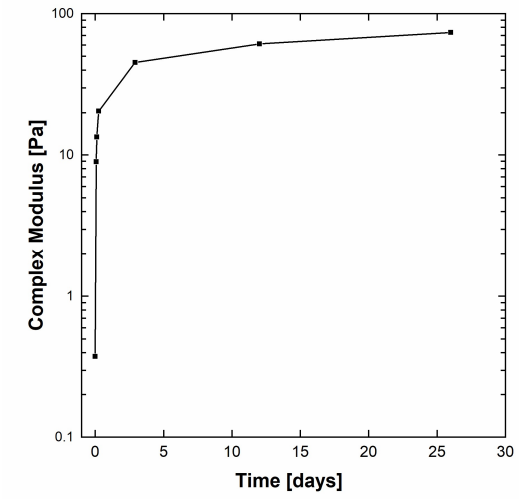

Figure A.4.4. Complex modulus at the frequency of 8.9 rad s^{-1} of 4 wt% CNC-Na^+ suspensions after freezing at −12 °C for various times between 0 and 26 days.